3 Figures

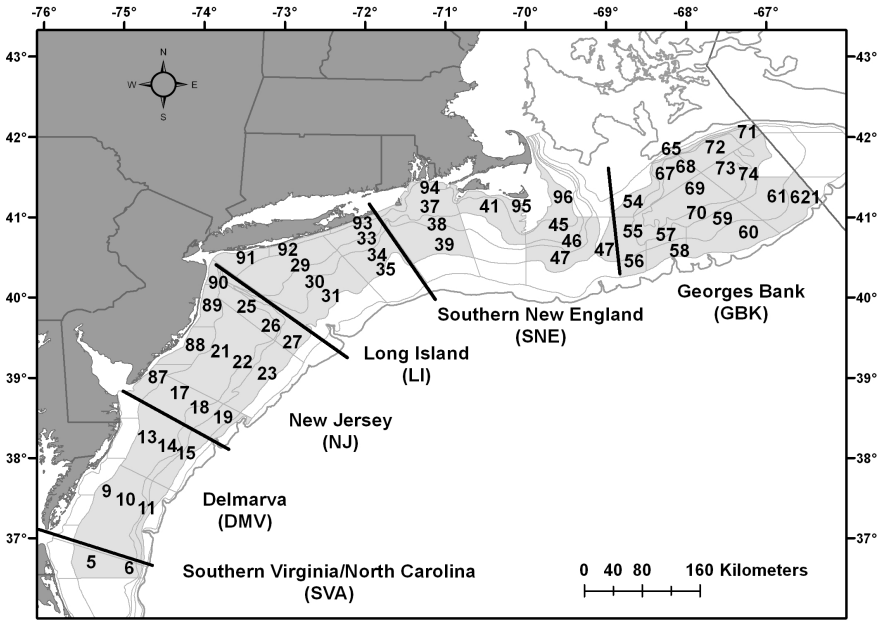

Figure 6: Ocean quahog stock assessment regions and NEFSC shellfish survey strata. The shaded strata are where ocean quahogs have been found and are used to estimate stock abundance in this assessment.

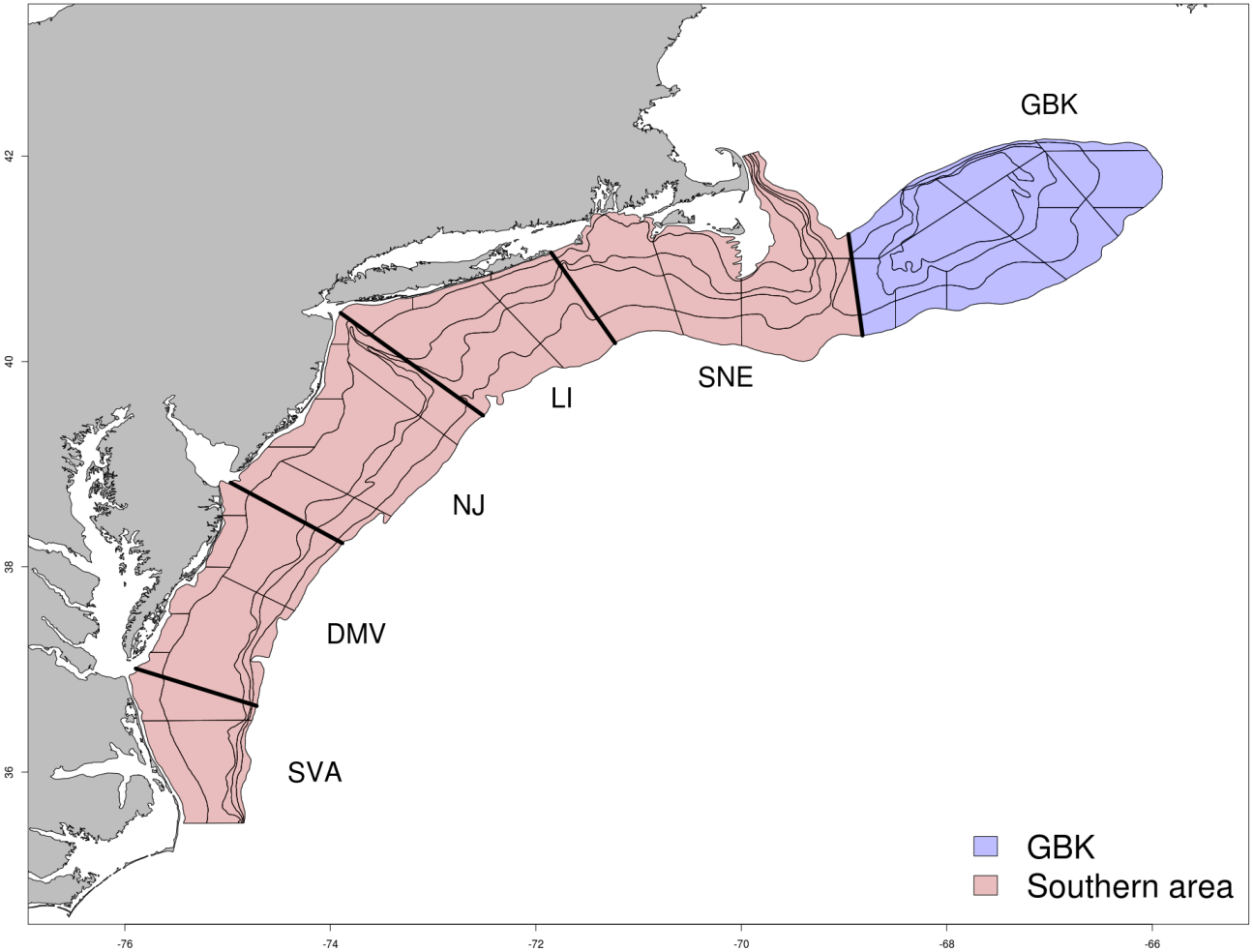

Figure 7: Ocean quahog regions divided into two areas.

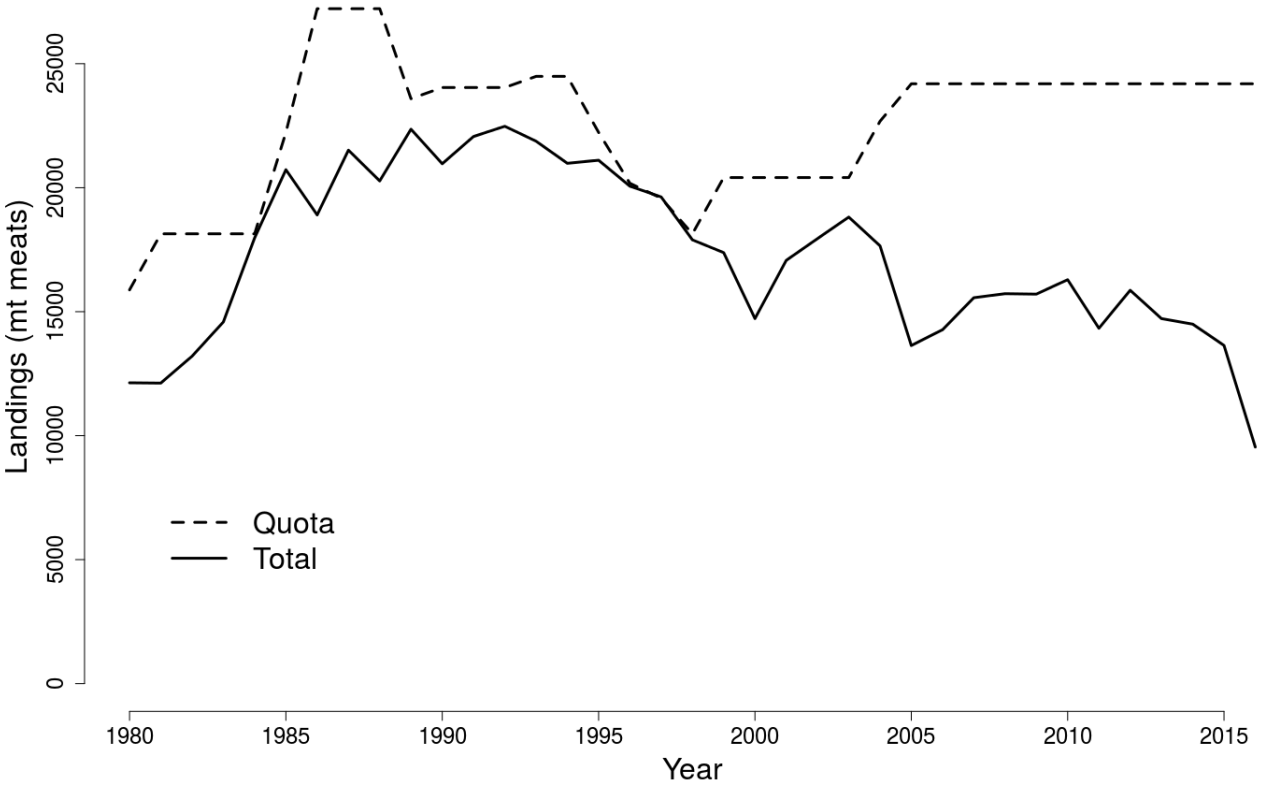

Figure 8: Total ocean quahog landings and quotas during 1980-2016.

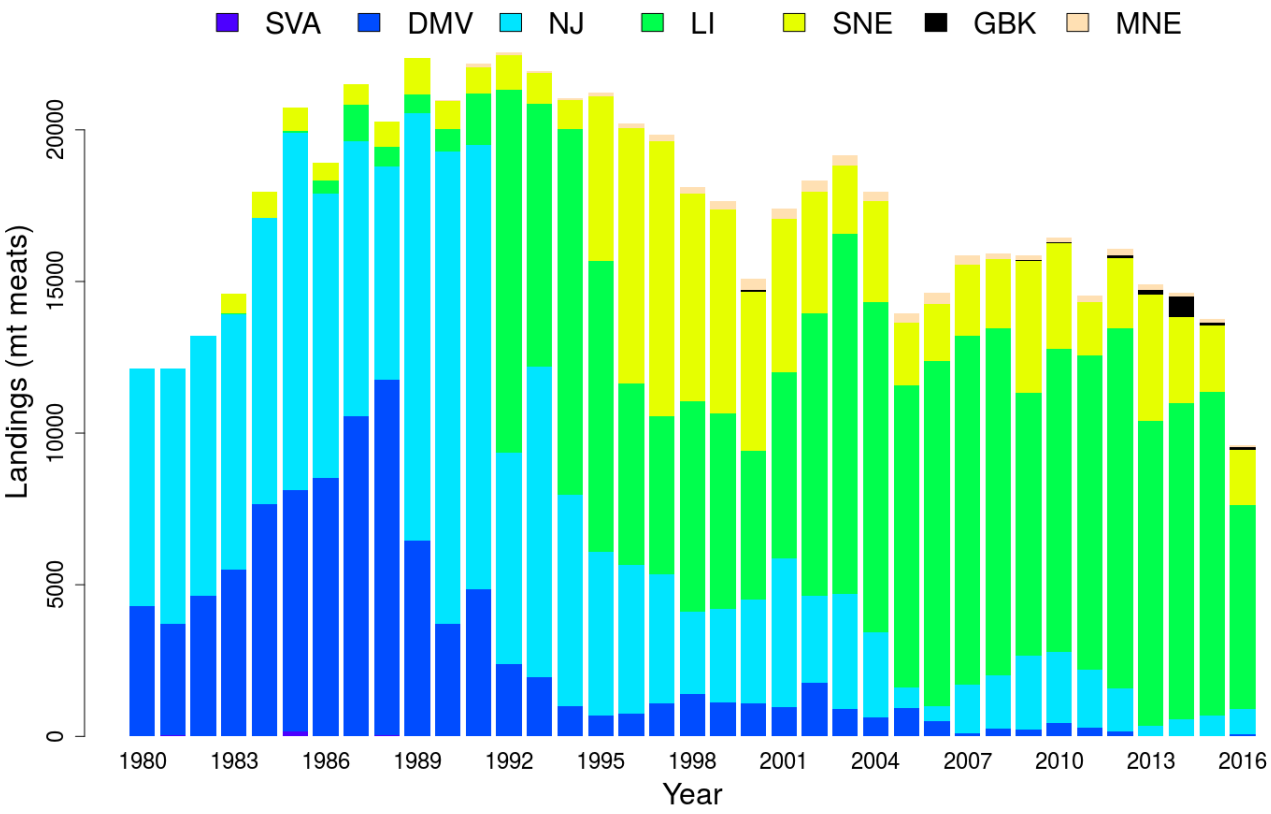

Figure 9: Ocean quahog landings from the US EEZ during 1980-2016, by stock assessment region.

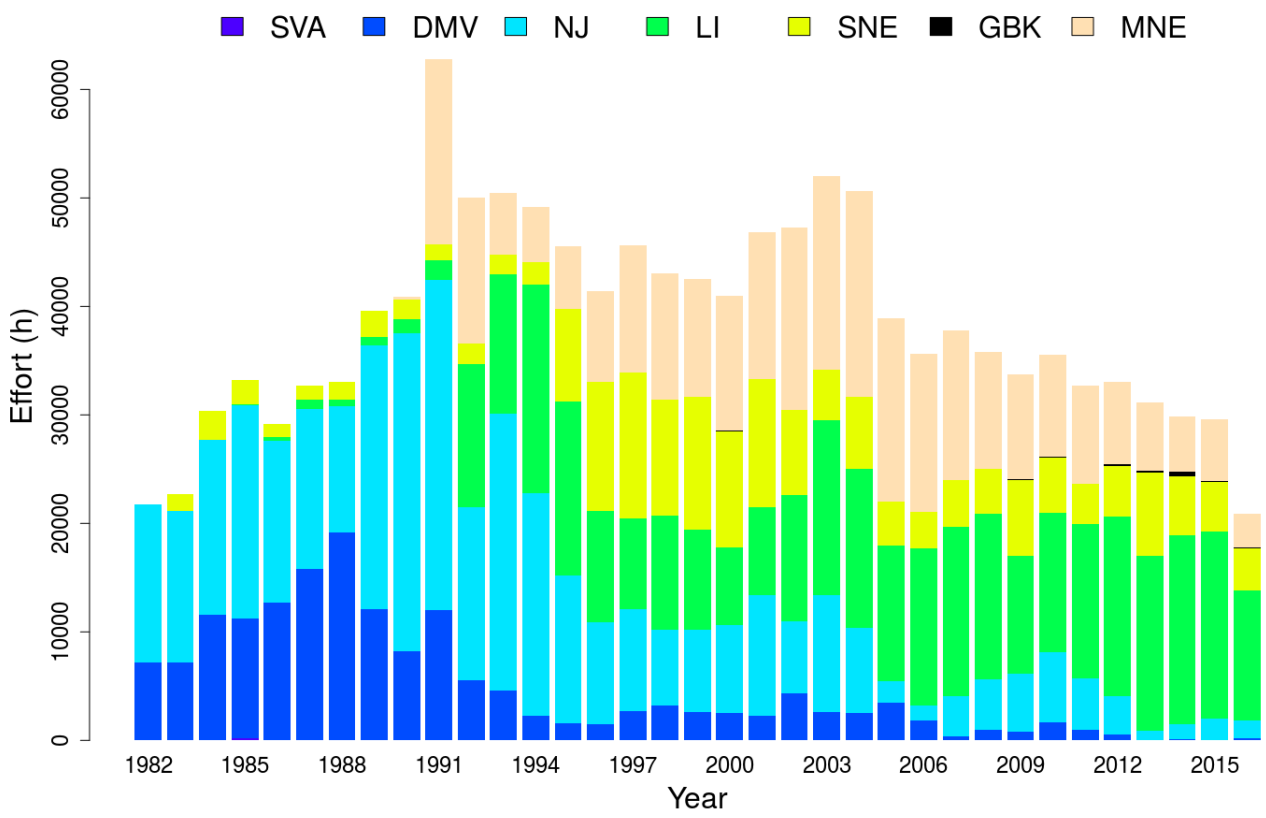

Figure 10: Ocean quahog hours fished from the US EEZ during 1982-2016, by stock assessment region.

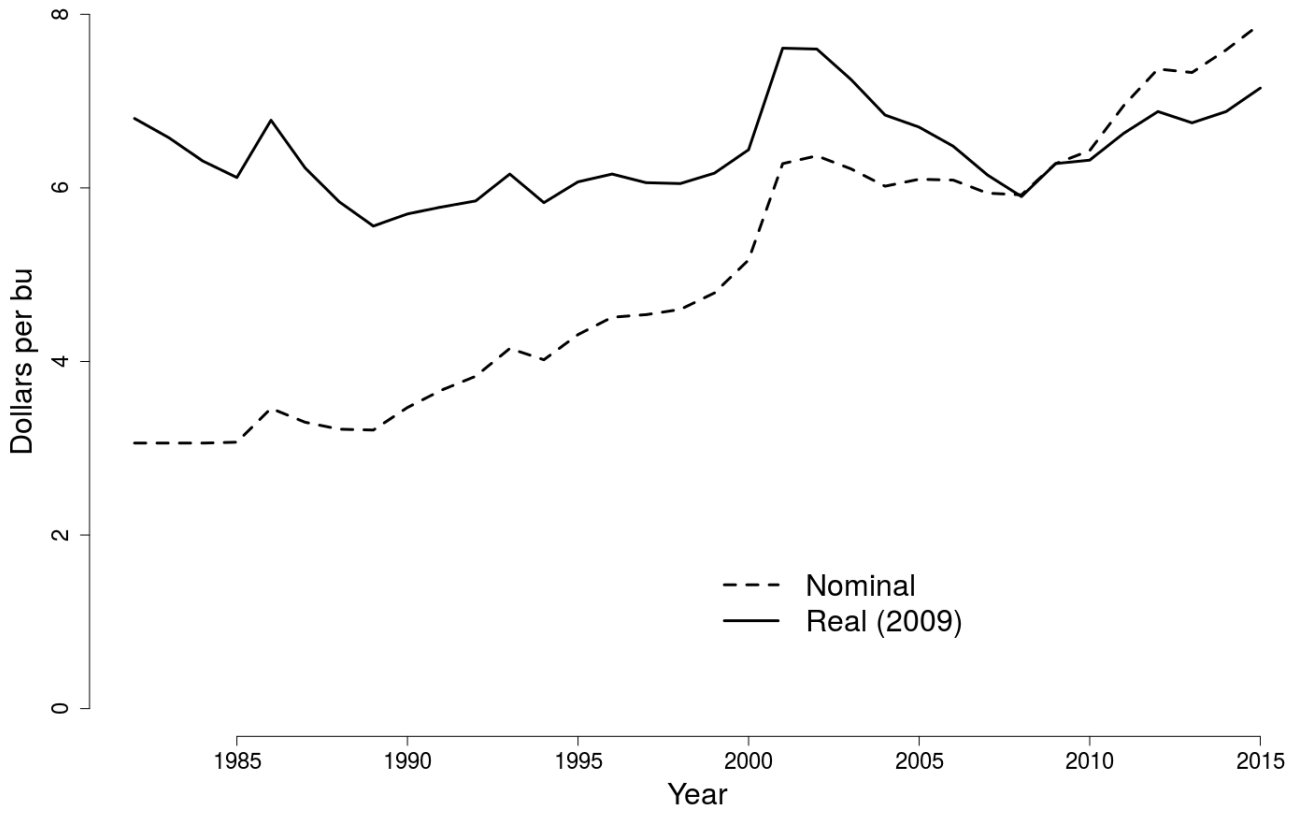

Figure 11: Nominal and real dollar equivalent prices for ocean quahog 1981-2016.

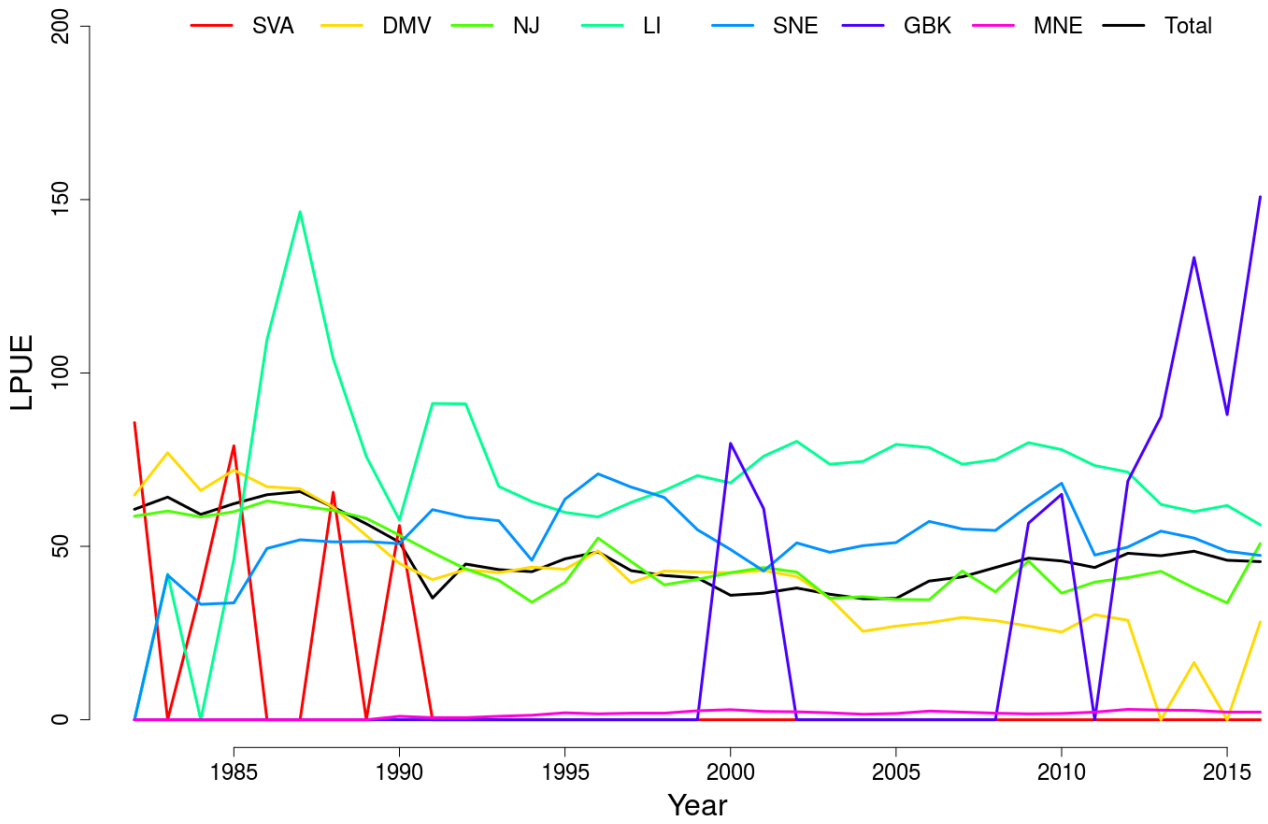

Figure 12: Nominal landings per unit effort (LPUE in bushels landed per hour fished) for ocean quahog, by region, 1981-2016. LPUE is total landings in bushels divided by total fishing effort.

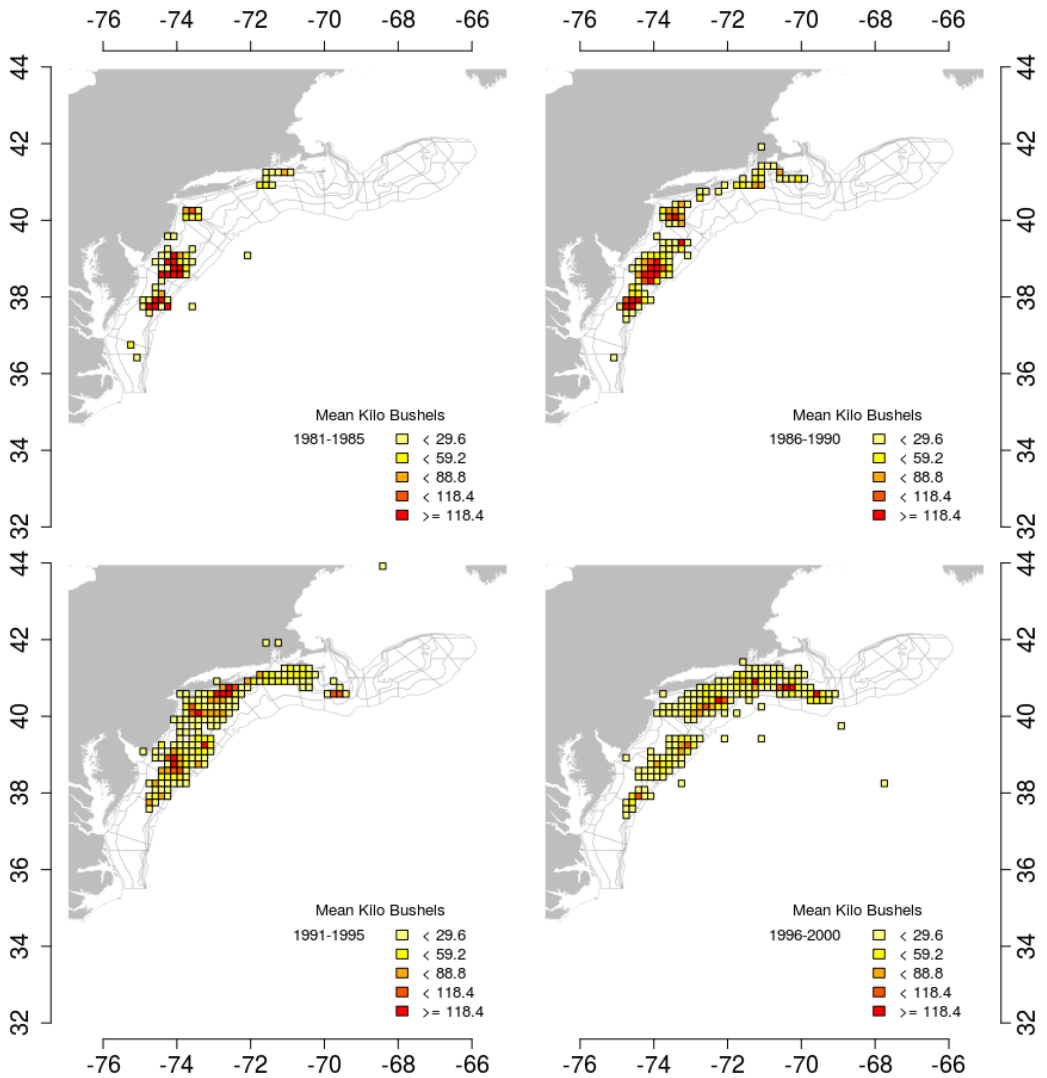

Figure 13: Average ocean quahog landings by ten-minute squares over time. Only squares where more the 5 kilo bushels were caught are shown.

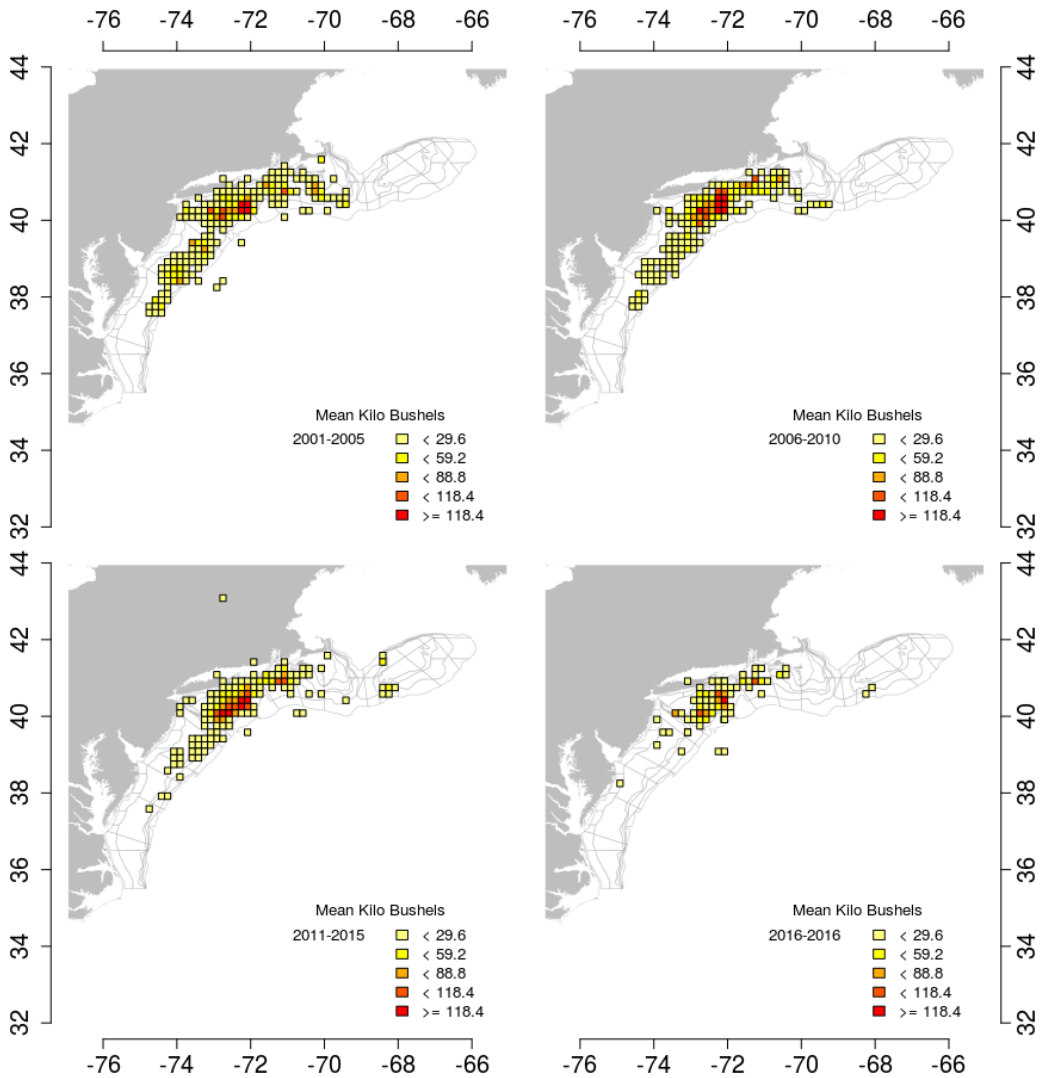

Figure 14: Average ocean quahog landings by ten-minute squares over time. Only squares where more the 5 kilo bushels were caught are shown.

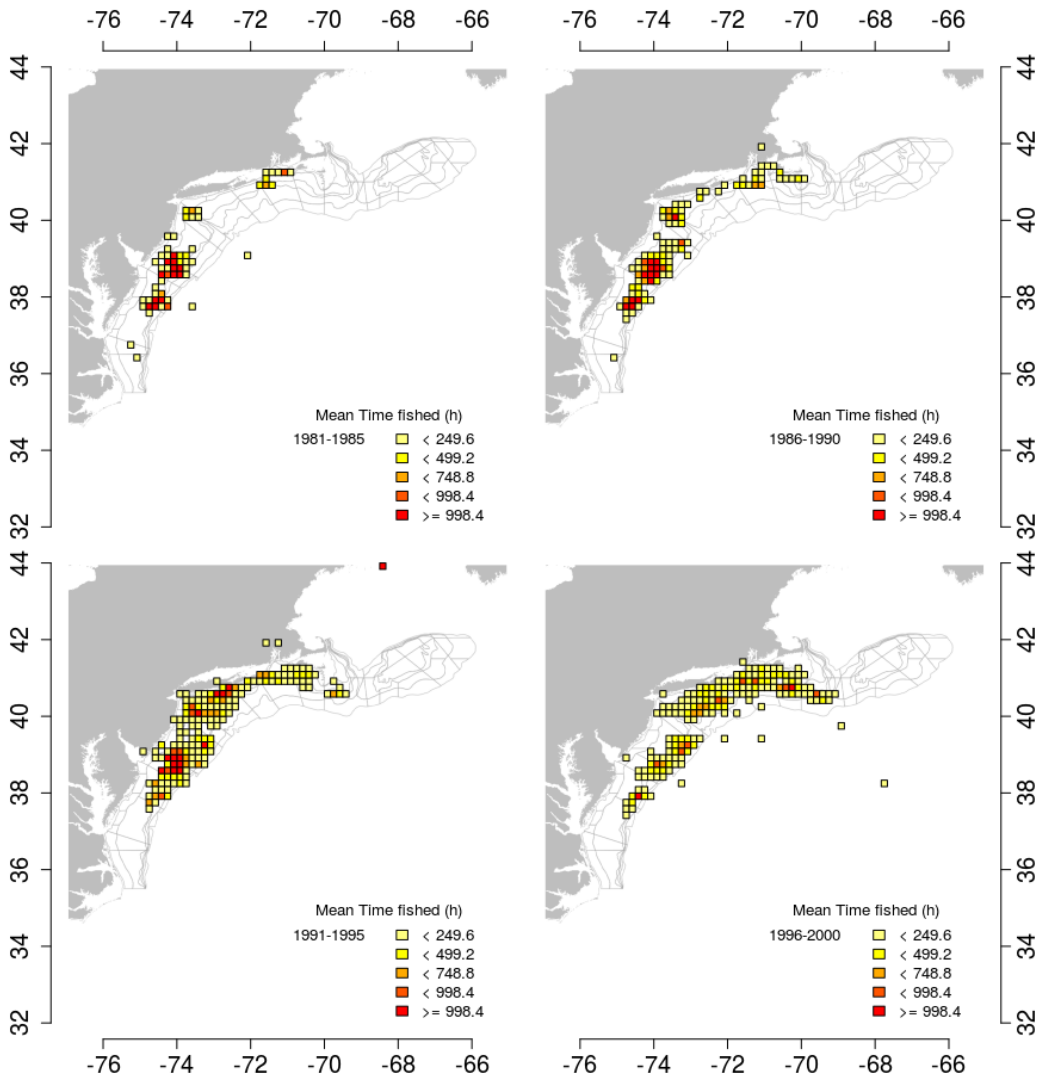

Figure 15: Average ocean quahog effort by ten-minute squares over time. Only squares where more the 5 kilo bushels were caught are shown.

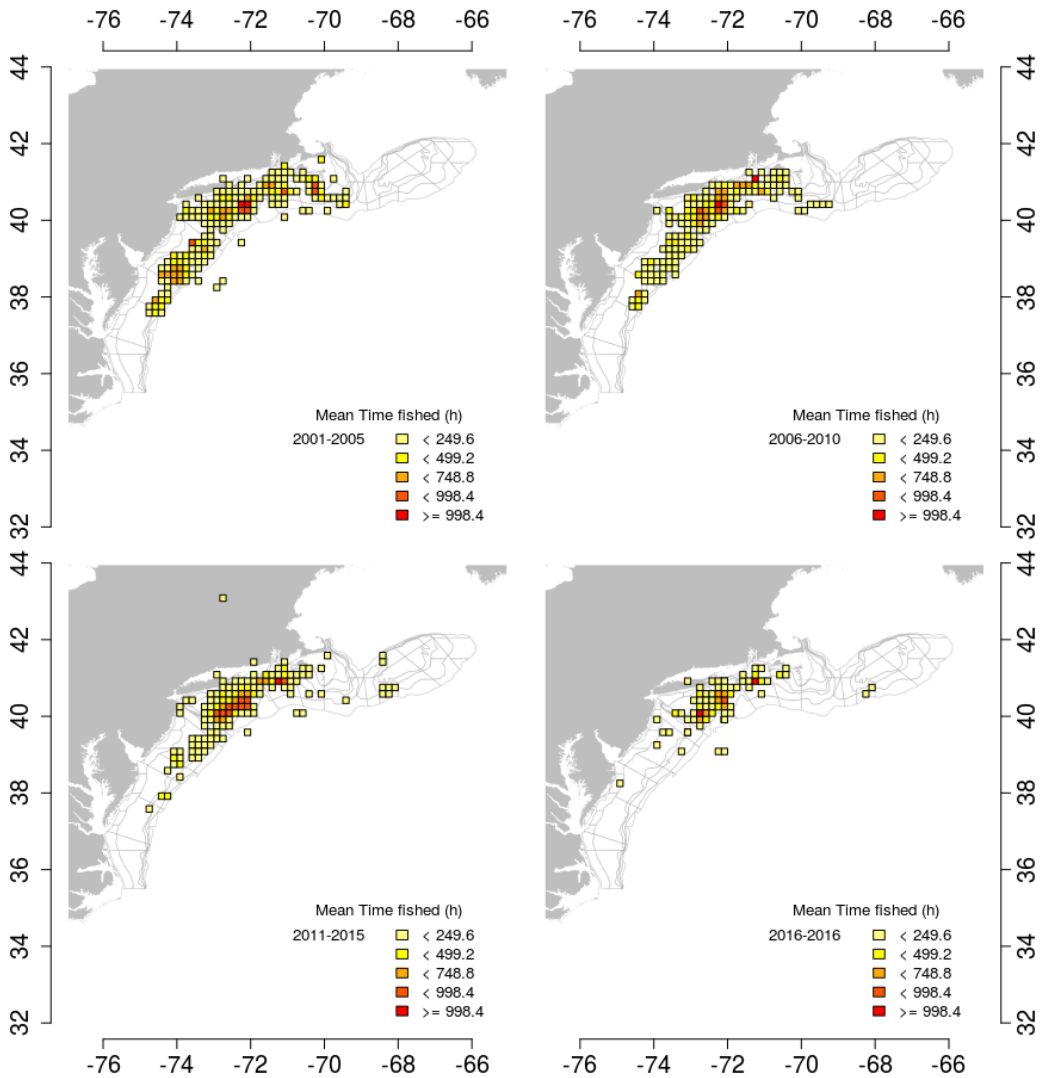

Figure 16: Average ocean quahog effort by ten-minute squares over time. Only squares where more the 5 kilo bushels were caught are shown.

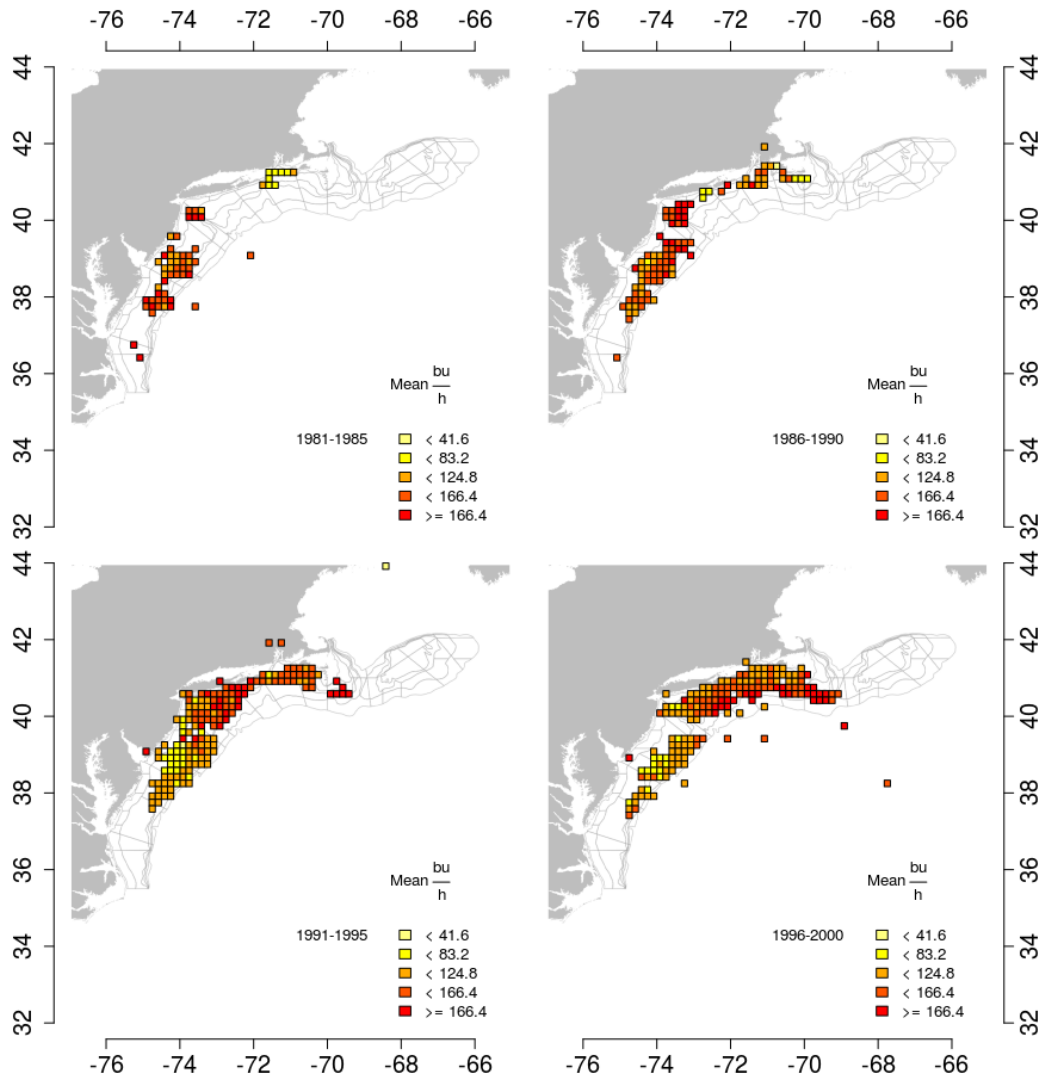

Figure 17: Average ocean quahog LPUE (bu. h^{-1}) by ten-minute squares over time. Only squares where more the 5 kilo bushels were caught are shown.

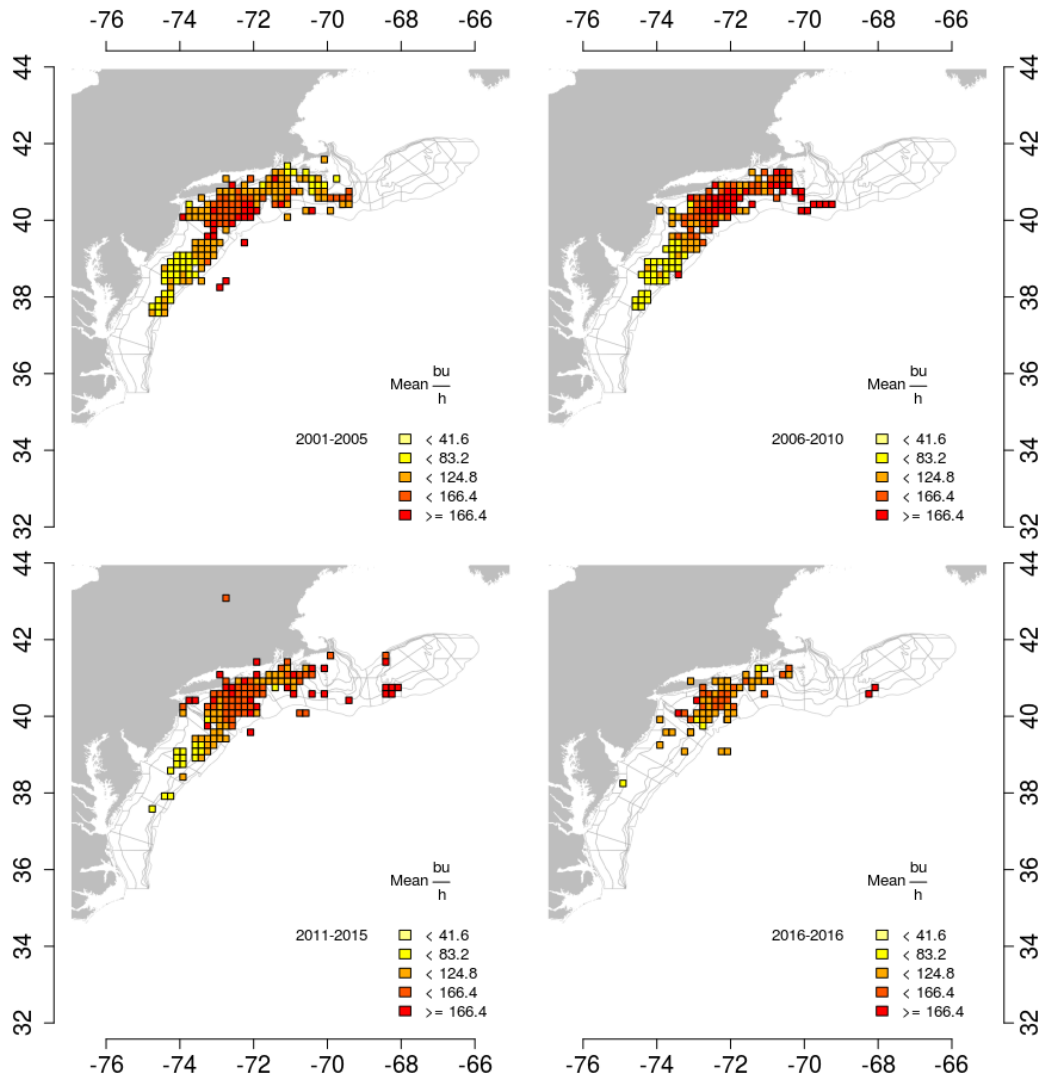

Figure 18: Average ocean quahog LPUE (bu. h^{-1}) by ten-minute squares over time. Only squares where more the 5 kilo bushels were caught are shown.

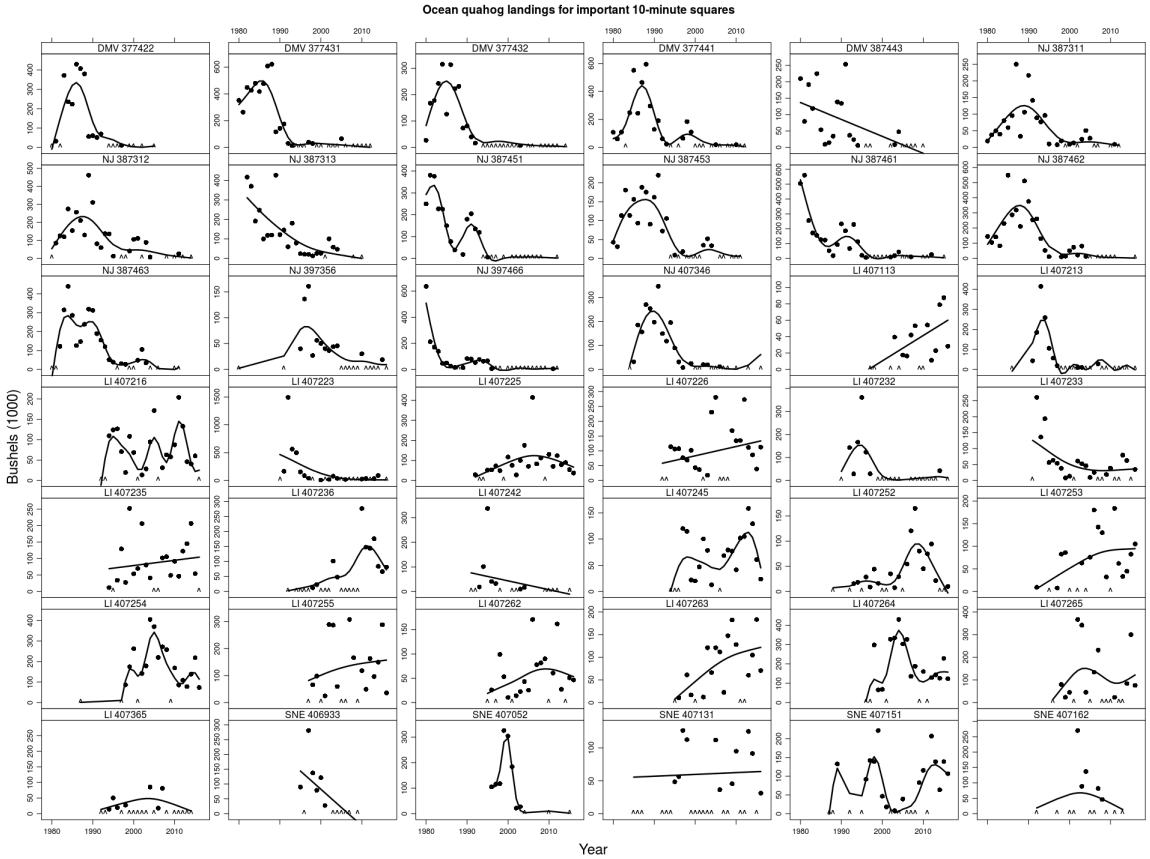

Figure 19: Annual ocean quahog landings in "important" ten minute squares (TNMS) during 1980-2016 based on logbook data. Important means that a square ranked in the top 10 TNMS for total landings during any five-year period (1980-1984, 1985-1989, ...). Data for 2016 are incomplete and preliminary. To protect the privacy of individual firms, data are not plotted if the number of vessels is less than 3. Instead, a "$\wedge$" is shown on the x-axis to indicate where data are missing. The solid dark line is a spline intended to show trends. The spline was fit to all available data, including data not plotted.

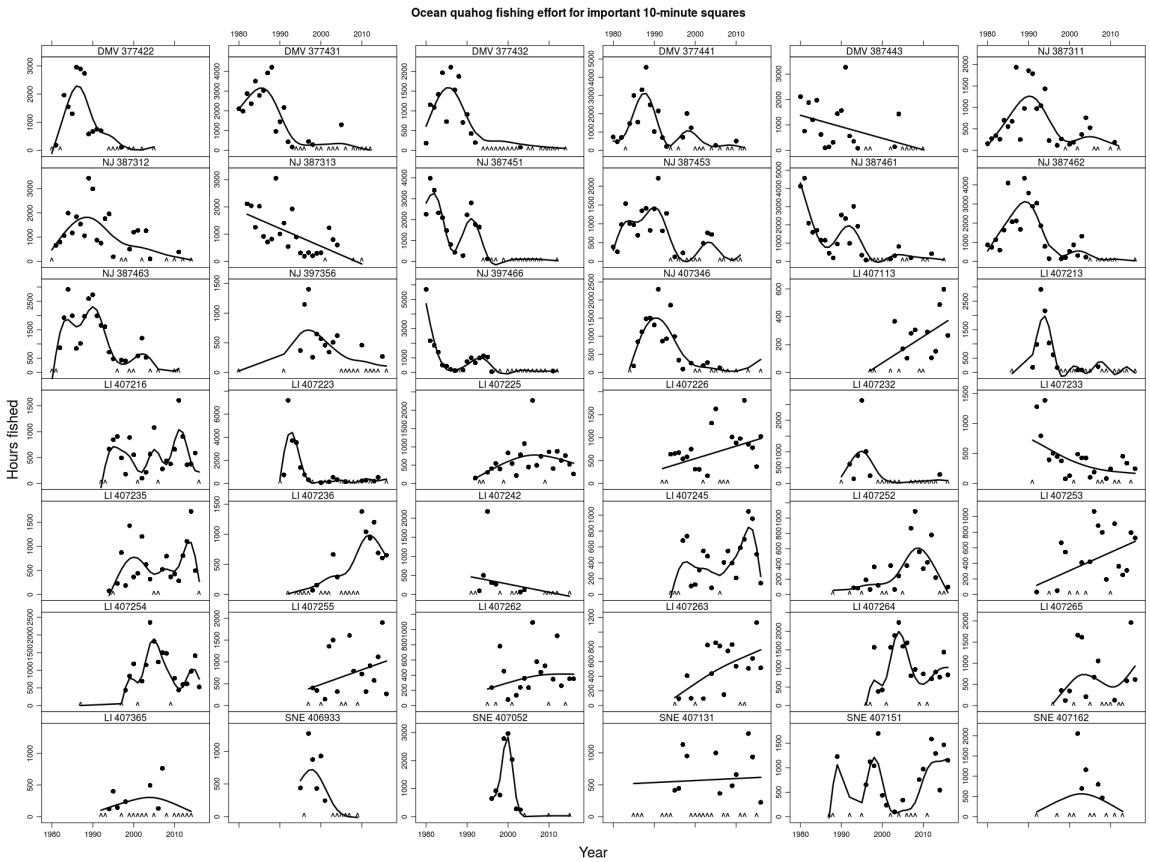

Figure 20: Annual ocean quahog effort (hours y^{-1}) in "important" ten minute squares (TNMS) during 1980-2016 based on logbook data. Important means that a square ranked in the top 10 TNMS for total landings during any five-year period. Data for 2016 are incomplete and preliminary. To protect the privacy of individual firms, data are not plotted if the number of vessels is less than 3. Instead, a "$\wedge$" is shown on the x-axis to indicate where data are missing. The solid dark line is a spline intended to show trends. The spline was fit to all available data, including data not plotted.

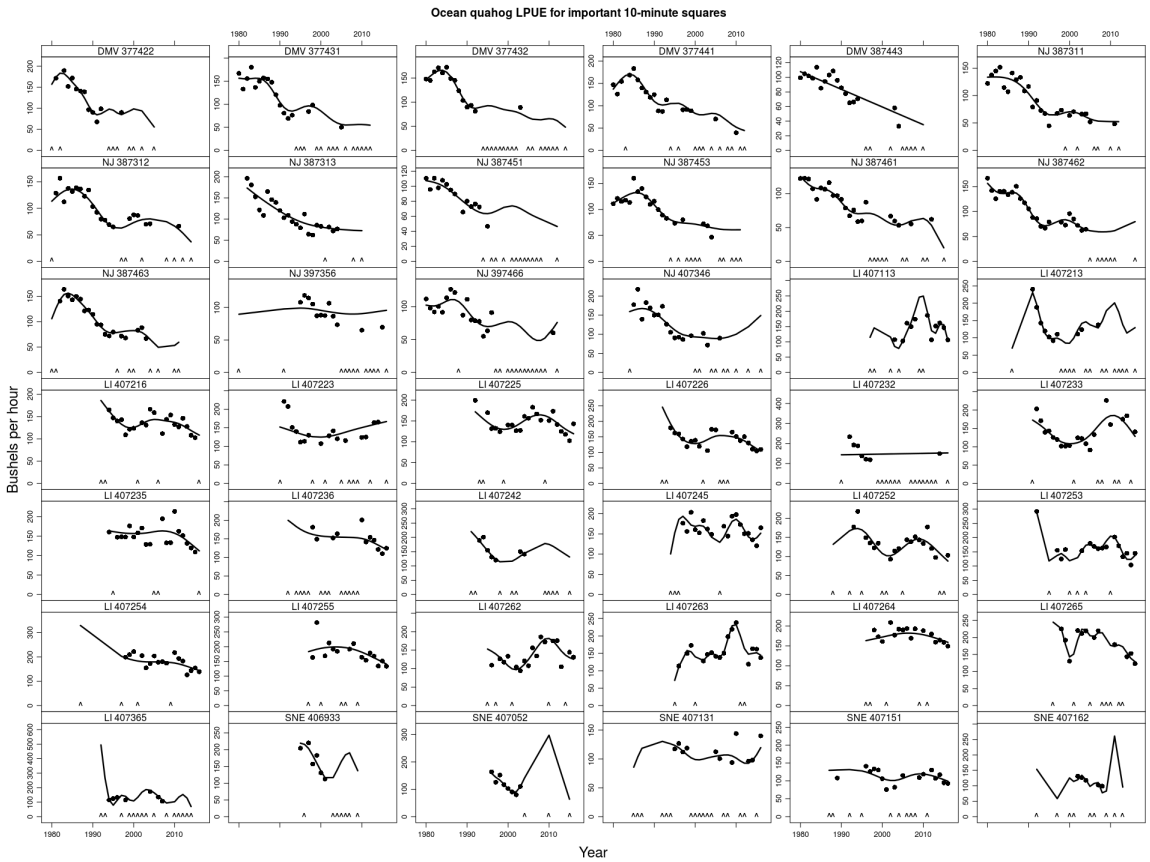

Figure 21: Annual ocean quahog LPUE (bu h^{-1}) in "important" ten minute squares (TNMS) during 1980-2016 based on logbook data. Important means that a square ranked in the top 10 TNMS for total landings during any five-year period . Data for 2016 are incomplete and preliminary. To protect the privacy of individual firms, data are not plotted if the number of vessels is less than 3. Instead, a "$\wedge$" is shown on the x-axis to indicate where data are missing. The solid dark line is a spline intended to show trends. The spline was fit to all available data, including data not plotted.

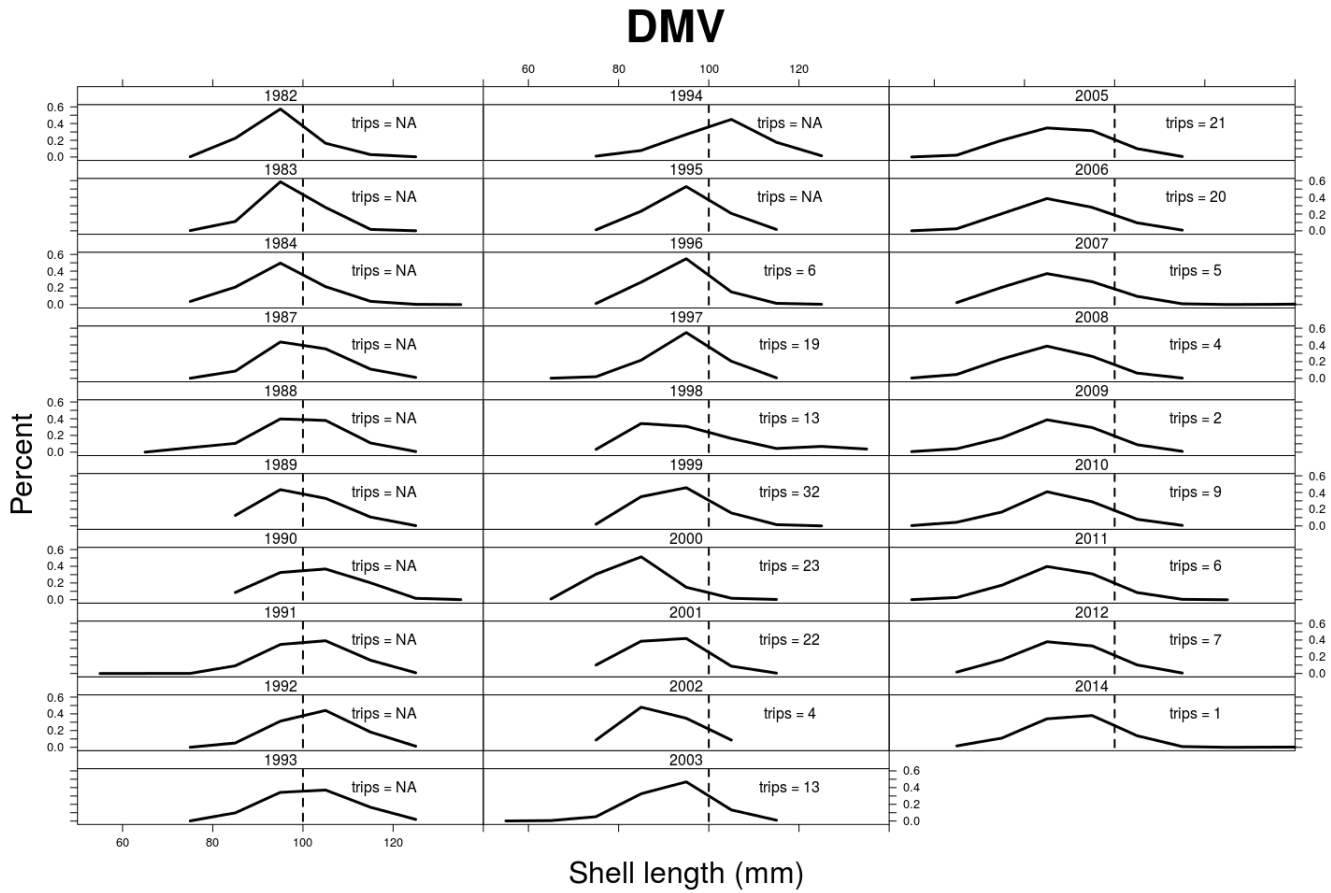

Figure 22: Length compositions of port-sampled landed ocean quahogs from the DMV region. Sample sizes are the number of trips sampled in each year. Number of trips sampled before 1996 are unknown.

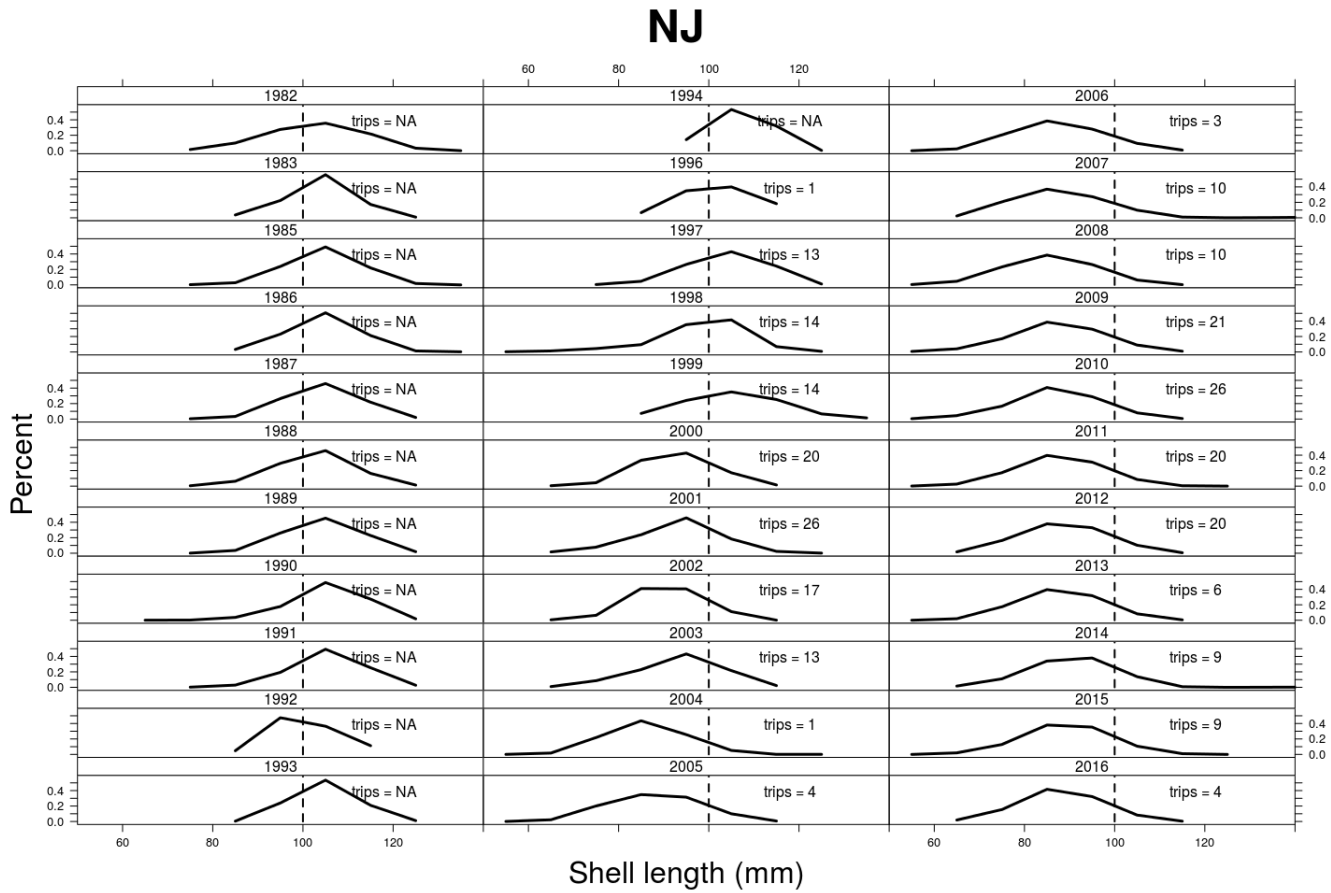

Figure 23: Length compositions of port-sampled landed ocean quahogs from the NJ region. Sample sizes are the number of trips sampled in each year. Number of trips sampled before 1996 are unknown.

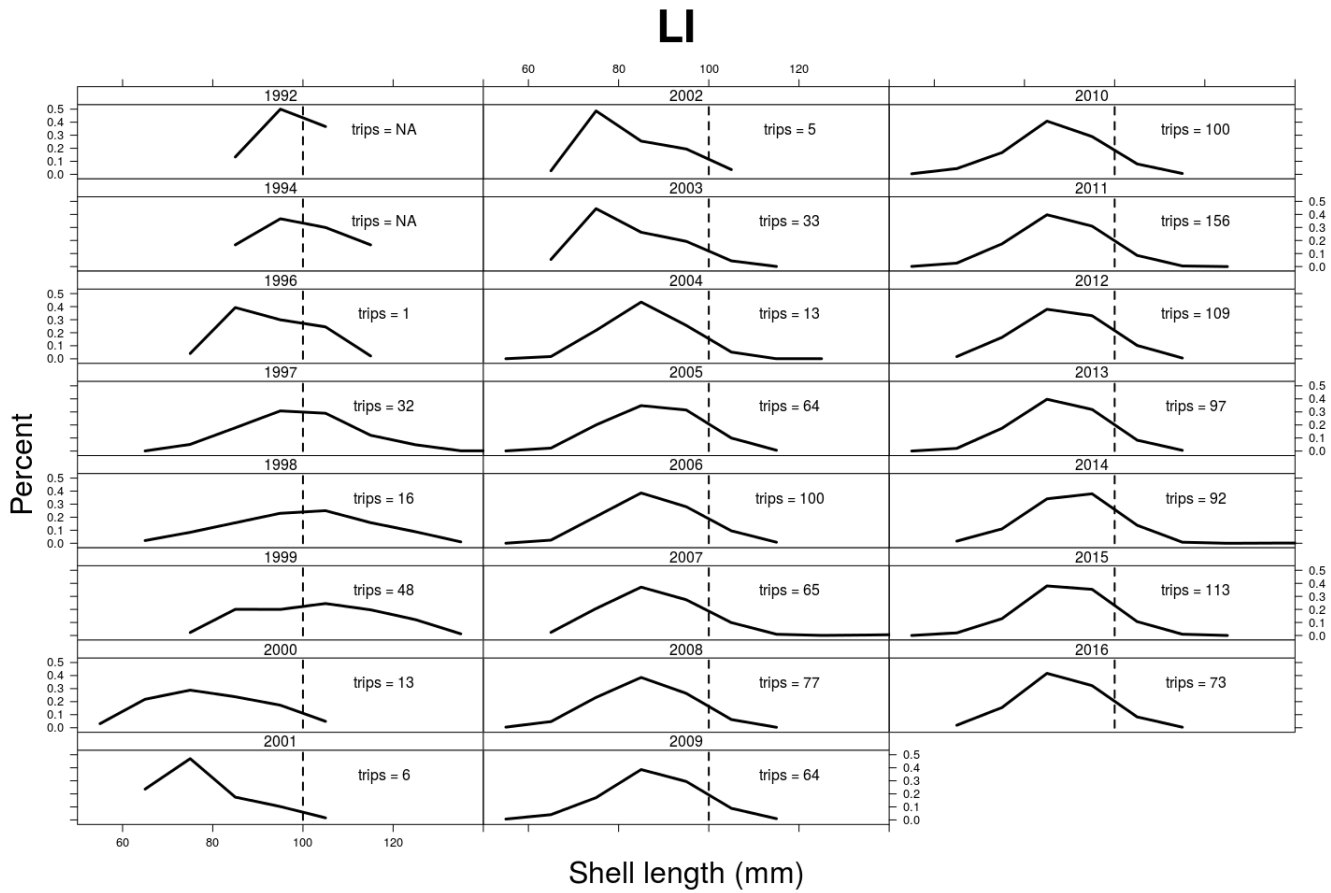

Figure 24: Length compositions of port-sampled landed ocean quahogs from the LI region. Sample sizes are the number of trips sampled in each year. Number of trips sampled before 1996 are unknown.

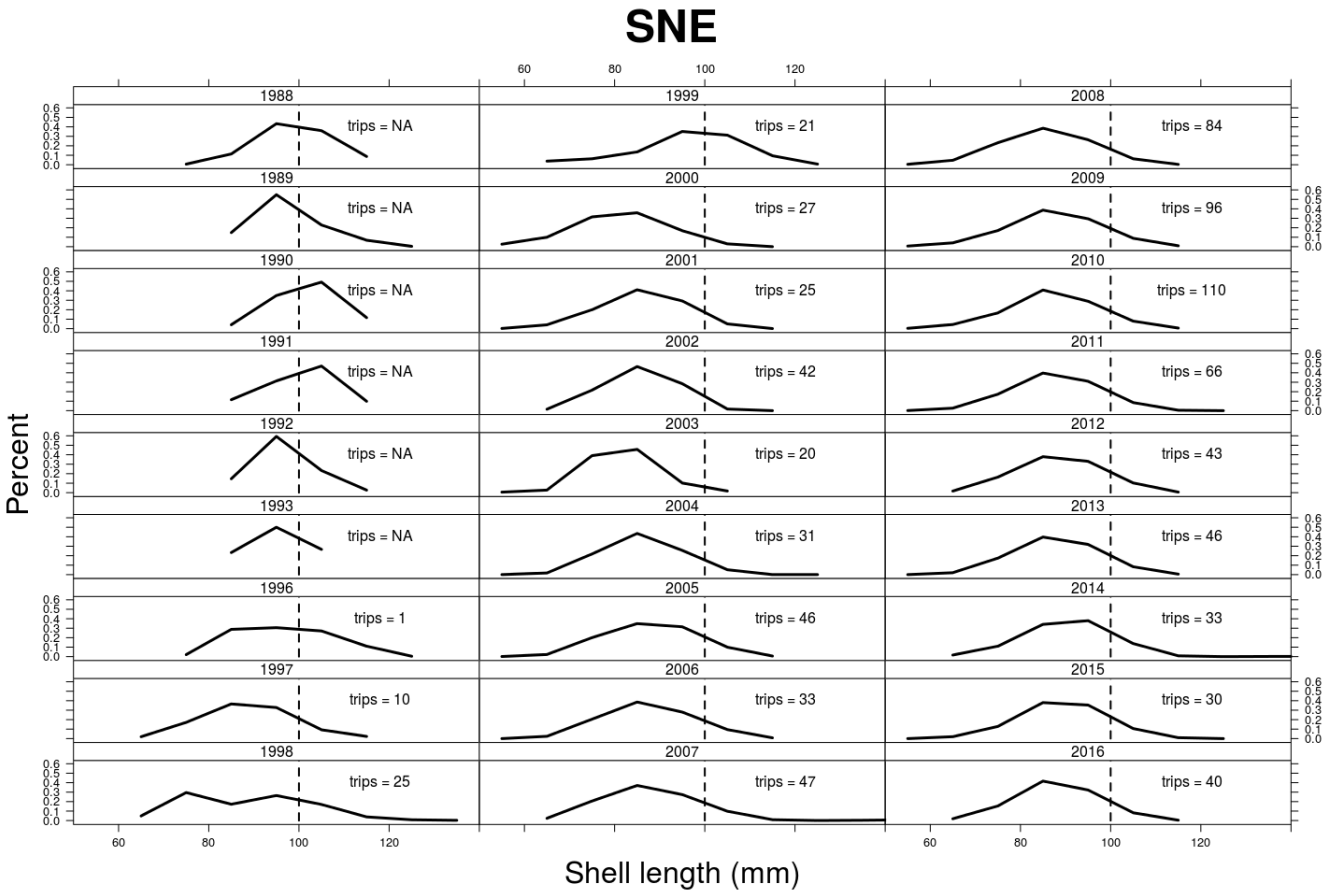

Figure 25: Length compositions of port-sampled landed ocean quahogs from the SNE region. Sample sizes are the number of trips sampled in each year. Number of trips sampled before 1996 are unknown.

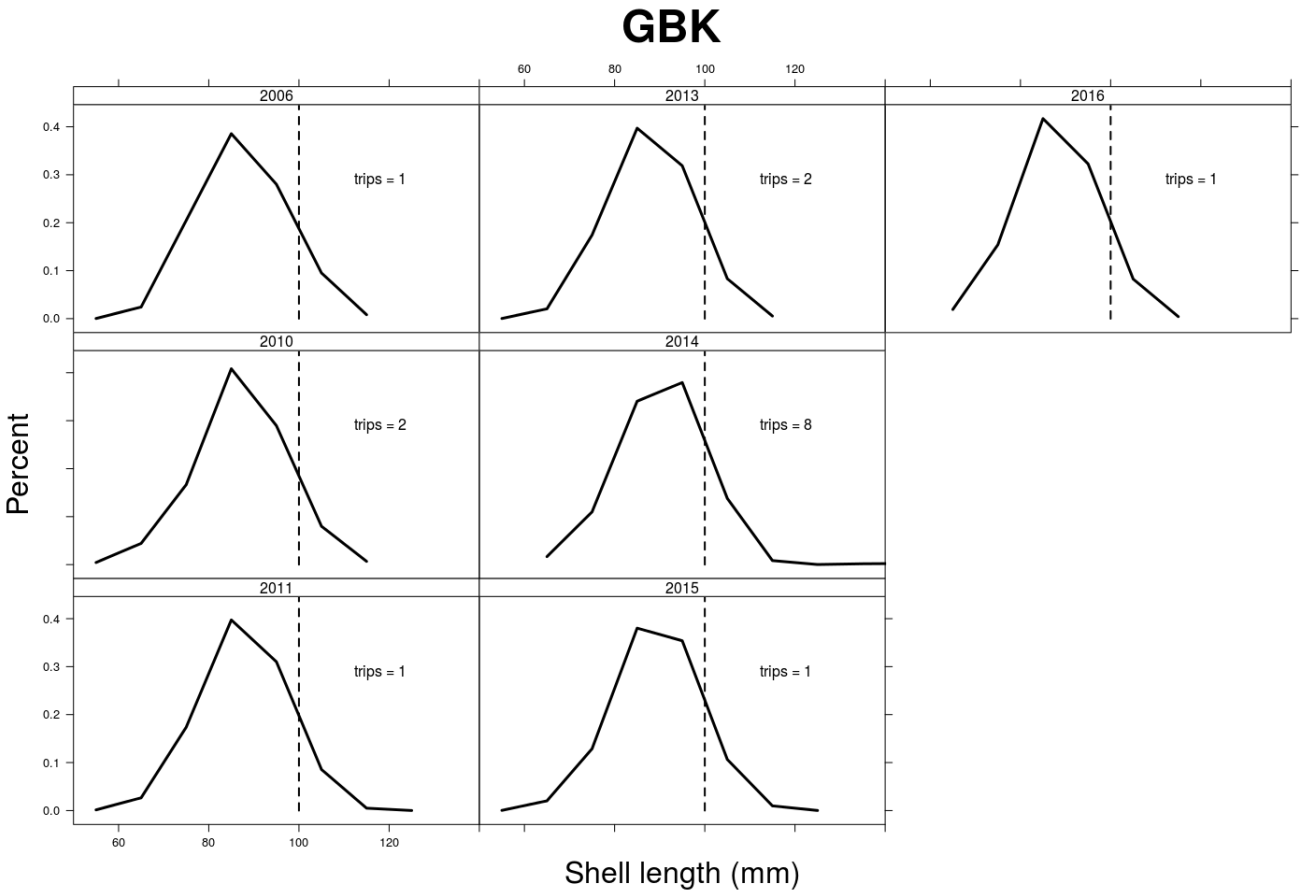

Figure 26: Length compositions of port-sampled landed ocean quahogs from the GBK region. Sample sizes are the number of trips sampled in each year. Number of trips sampled before 1996 are unknown.

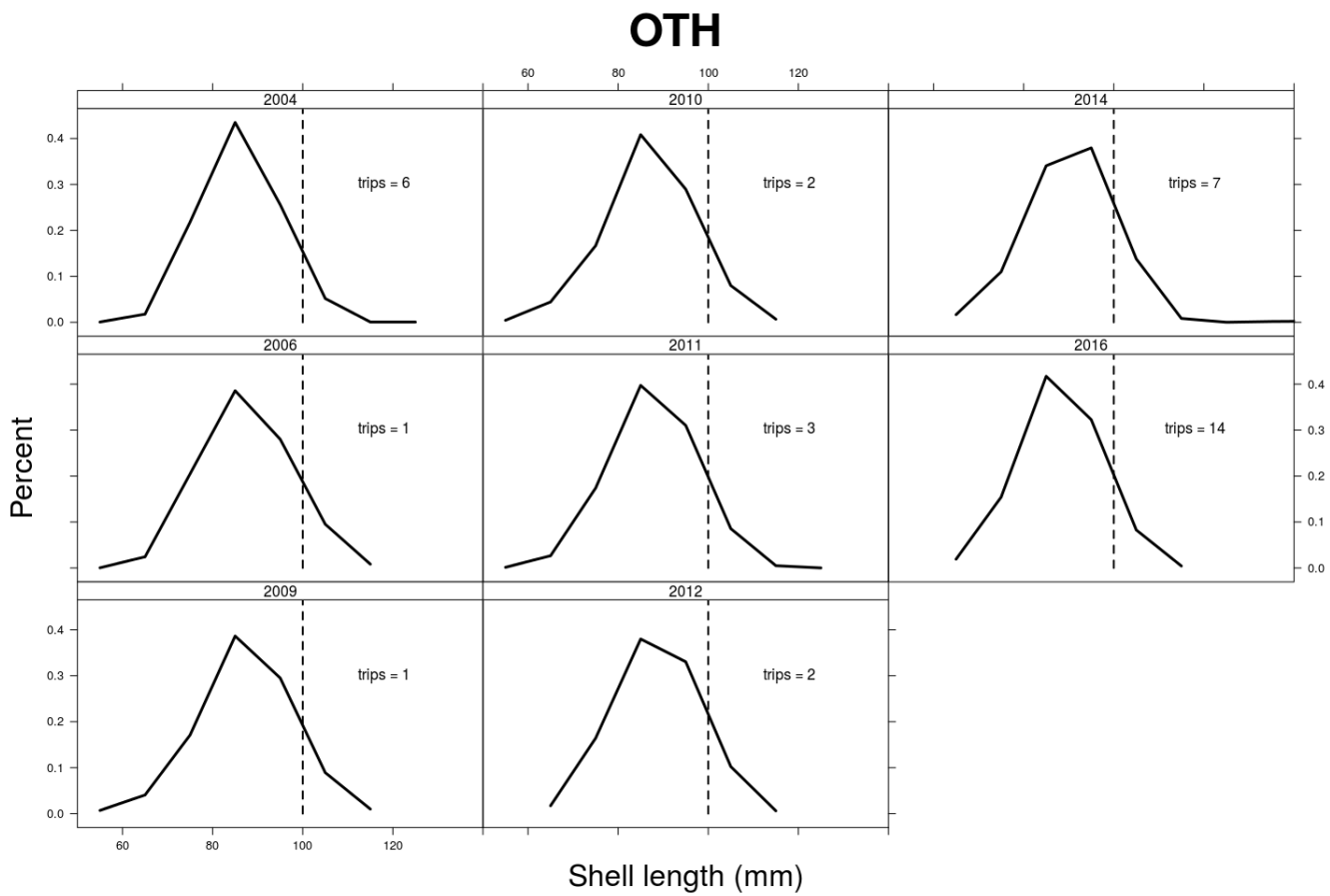

Figure 27: Length compositions of port-sampled landed ocean quahogs for which no area was recorded. Sample sizes are the number of trips sampled in each year. Number of trips sampled before 1996 are unknown.

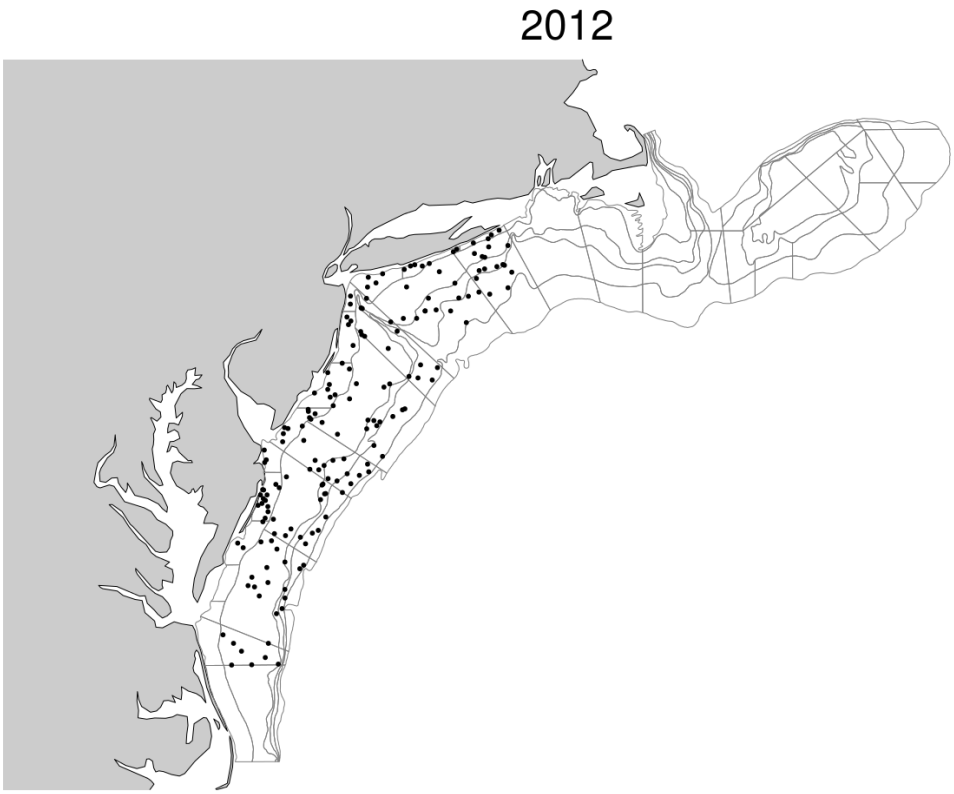

Figure 28: Station locations from the 2012 survey.

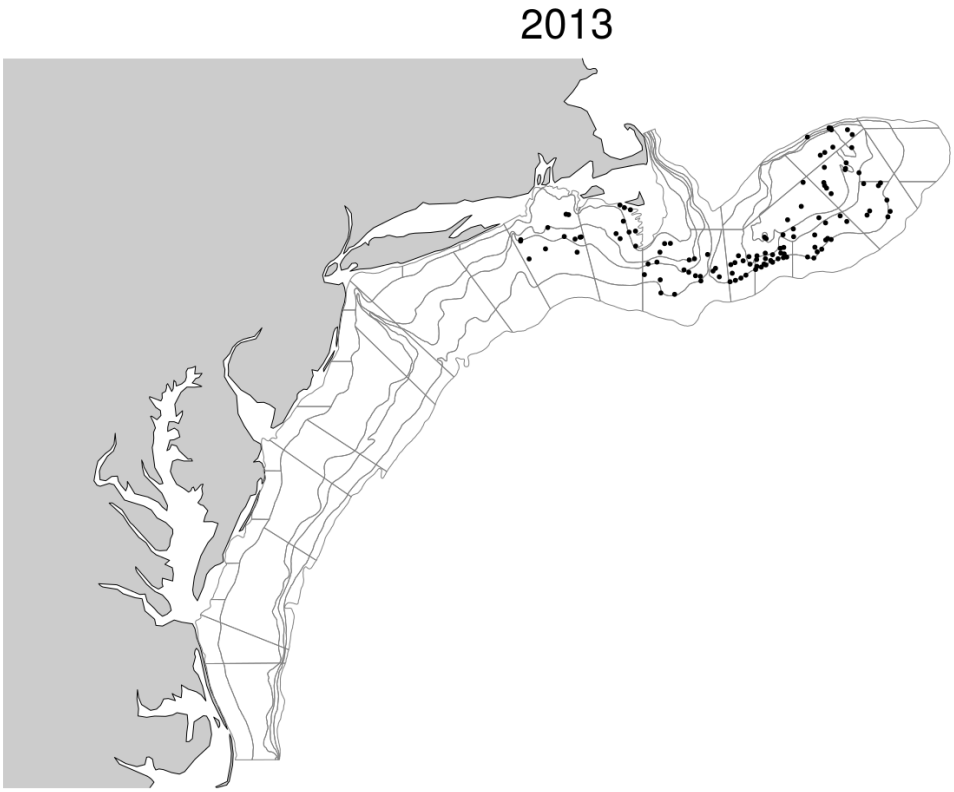

Figure 29: Station locations from the 2013 survey.

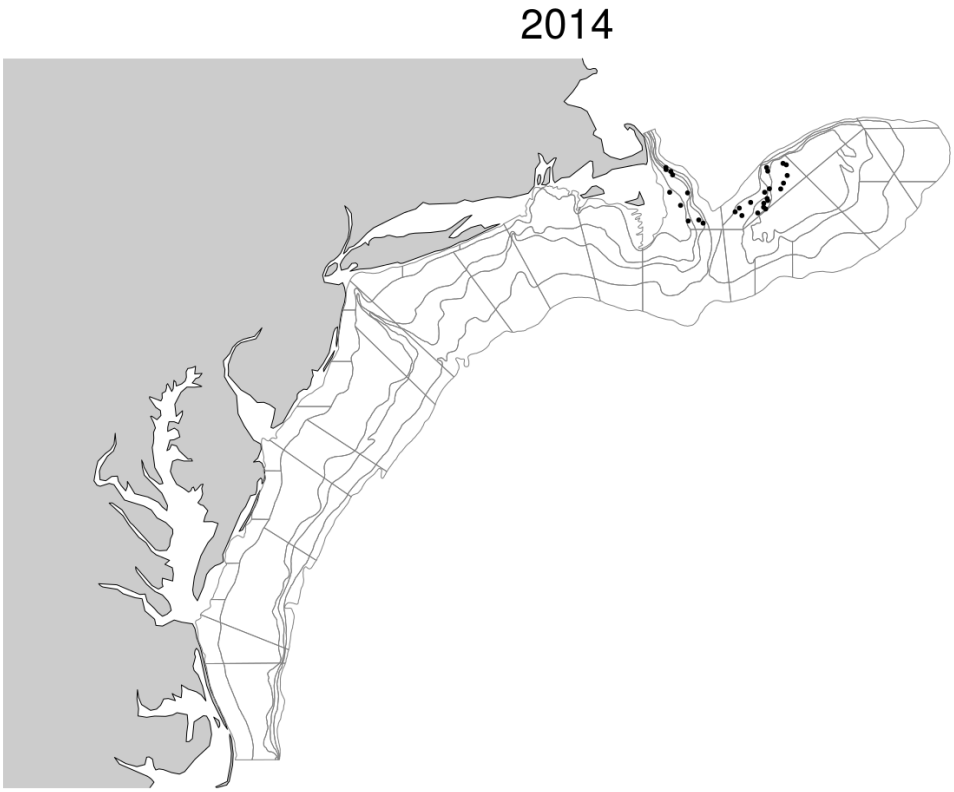

Figure 30: Station locations from the 2014 survey.

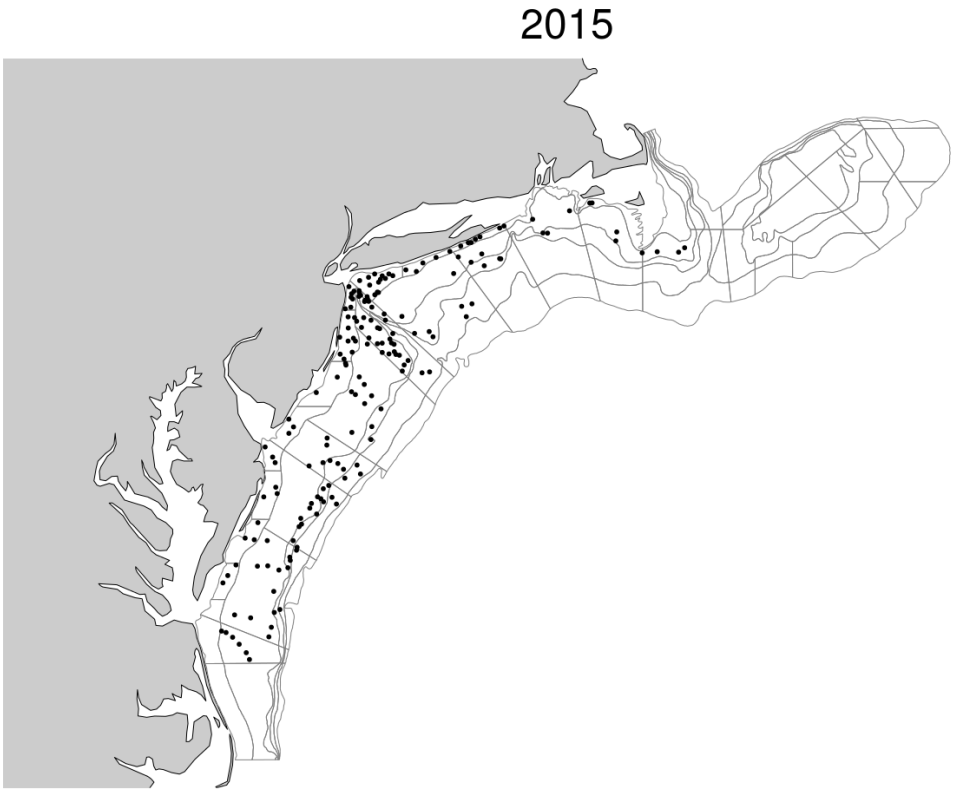

Figure 31: Station locations from the 2015 survey.

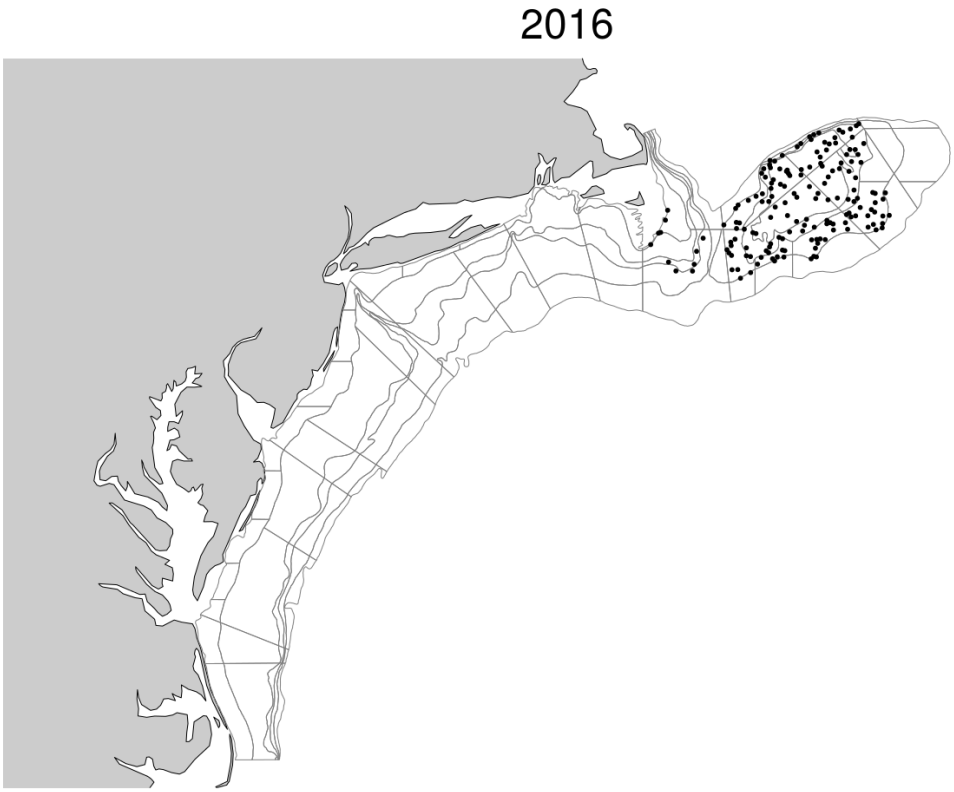

Figure 32: Station locations from the 2016 survey.

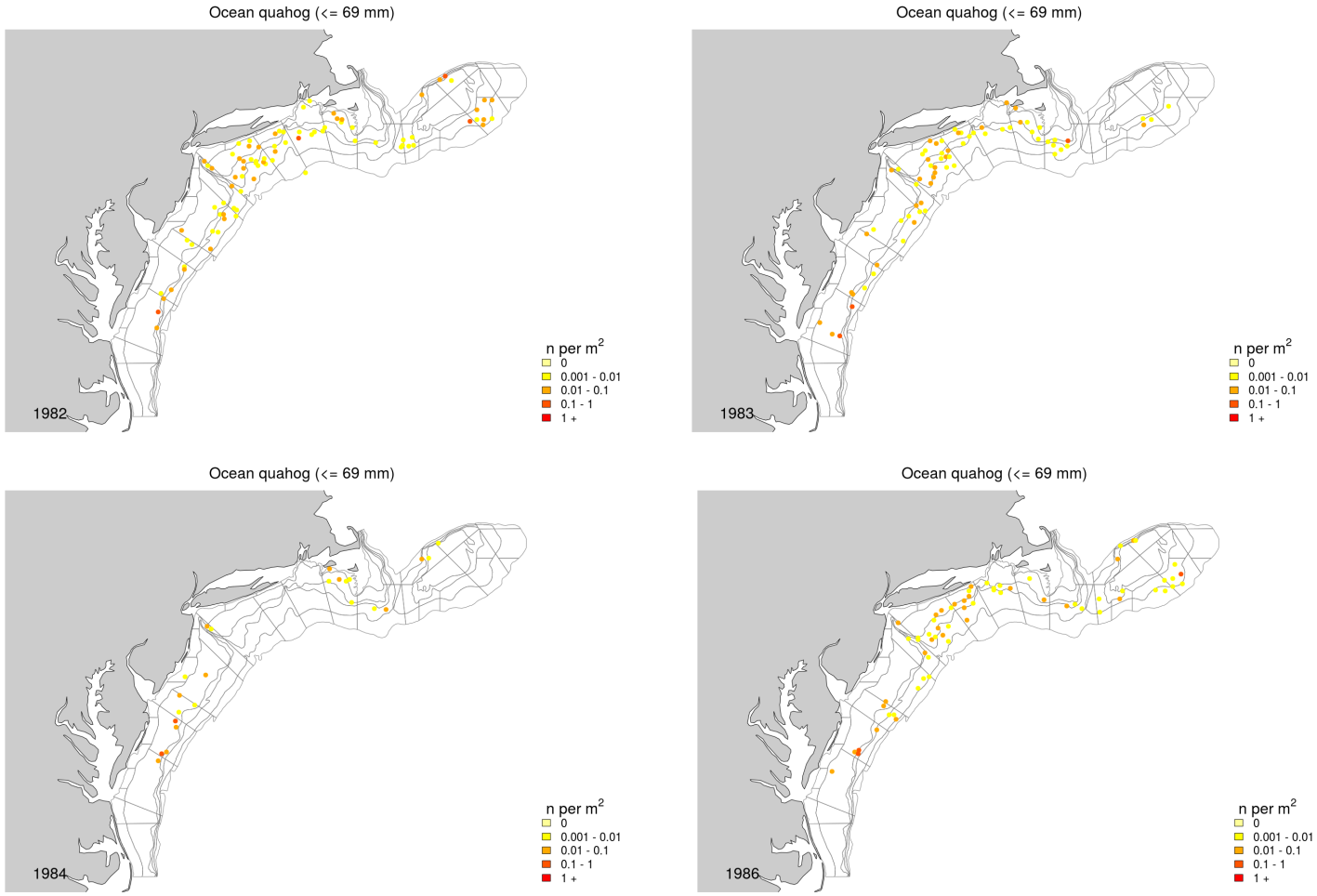

Figure 33: Survey stations where small ($<= 69\ mm$) ocean quahog were caught, by year.

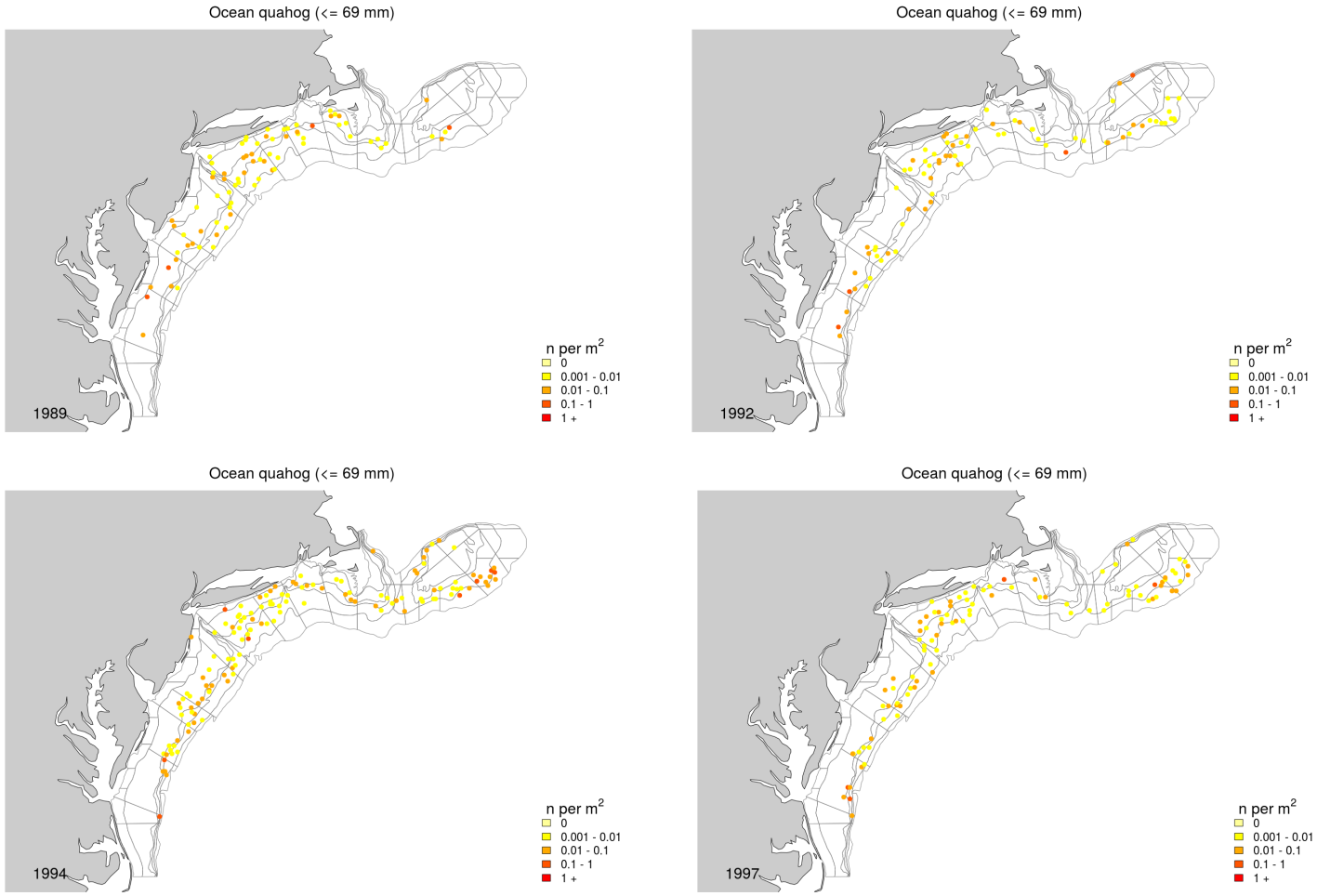

Figure 33 cont.

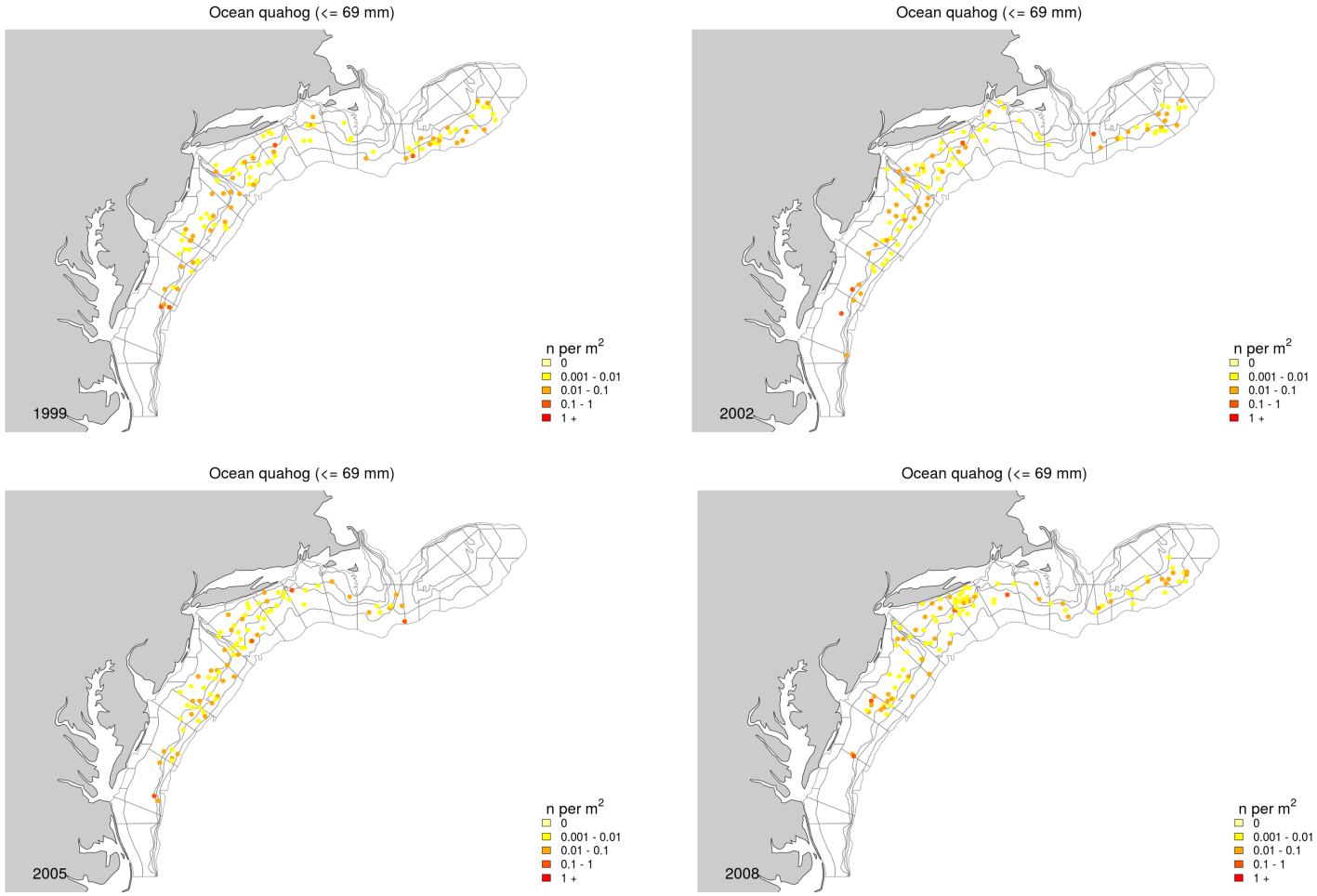

Figure 33 cont.

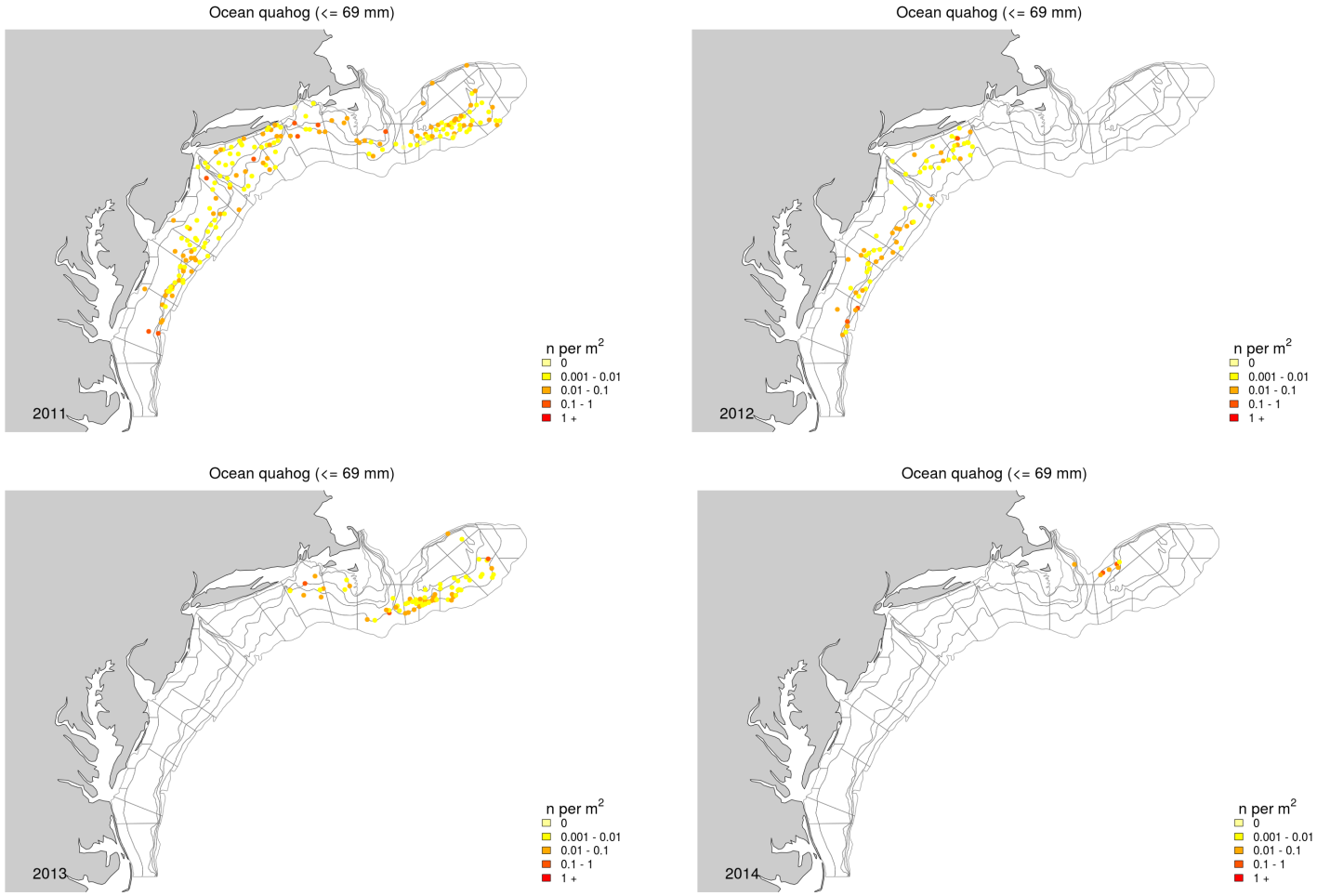

Figure 33 cont.

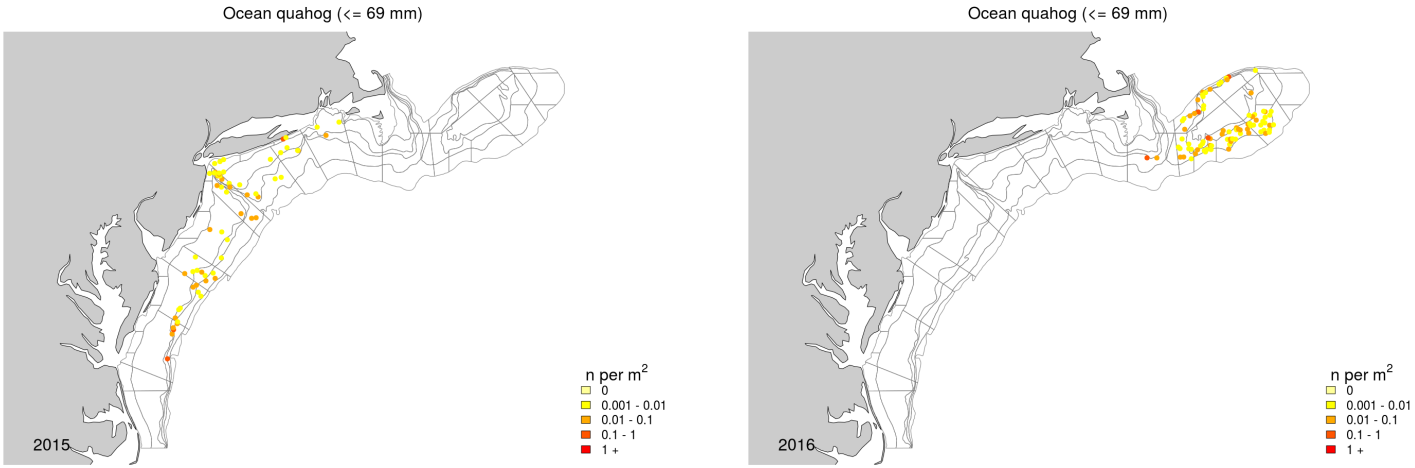

Figure 33 cont.

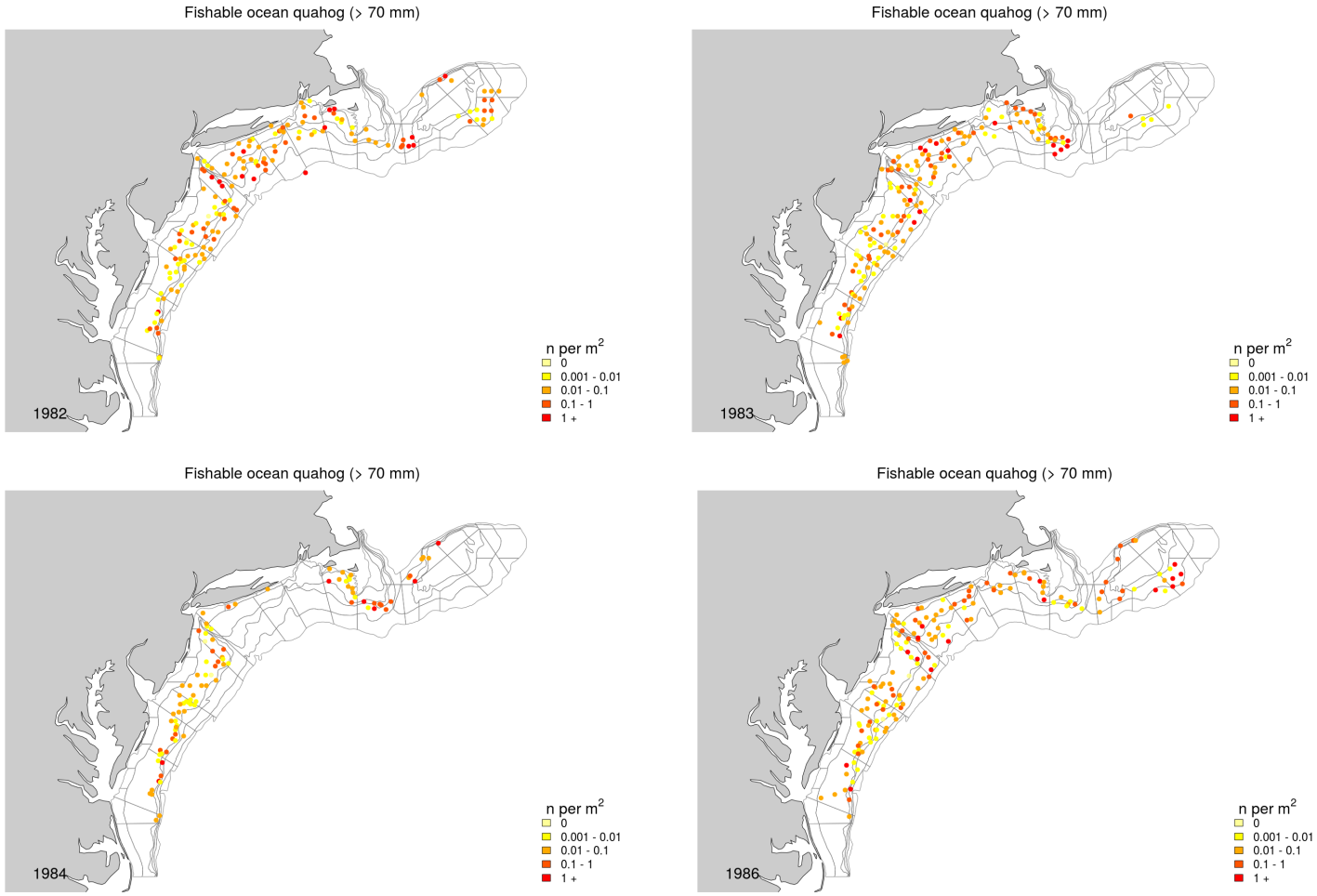

Figure 34: Survey stations where large ($>= 70\ mm$) ocean quahog were caught, by year.

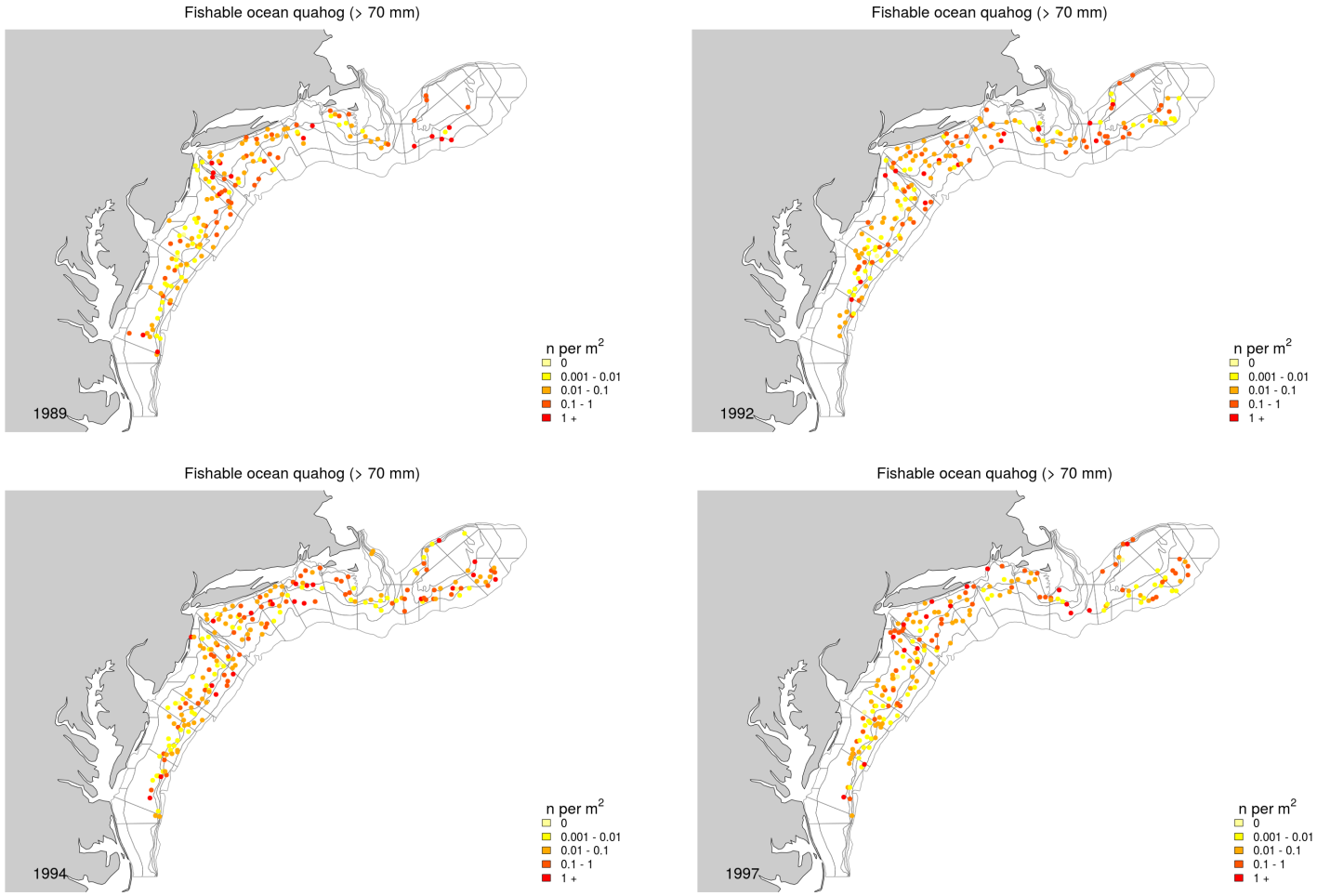

Figure 34 cont.

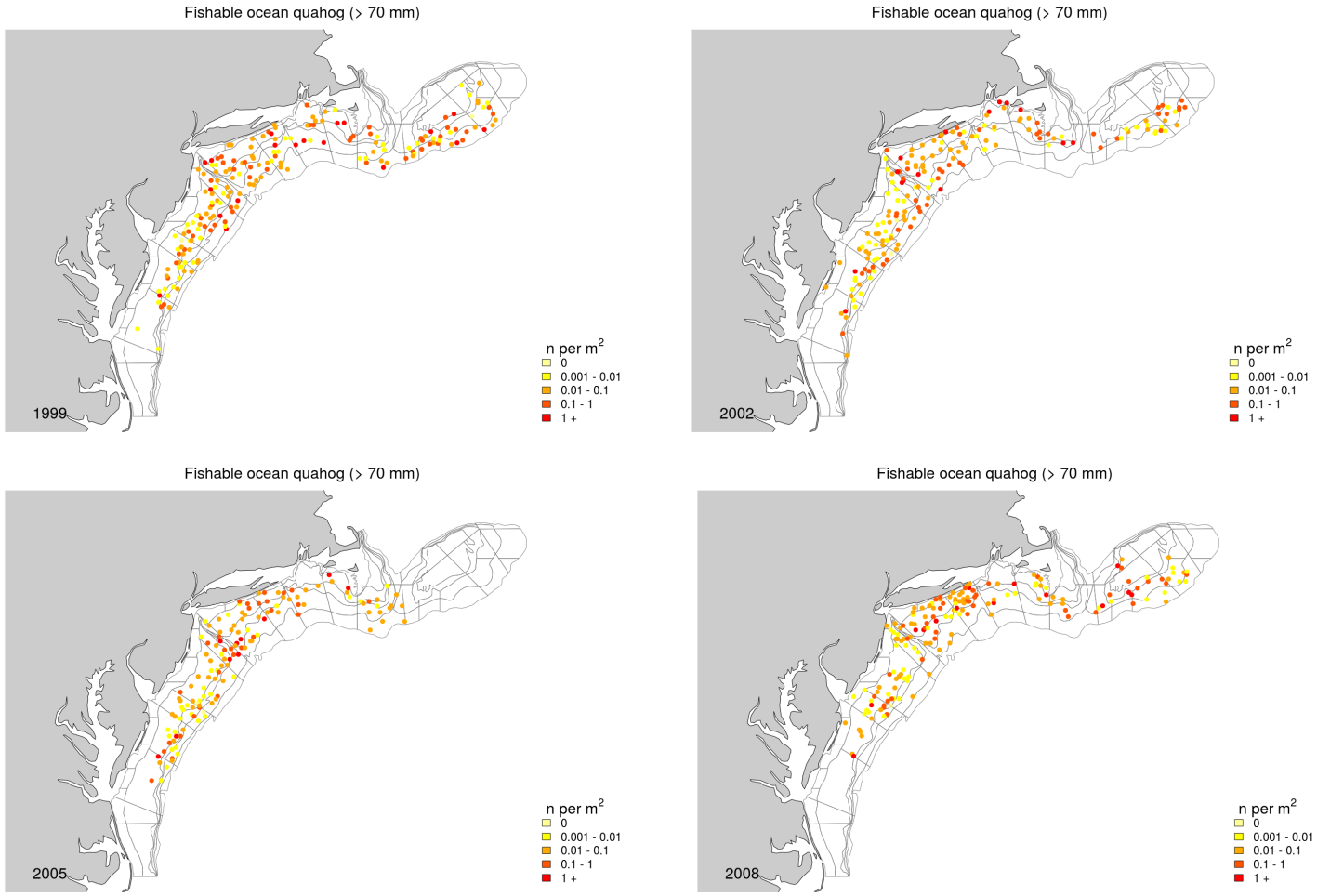

Figure 34 cont.

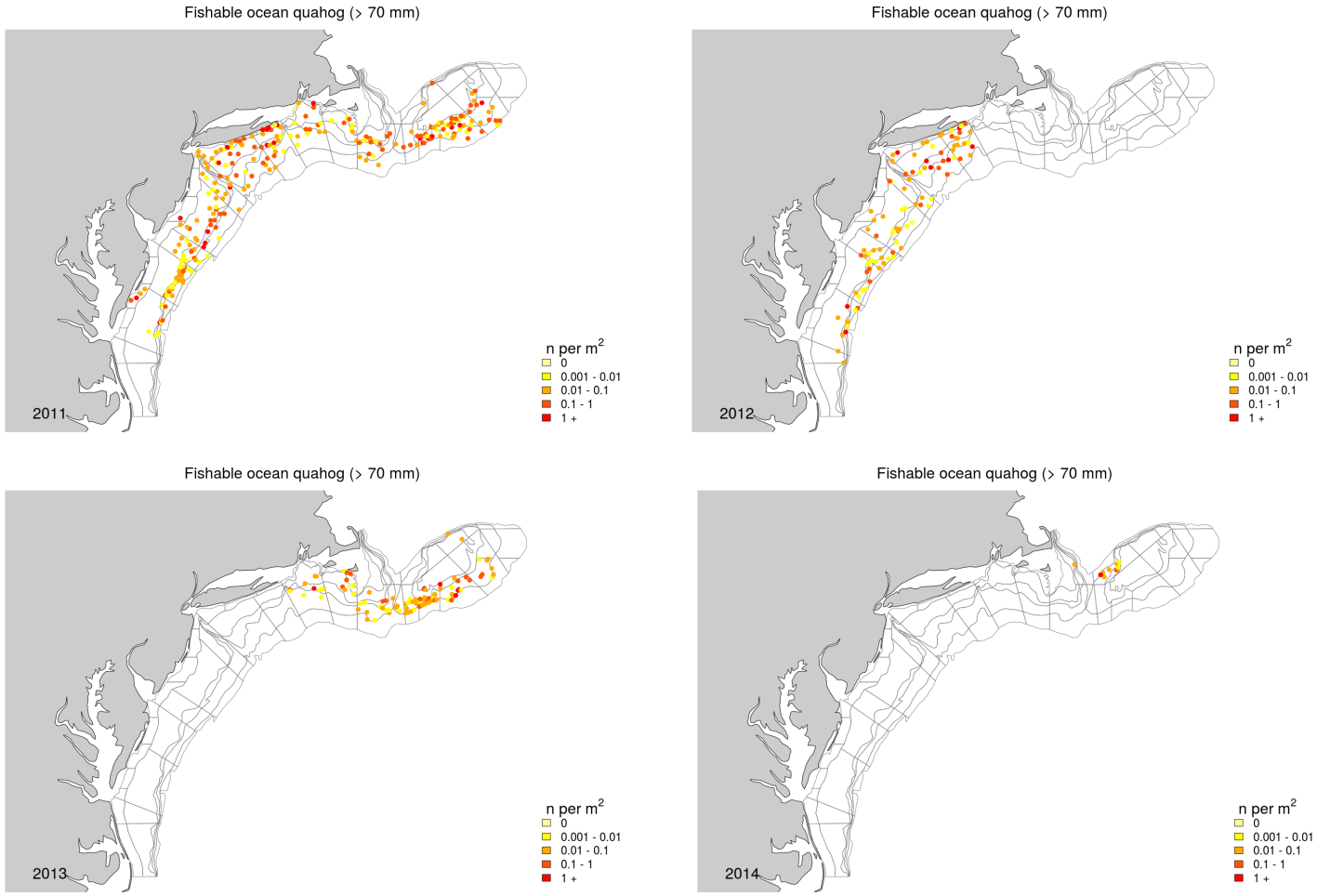

Figure 34 cont.

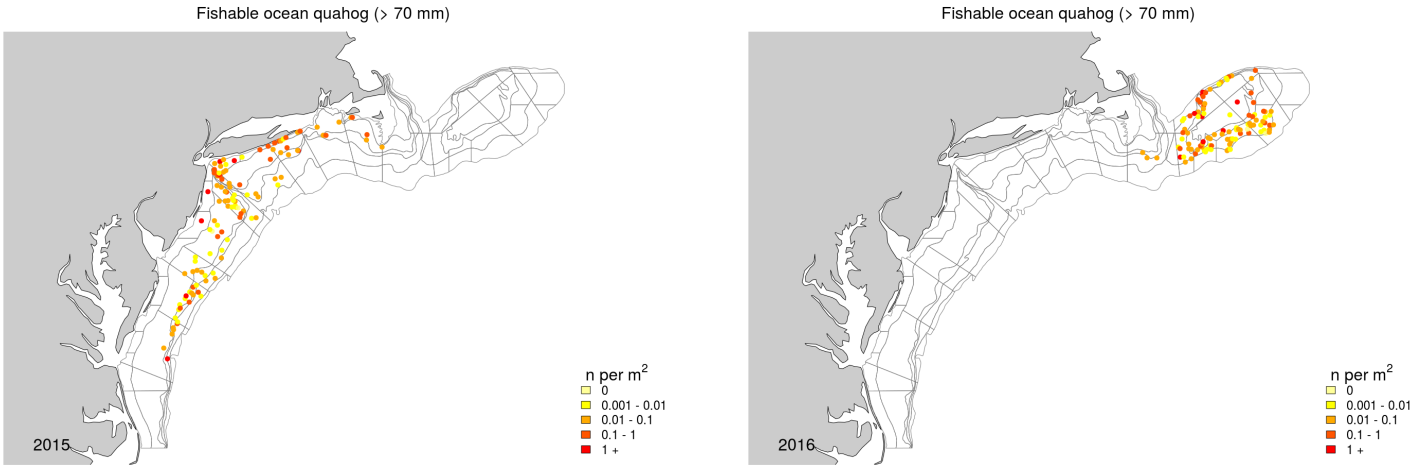

Figure 34 cont.

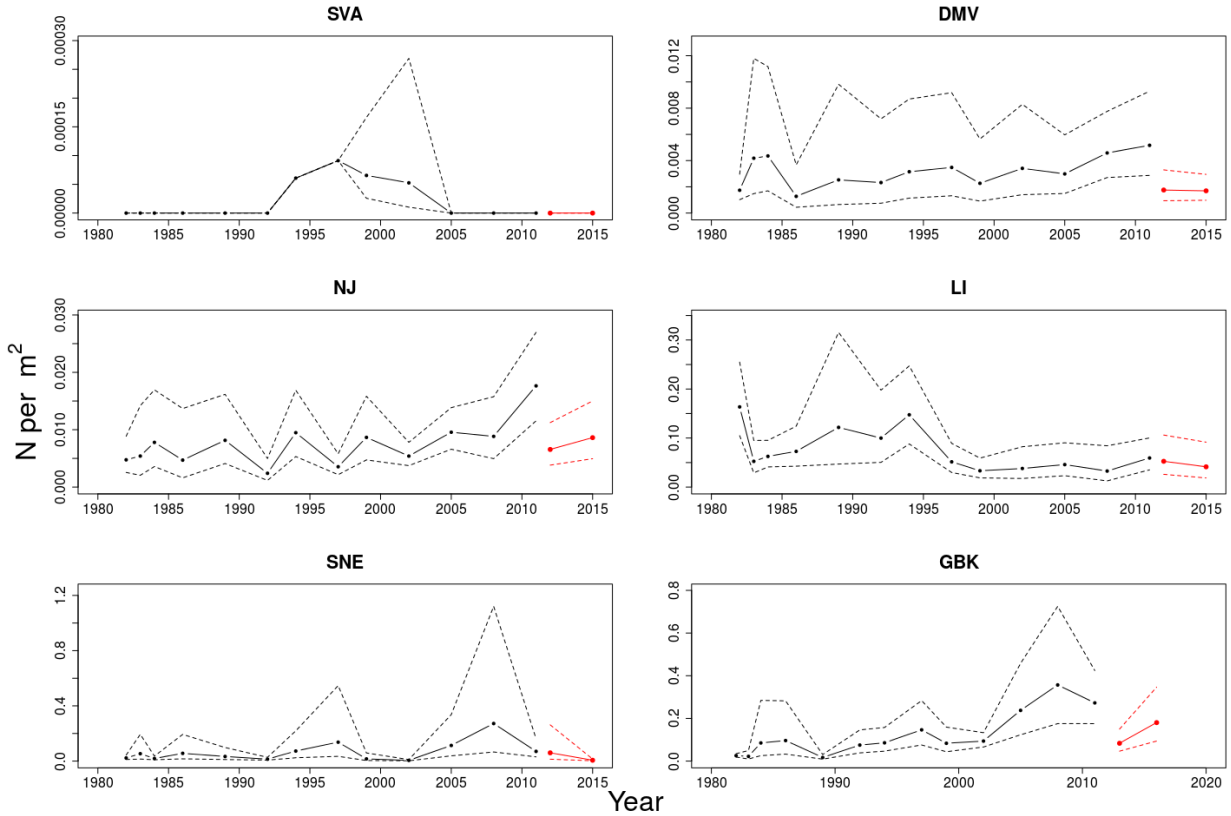

Figure 35: Trends in small ocean quahog abundance < 70 mm SL from NEFSC surveys adjusted for selectivity, but not efficiency changes in 2012, with approximate 95% asymmetric confidence intervals. Beginning in 2012, the survey was conducted from a commercial platform using a dredge with higher capture efficiency. Results from the new survey platform are shown as a separate series in red. GBK and SNE were not sampled in 2012 and SVA, DMV, NJ and LI were not sampled in 2013 or 2014.

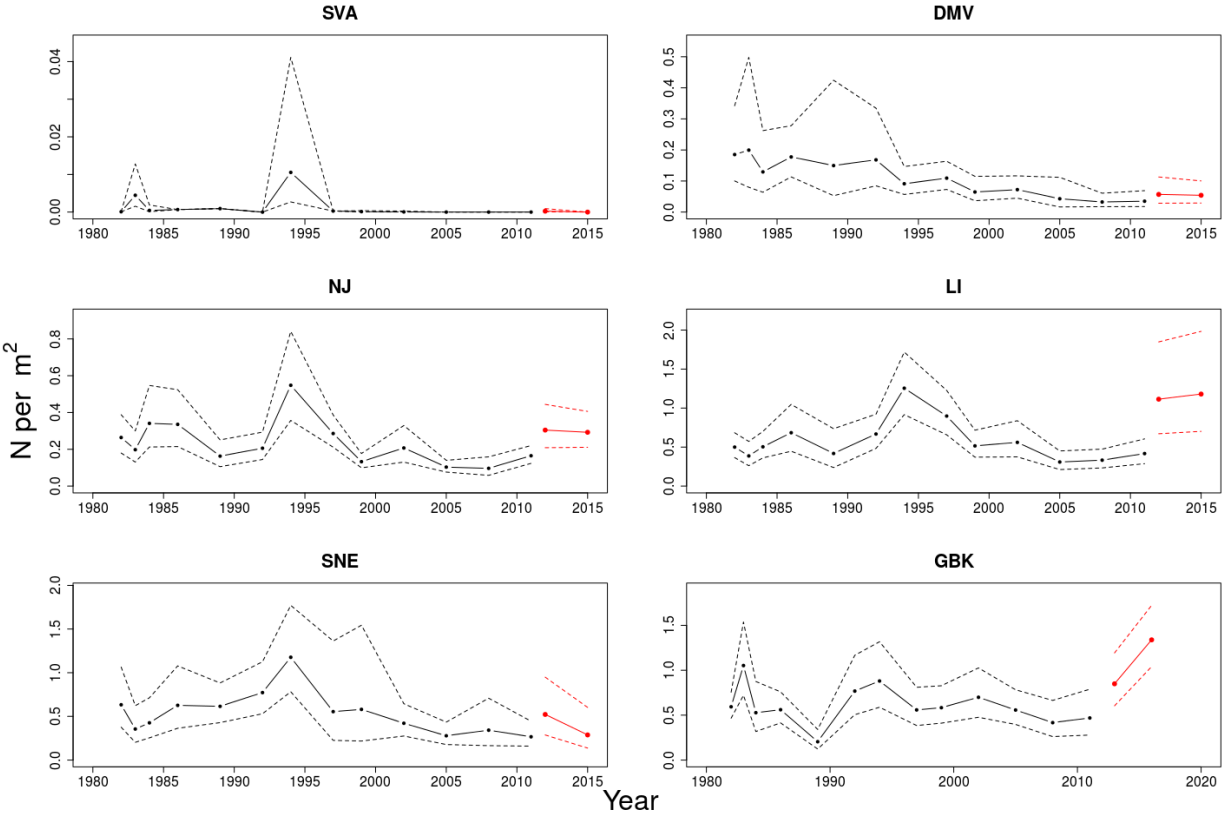

Figure 36: Trends in large ocean quahog abundance > 69 mm SL from NEFSC surveys adjusted for selectivity, but not efficiency changes in 2012, with approximate 95% asymmetric confidence intervals. Beginning in 2012, the survey was conducted from a commercial platform using a dredge with higher capture efficiency. Results from the new survey platform are shown as a separate series in red. GBK and SNE were not sampled in 2012 and SVA, DMV, NJ and LI were not sampled in 2013 or 2014.

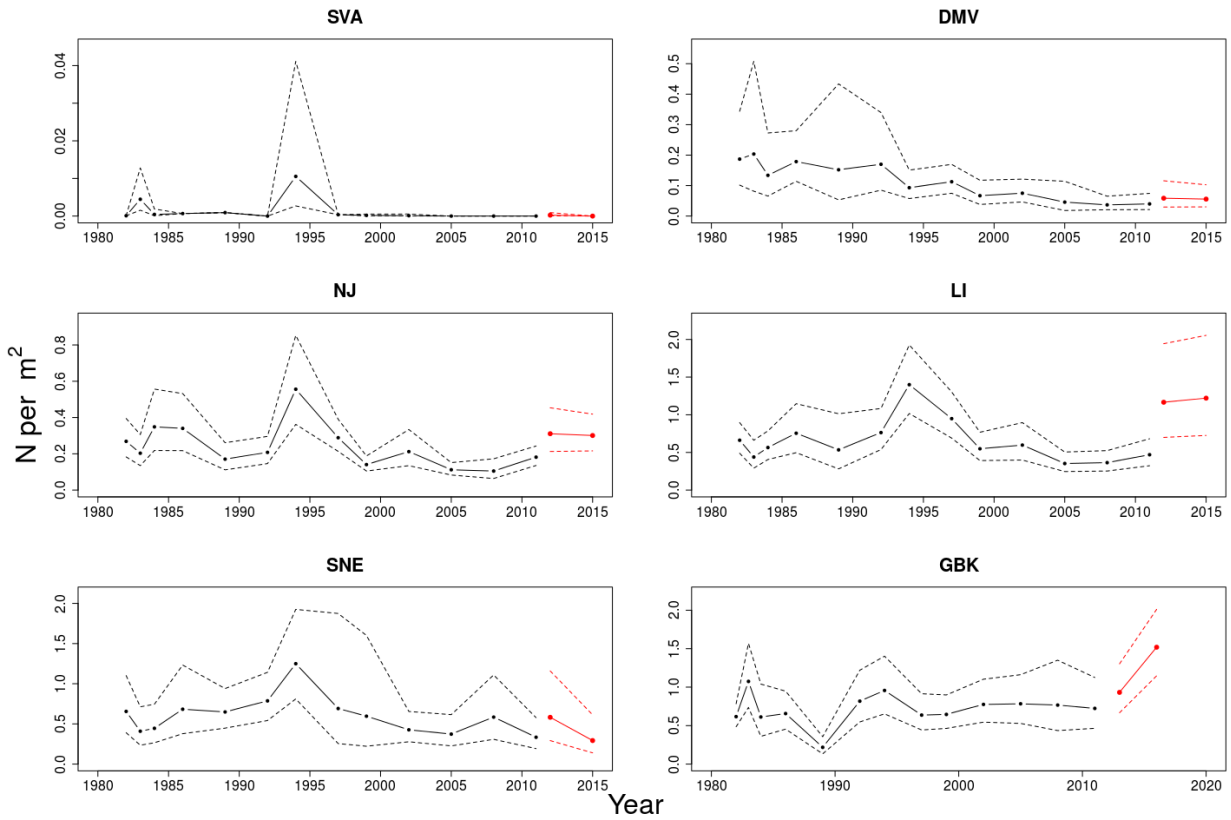

Figure 37: Trends in total ocean quahog abundance > 50 mm SL from NEFSC surveys adjusted for selectivity, but not efficiency changes in 2012, with approximate 95% asymmetric confidence intervals. Beginning in 2012, the survey was conducted from a commercial platform using a dredge with higher capture efficiency. Results from the new survey platform are shown as a separate series in red. GBK and SNE were not sampled in 2012 and SVA, DMV, NJ and LI were not sampled in 2013 or 2014.

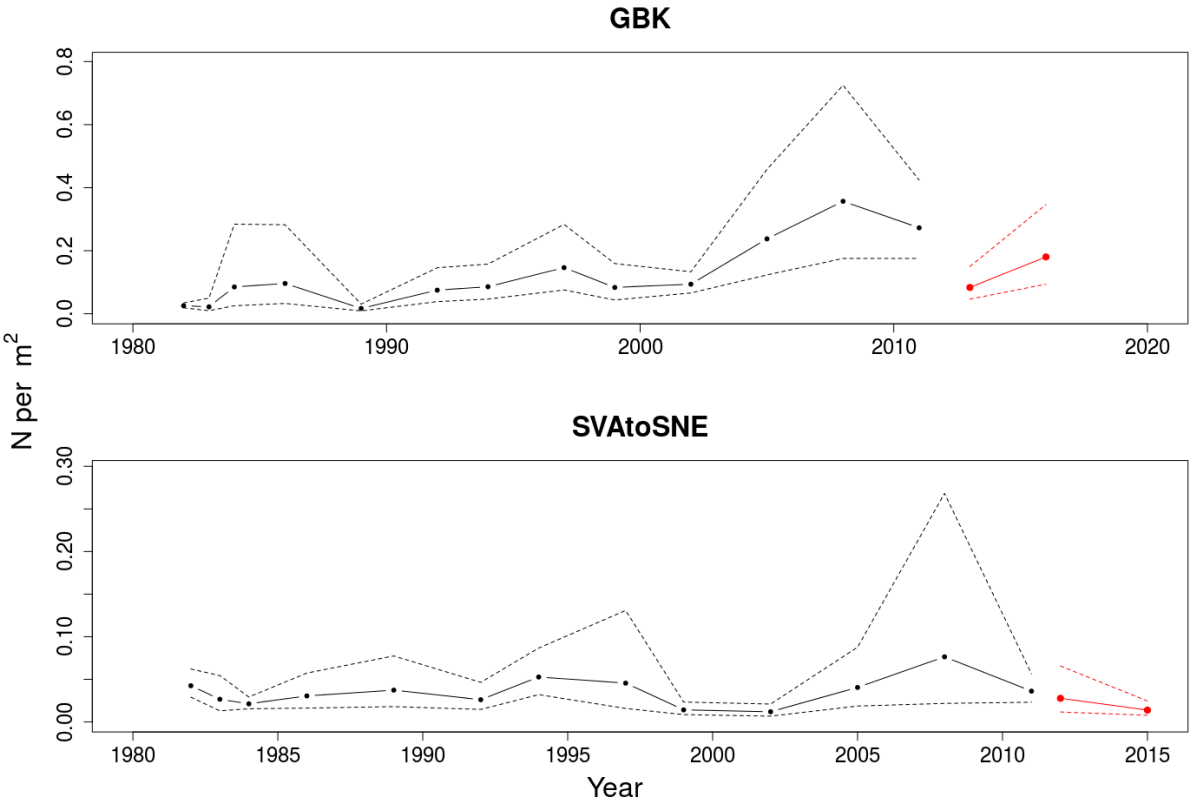

Figure 38: Trends in small ocean quahog abundance < 70 mm SL from NEFSC surveys adjusted for selectivity, but not efficiency changes in 2012, with approximate 95% asymmetric confidence intervals. Beginning in 2012, the survey was conducted from a commercial platform using a dredge with higher capture efficiency. Results from the new survey platform are shown as a separate series in red. GBK and SNE were not sampled in 2012 and SVA, DMV, NJ and LI were not sampled in 2013 or 2014.

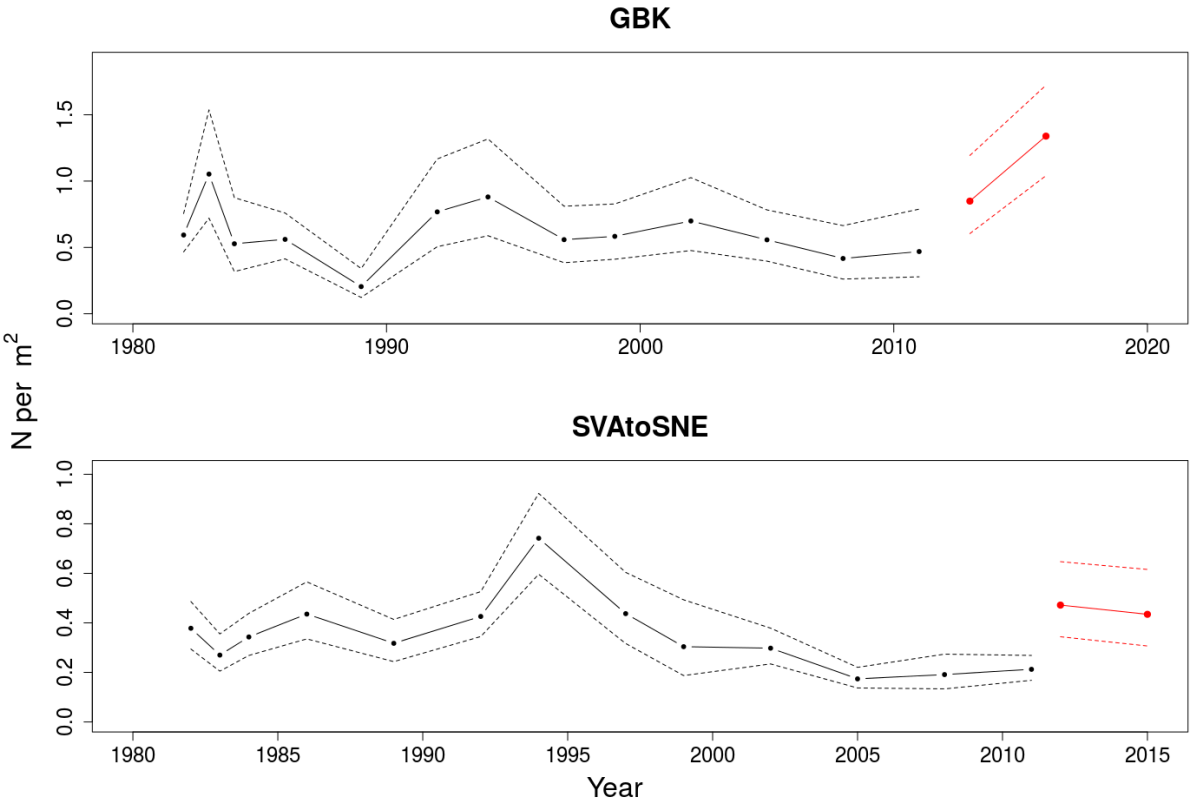

Figure 39: Trends in large Ocean quahog abundance > 69 mm SL from NEFSC surveys adjusted for selectivity, but not efficiency changes in 2012, with approximate 95% asymmetric confidence intervals. Beginning in 2012, the survey was conducted from a commercial platform using a dredge with higher capture efficiency. Results from the new survey platform are shown as a separate series in red. GBK and SNE were not sampled in 2012 and SVA, DMV, NJ and LI were not sampled in 2013 or 2014.

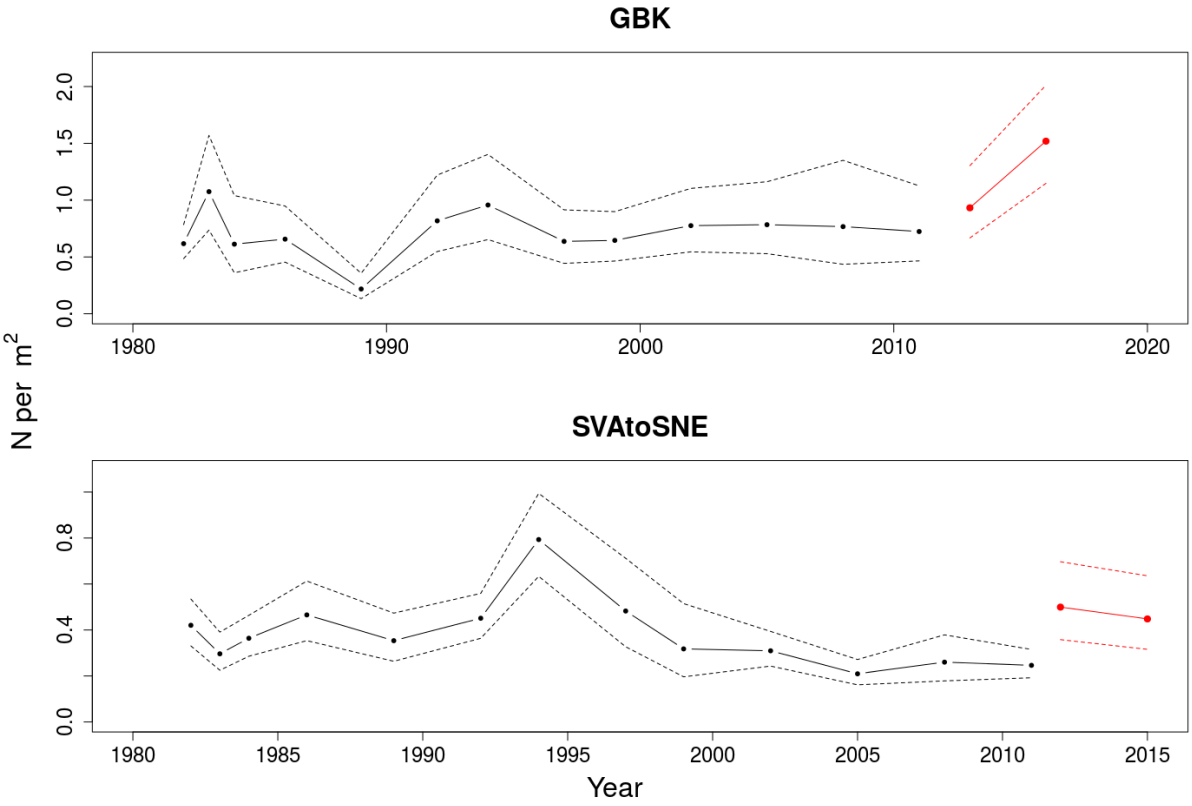

Figure 40: Trends in total Ocean quahog abundance > 50 mm SL from NEFSC surveys adjusted for selectivity, but not efficiency changes in 2012, with approximate 95% asymmetric confidence intervals. Beginning in 2012, the survey was conducted from a commercial platform using a dredge with higher capture efficiency. Results from the new survey platform are shown as a separate series in red. GBK and SNE were not sampled in 2012 and SVA, DMV, NJ and LI were not sampled in 2013 or 2014.

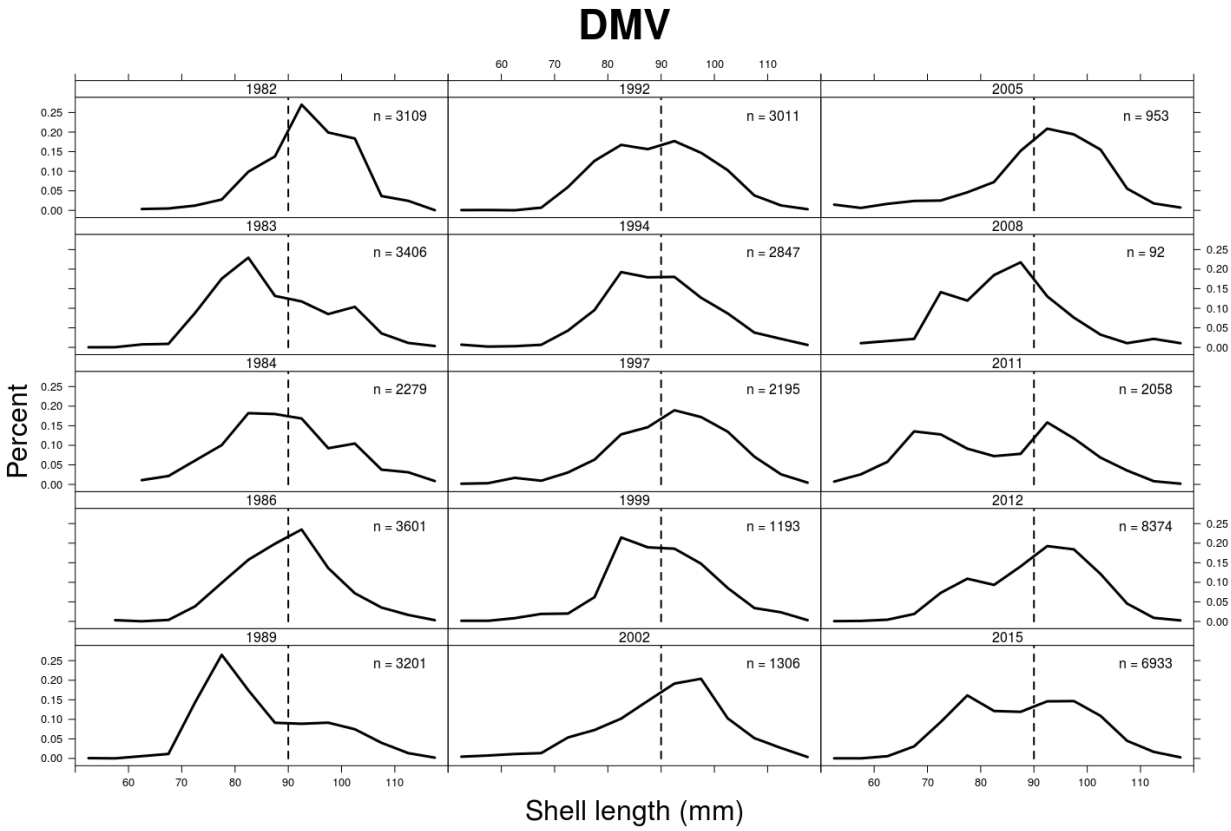

Figure 41: Length composition of NEFSC surveys in DMV. The sample sizes shown in each plot are the total number of clams caught in each survey year, not the number actually measured because a subsample of the total catch is taken when the total catch is larger than approximately 400 ocean quahog.

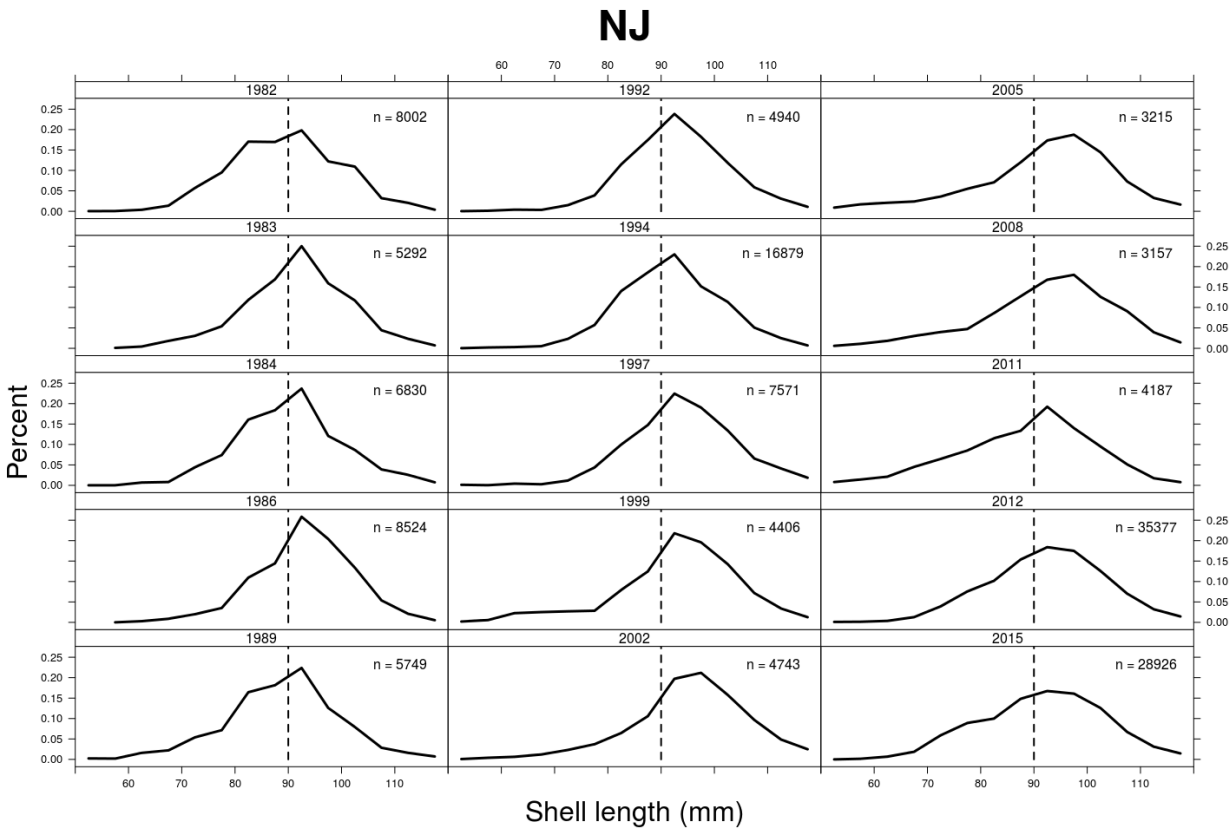

Figure 42: Length composition of NEFSC surveys in NJ. The sample sizes shown in each plot are the total number of clams caught in each survey year, not the number actually measured because a subsample of the total catch is taken when the total catch is larger than approximately 400 ocean quahog.

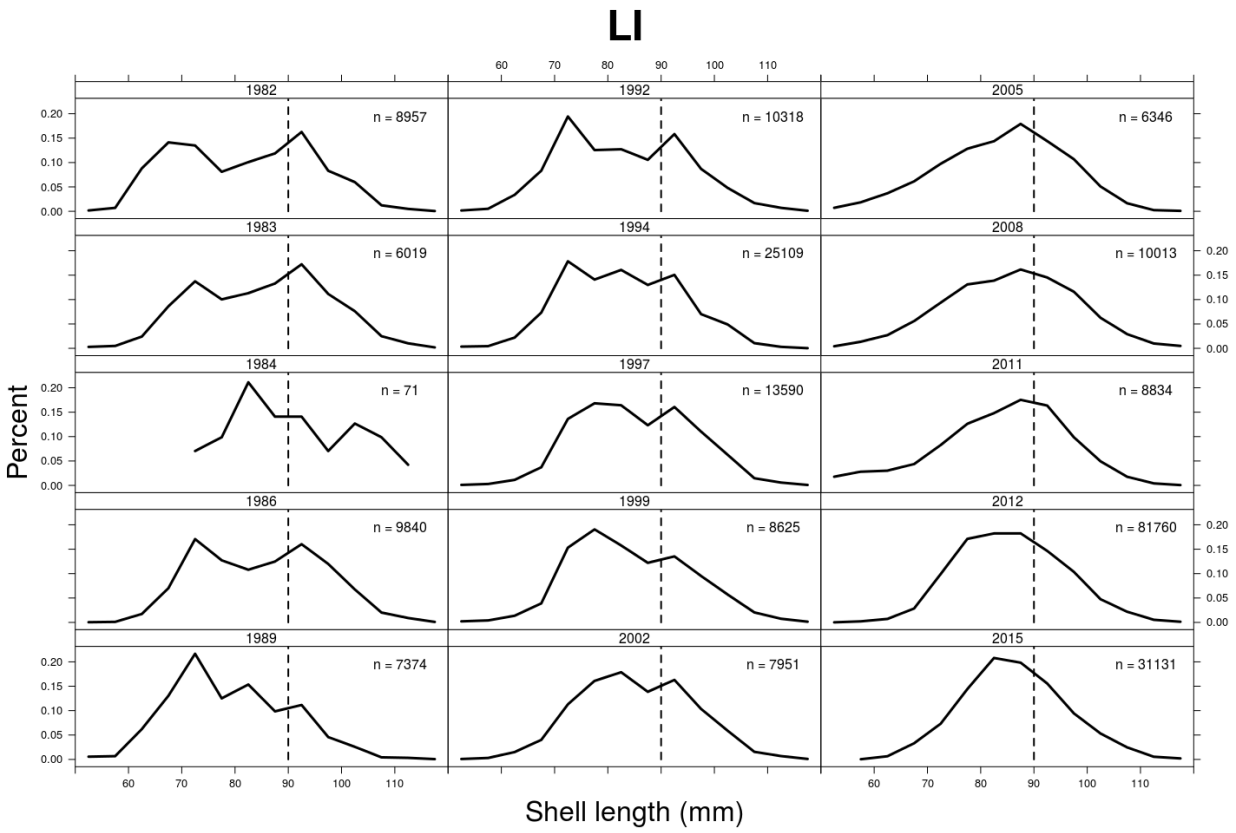

Figure 43: Length composition of NEFSC surveys in LI. The sample sizes shown in each plot are the total number of clams caught in each survey year, not the number actually measured because a subsample of the total catch is taken when the total catch is larger than approximately 400 ocean quahog.

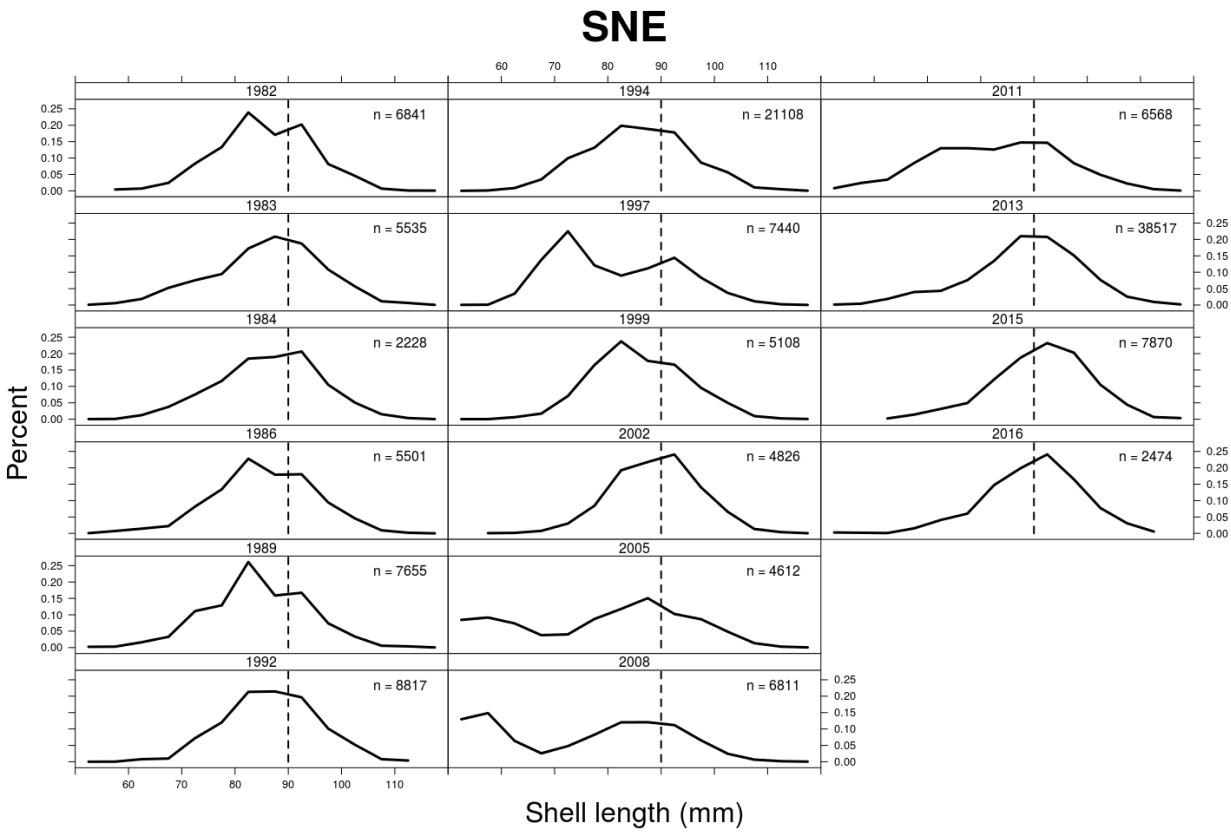

Figure 44: Length composition of NEFSC surveys in SNE. The sample sizes shown in each plot are the total number of clams caught in each survey year, not the number actually measured because a subsample of the total catch is taken when the total catch is larger than approximately 400 ocean quahog.

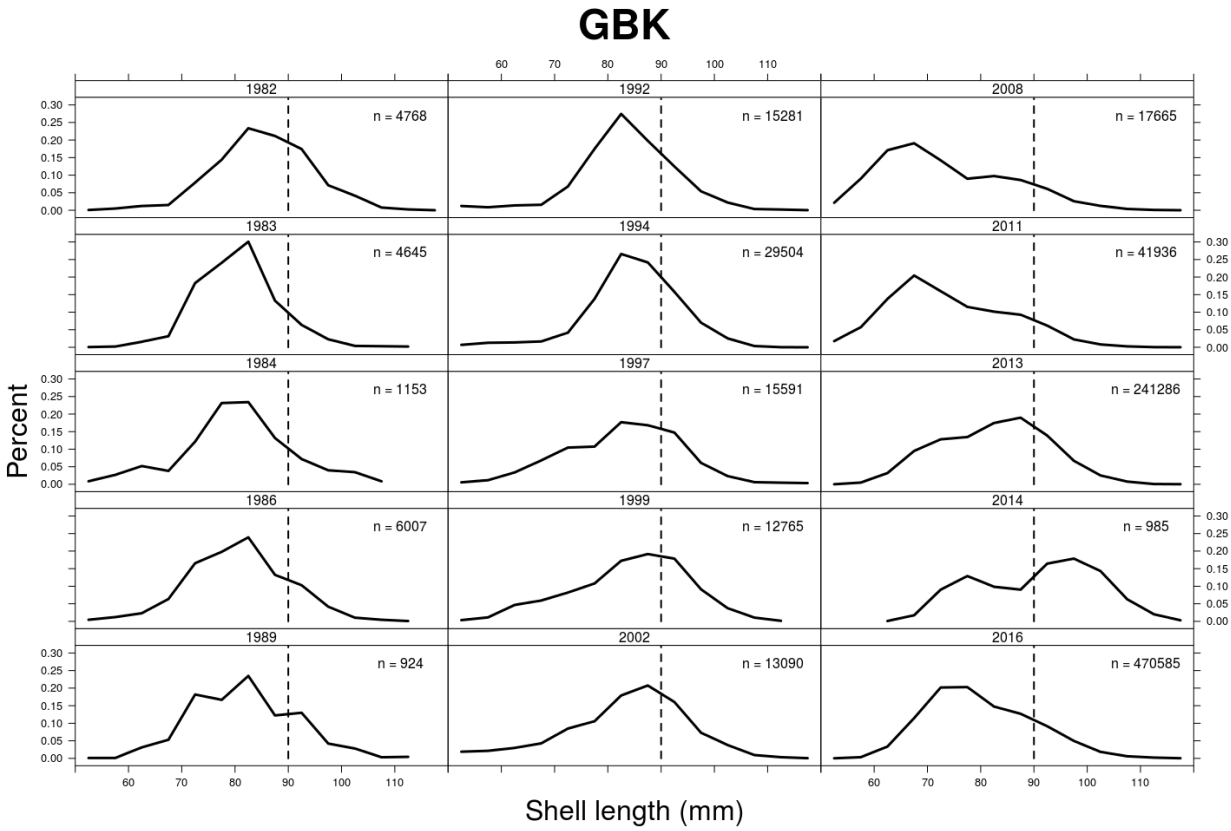

Figure 45: Length composition of NEFSC surveys in GBK. The sample sizes shown in each plot are the total number of clams caught in each survey year, not the number actually measured because a subsample of the total catch is taken when the total catch is larger than approximately 400 ocean quahog.

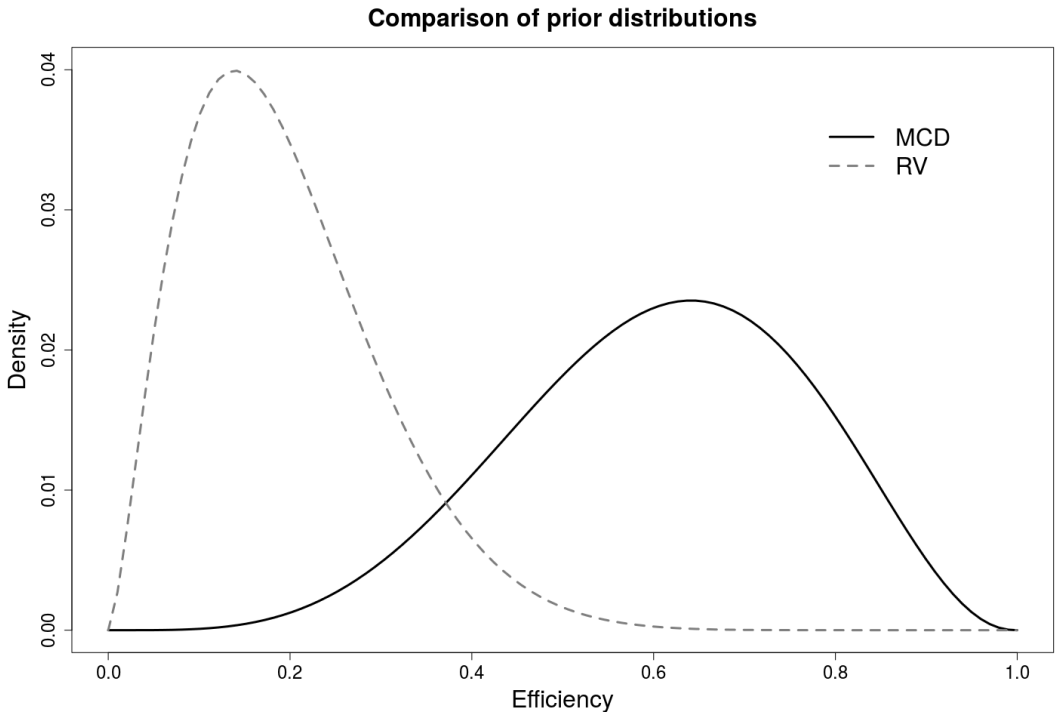

Figure 46: A comparison of the prior probability distributions for survey catchability for ocean quahog in the research dredge (RD) used prior to 2012 and the modified commercial dredge (MCD) used after 2011 based on depletion experiments. The MCD has a higher and more precisely determined estimated capture efficiency.

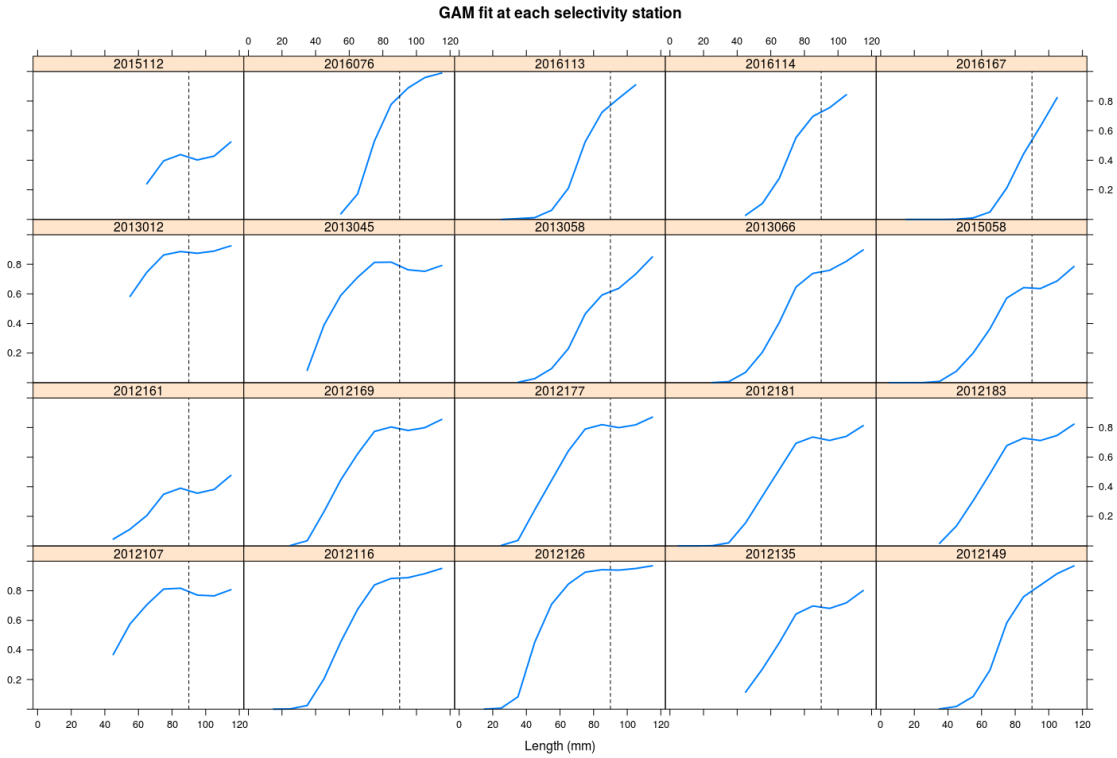

Figure 47: GAM fits to the selectivity data (modified commercial dredge compared to lined dredge) at each year and station combination. The plots generally indicate flat topped selectivity curves.

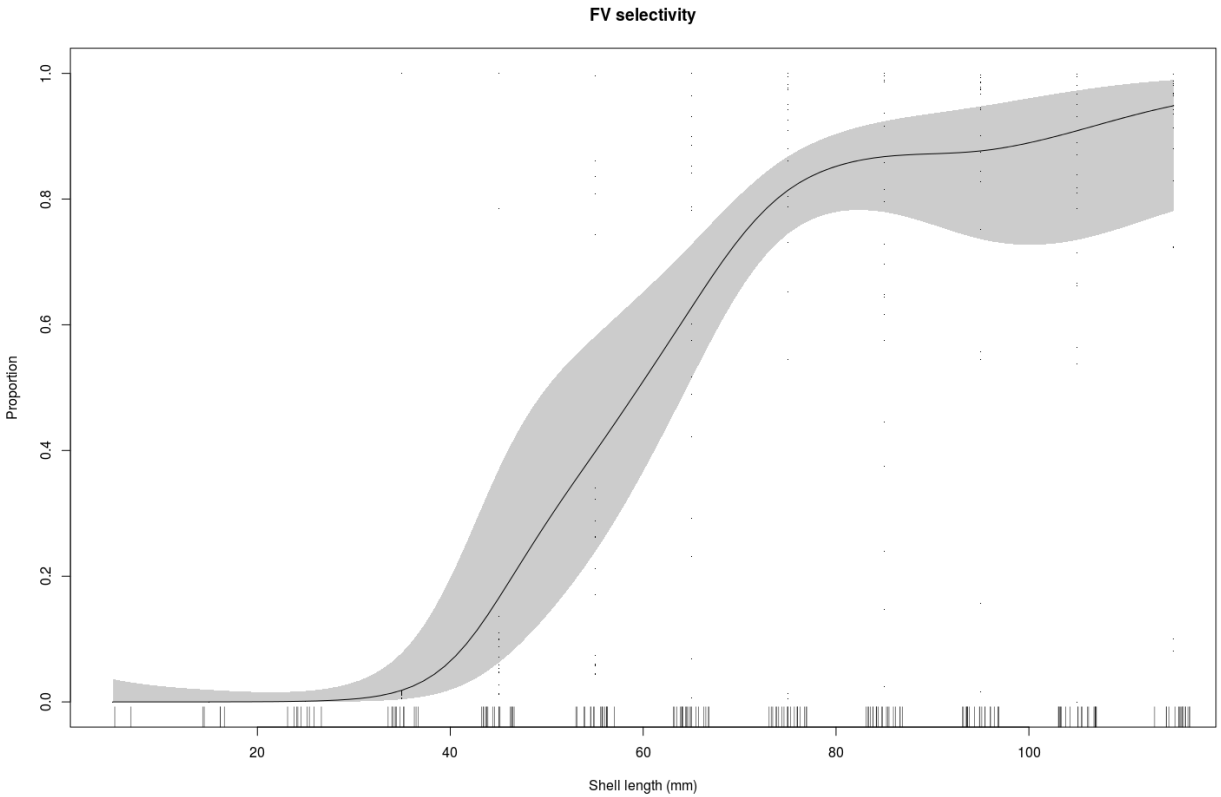

Figure 48: The GAM fit to all the selectivity data in all years. The best (by AIC) model included random effects in both the intercept and spline over length. The data density is shown in the rug plot along the horizontal axis and relative confidence is represented by the shaded region.

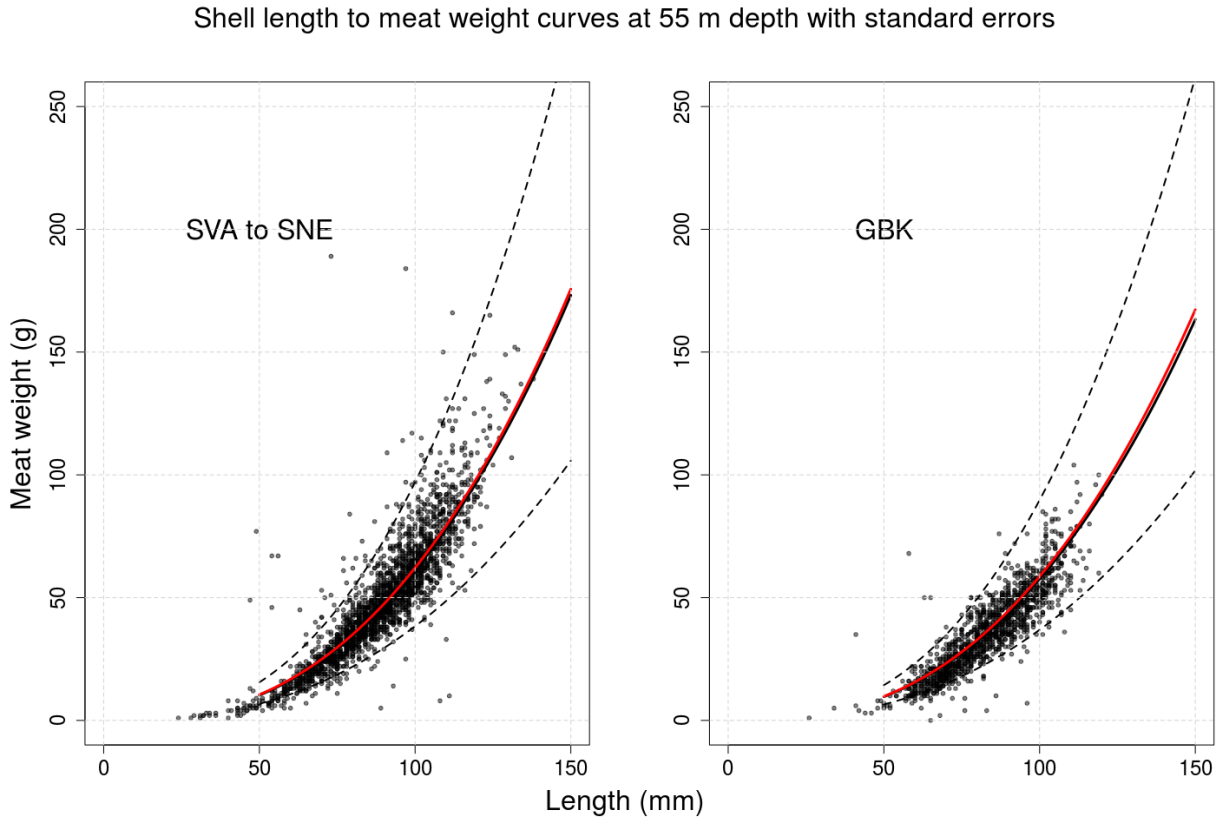

Figure 49: Broad scale area differences in allometric relationships for ocean quahog. The same depth (55 m) was used to generate the curves for each area. The 95% confidence regions are represented by the dotted line.

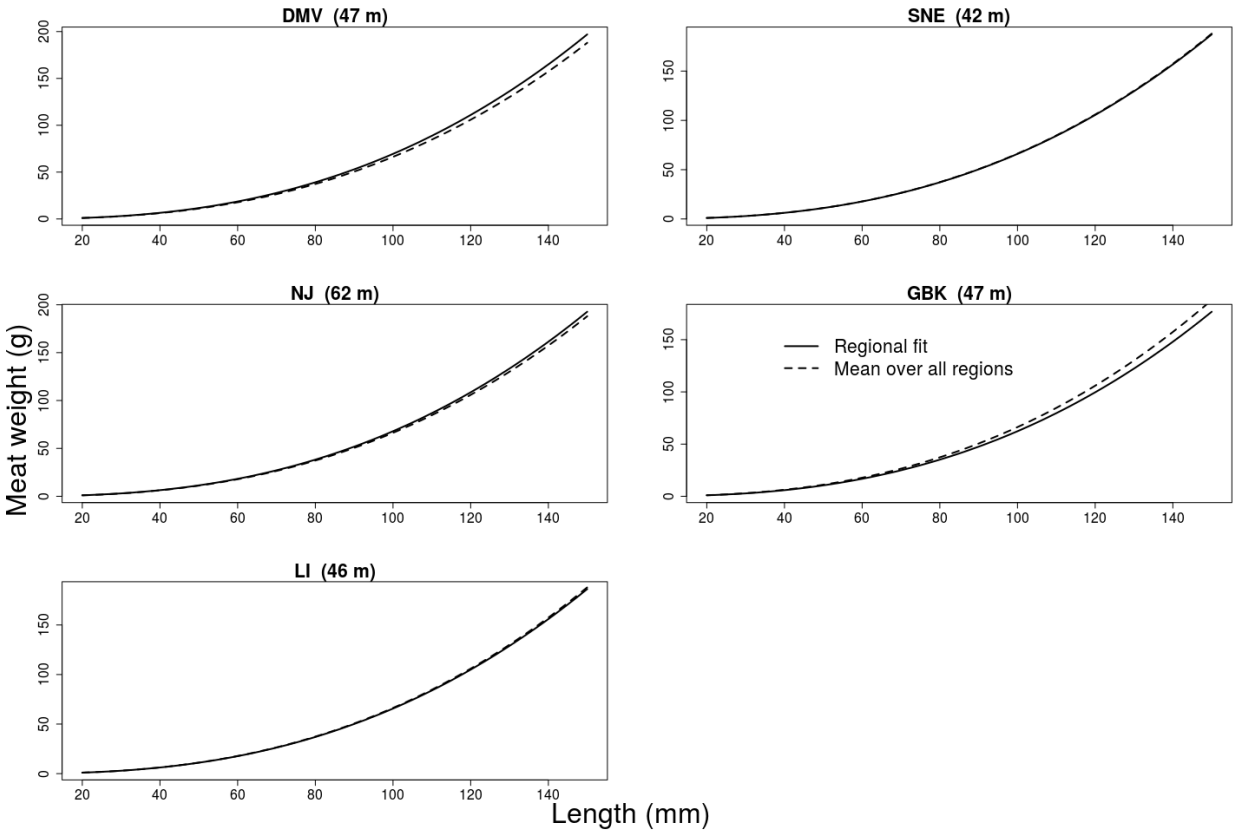

Figure 50: Regional differences in allometric relationships for ocean quahog. The median depth in each region was used to generate the curves. The global mean is represented by the dashed line.

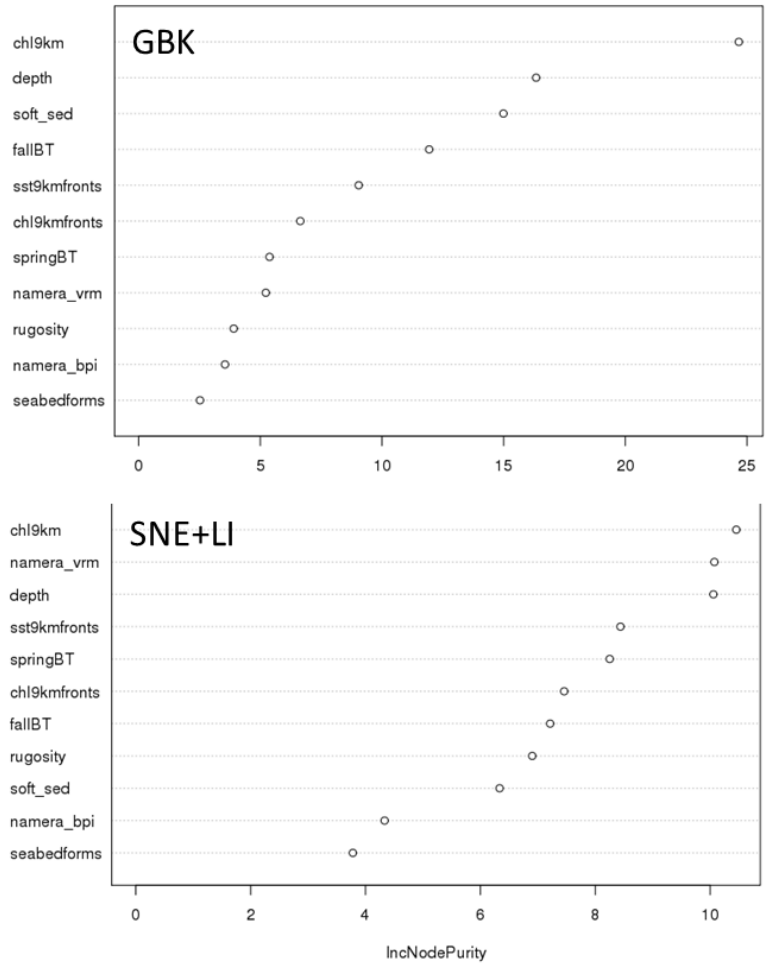

Figure 51: Variable importance plots for random forest models fit to NEFSC clam survey catches of ocean quahog in the GBK (top) and SNE+LI regions (bottom) during 1997-2011. The increase in node purity (IncNodePurity) is the average reduction in mean squared error when a variable is removed (permuted randomly) over all splits in all trees. The most important variable is at the top and other variables are listed in order of decreasing importance.

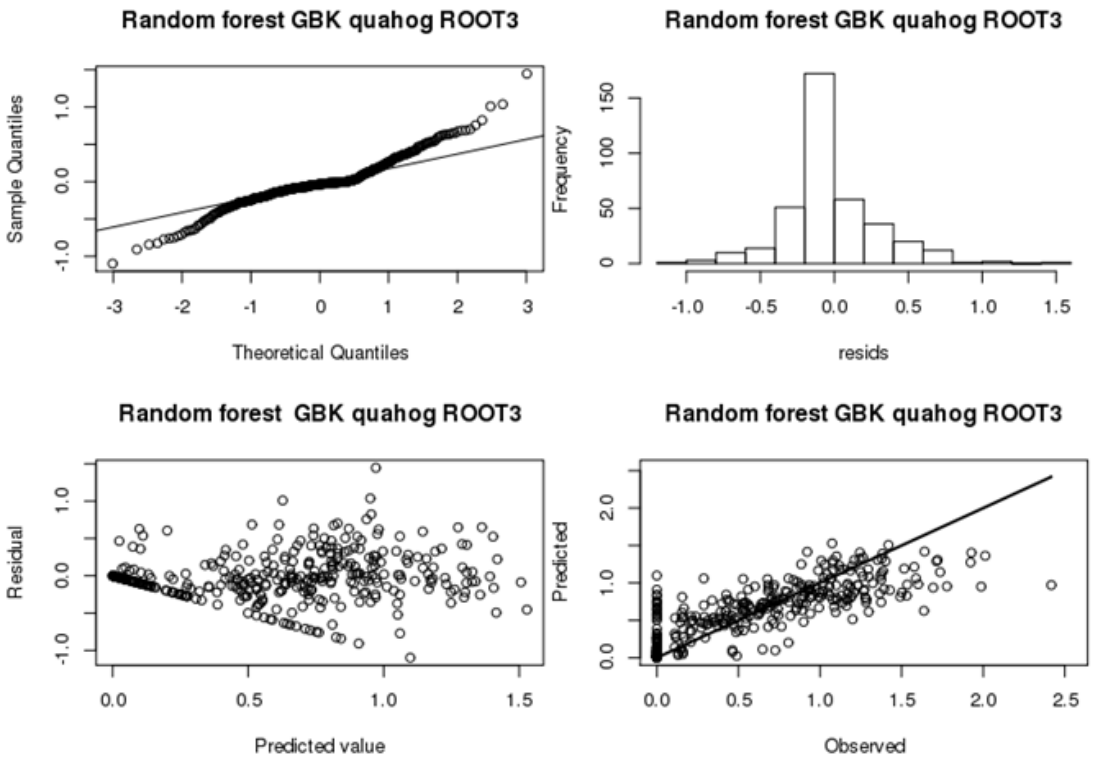

Figure 52: Ranked importance of predictor variables in random forest regression tree models for the GBK and SNE+LI regions. Rank 1 is the highest importance levels and rank 11 is the lowest.

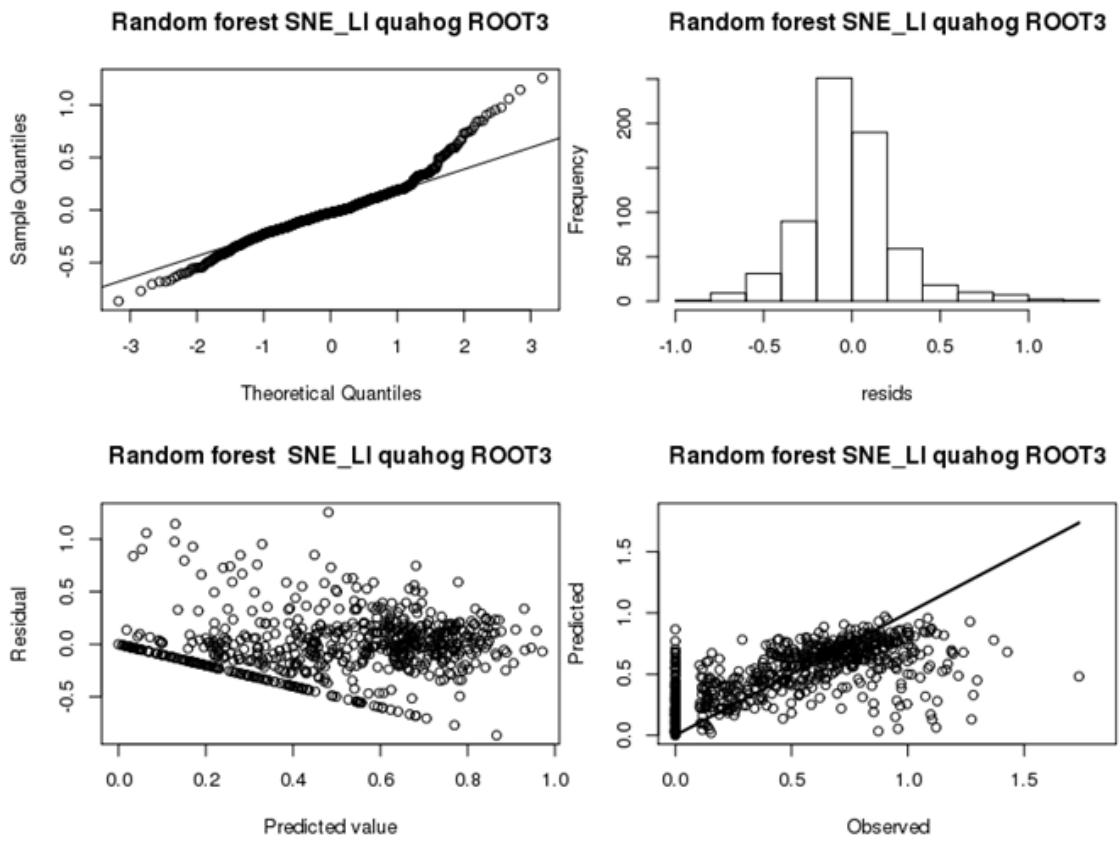

Figure 53: Residual plots for a random forest model fit to NEFSC clam survey catches of ocean quahog in the GBK region during 1997-2011. The residuals are sqrt(observed) - sqrt(predicted).

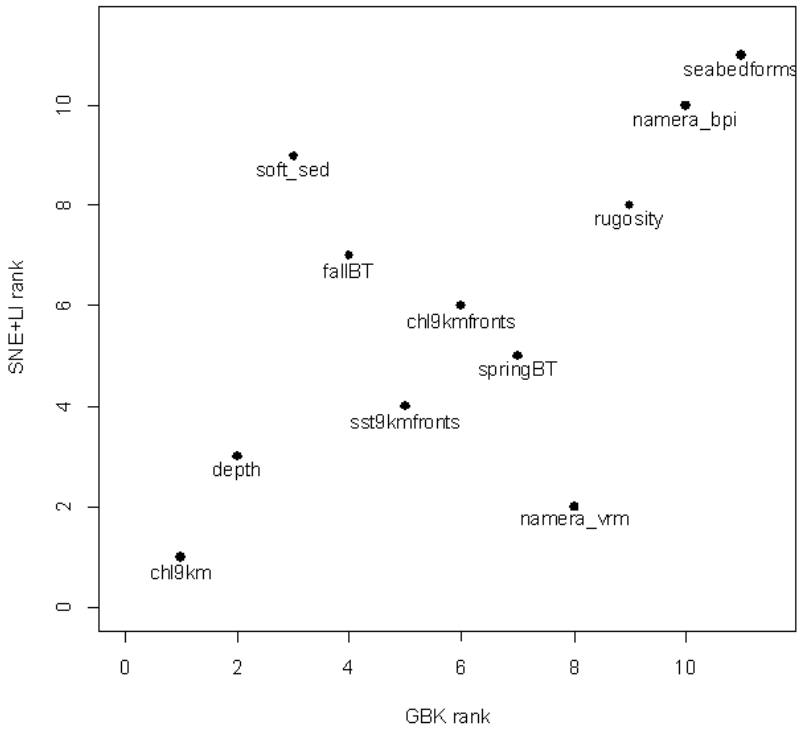

Figure 54: Residual plots for a random forest model fit for NEFSC clam survey catches of ocean quahog in the SNE+LI region during 1997-2011. The residuals are in cube root transformed units.

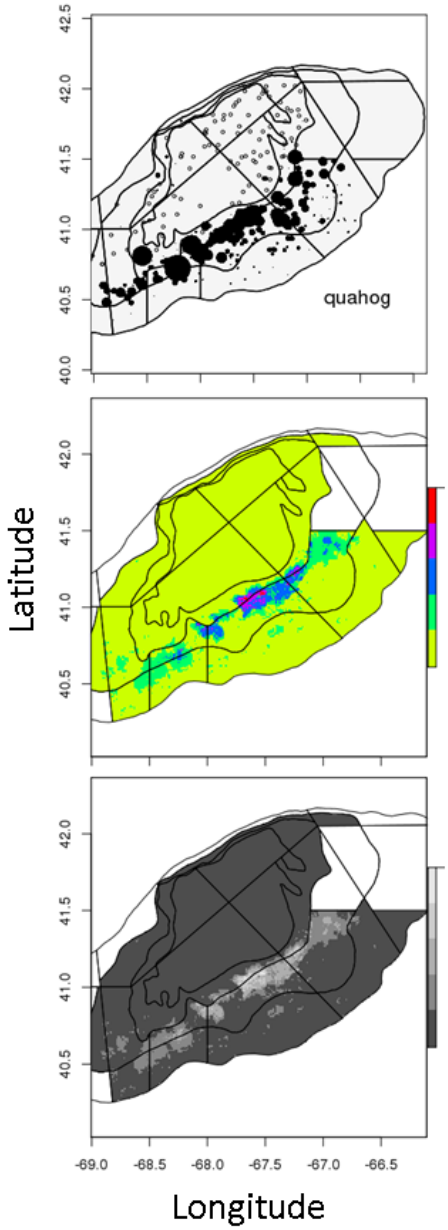

Figure 55: Survey catch data for GBK ocean quahog during 1997-2011 (top) and predicted values from a random forest regression tree (middle in color and bottom in shades of grey). Predicted values ranged from 0 to 1.4 ocean quahog m^2.

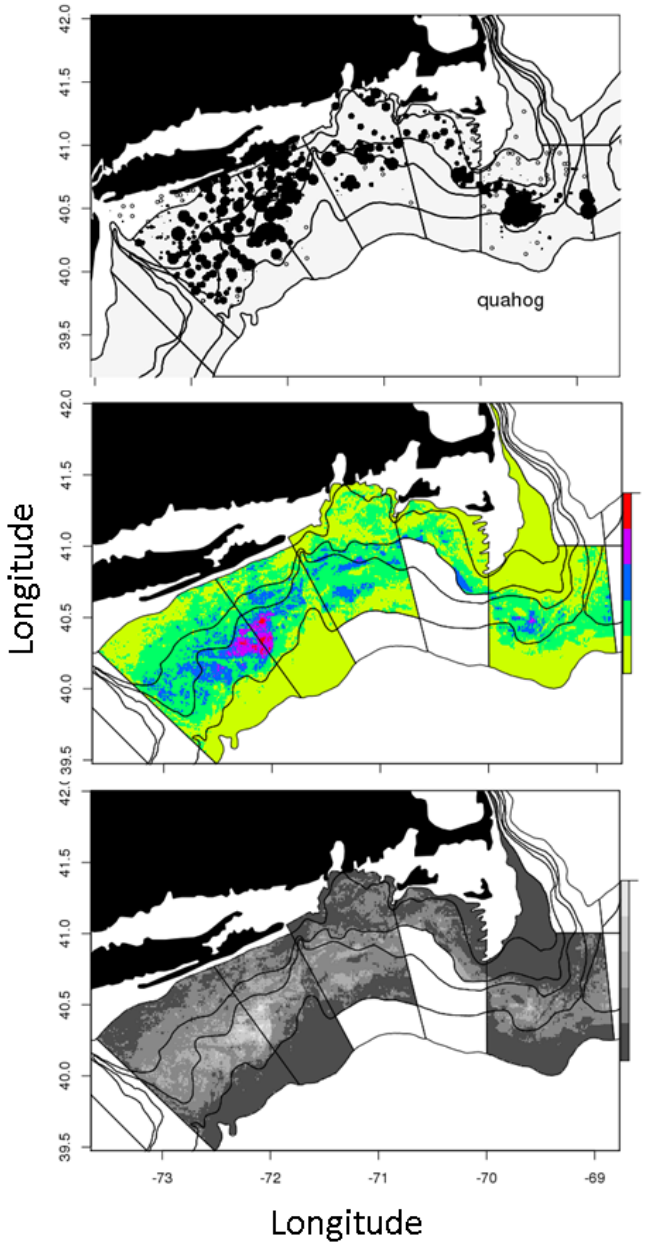

Figure 56: Survey catch data for LI+SNE ocean quahog during 1997-2011 (top) and predicted values from a random forest regression tree (middle in color and bottom in shades of grey). Predicted values ranged from 0 to 0.37 ocean quahog m^2.

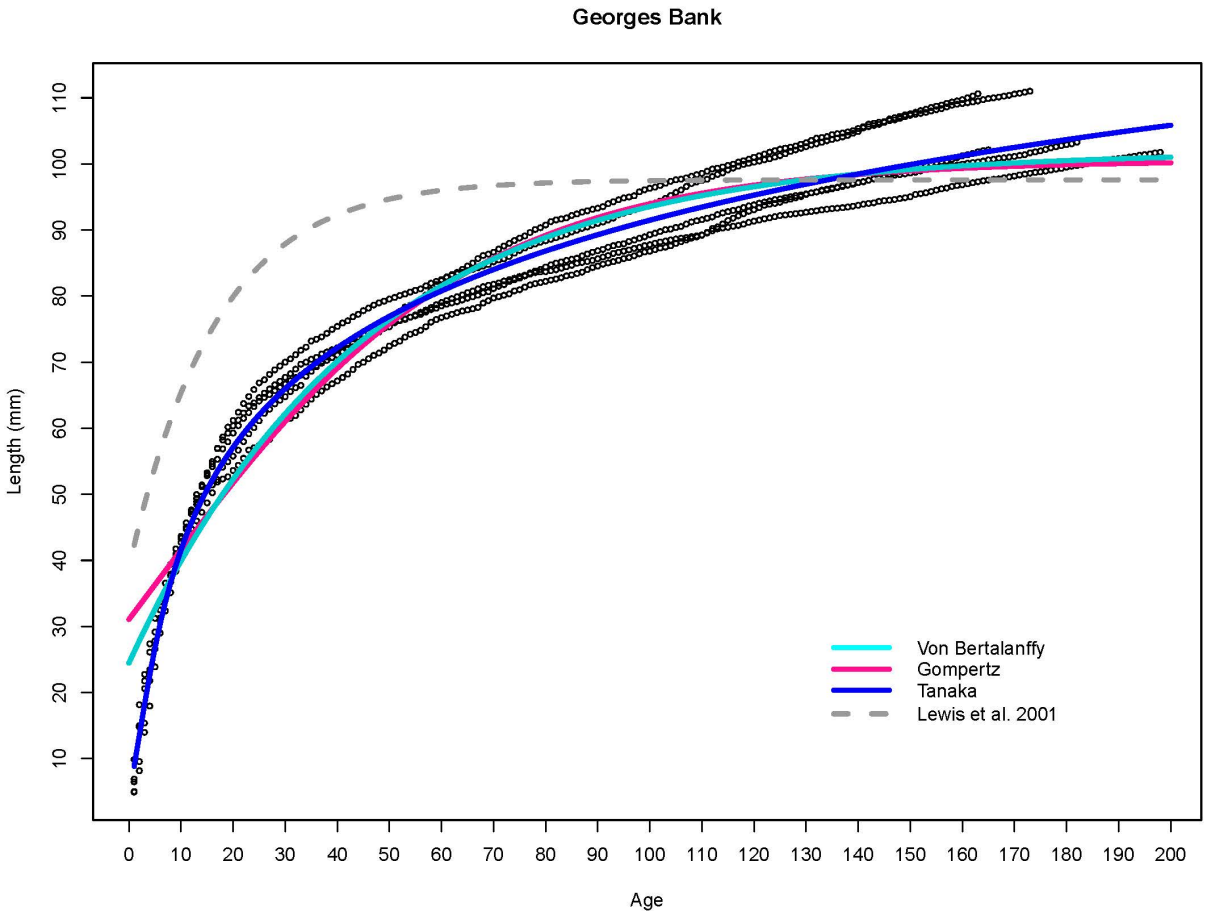

Figure 57: Top: Growth models for ocean quahog on GBK including Tanaka, Gompertz and von Bertalanffy curves fit to back calculated growth data for five ocean quahog collected at one station and a growth curve from 144 ocean quahog collected at a single survey station during 1994 (Lewis et al. 2001). This information was compiled after discussions by the Working Group.

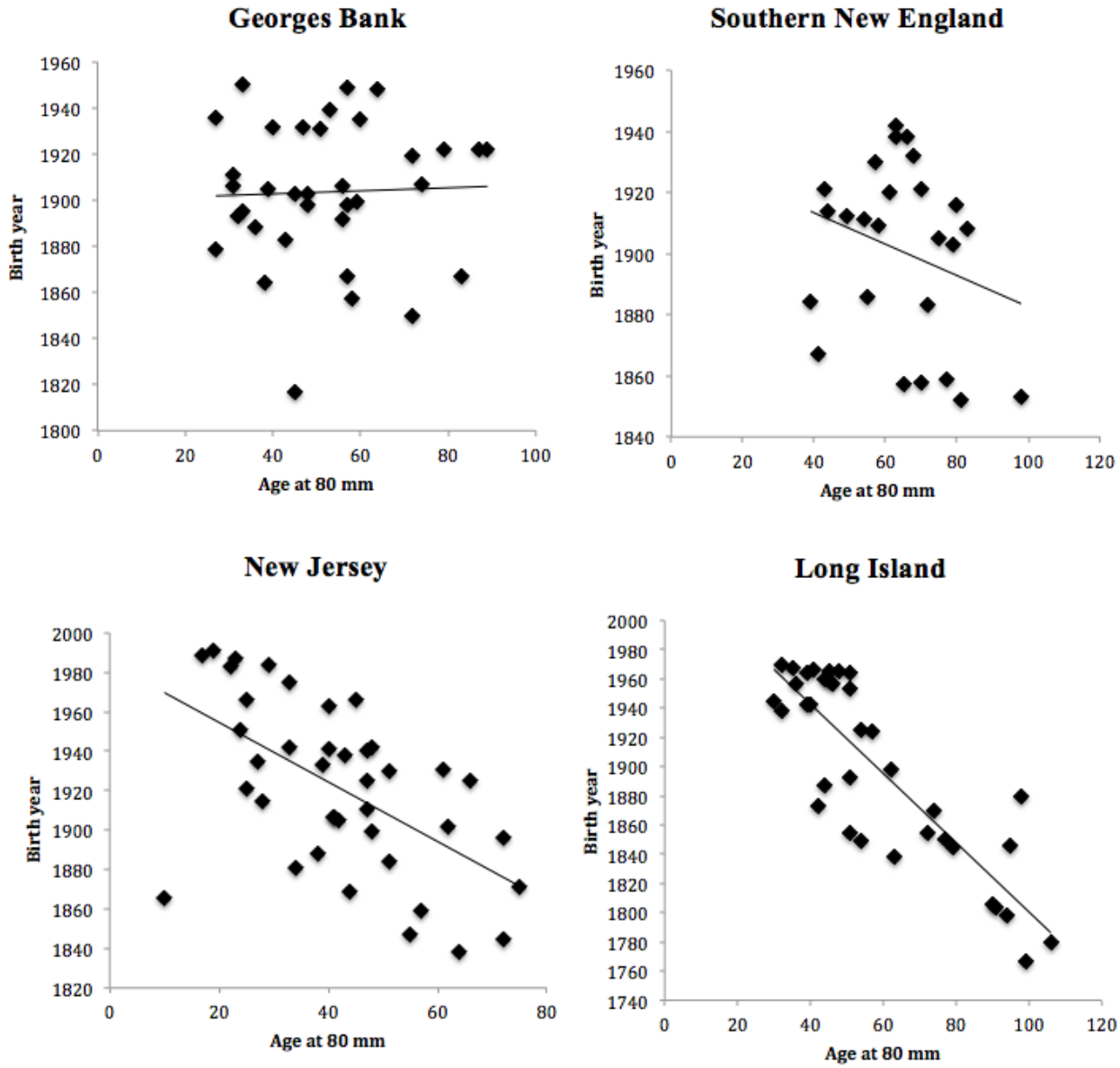

Figure 58: Birth year (age = 2015 - birth year) at 80 mm SL for ocean quahog collected at one station in each of four regions.

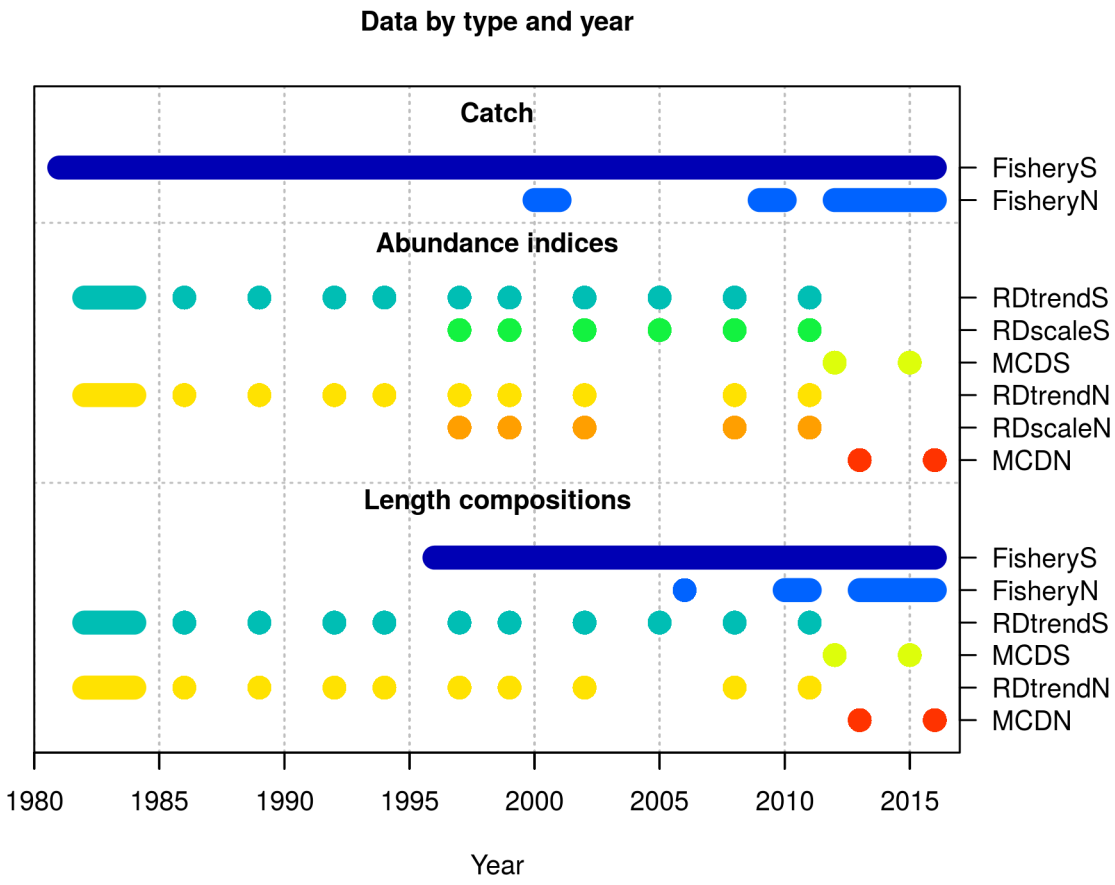

Figure 59: Data included in the ocean quahog assessment model. RD scale was not included in the likelihood.

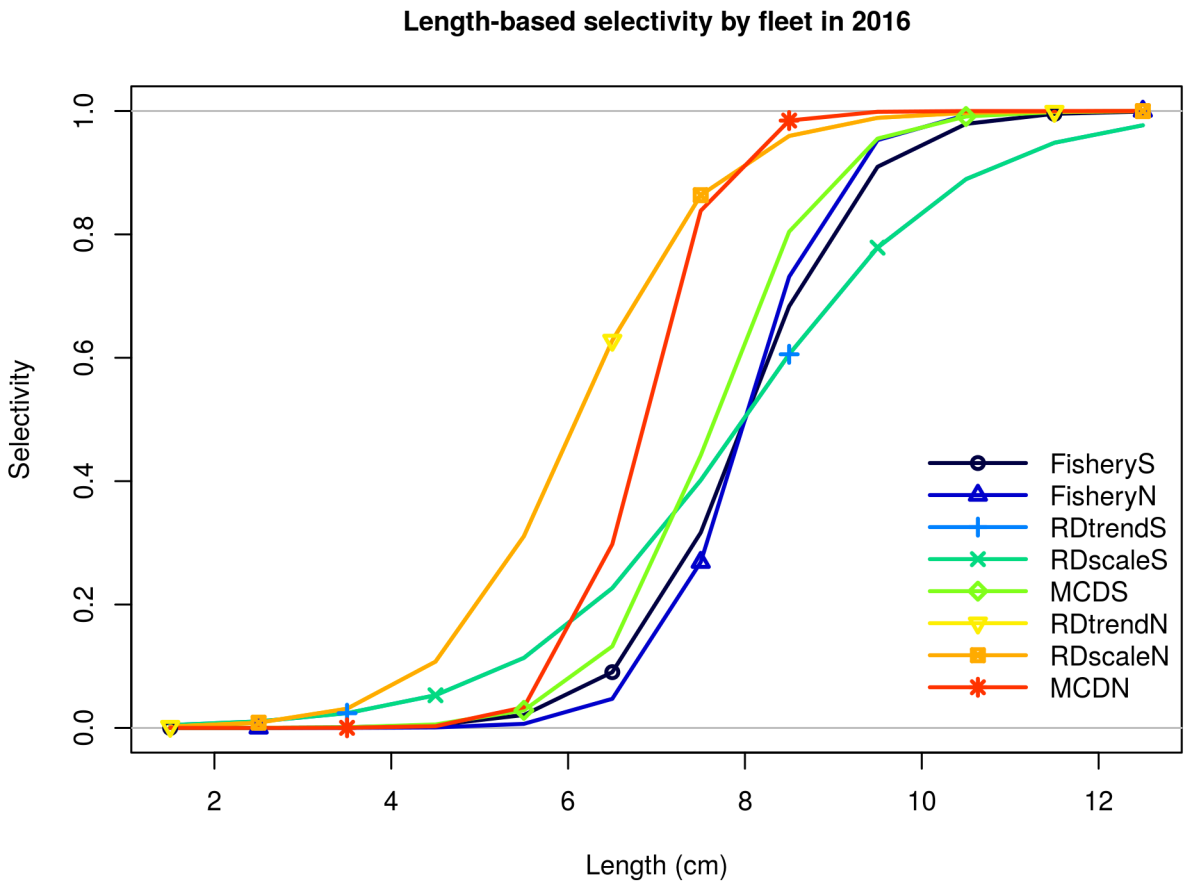

Figure 60: Comparison of selectivity curves for each fleet included in the assessment model for ocean quahog. RD trend and RD scale have identical selectivities because they are from the same survey (RD scale was not included in the likelihood).

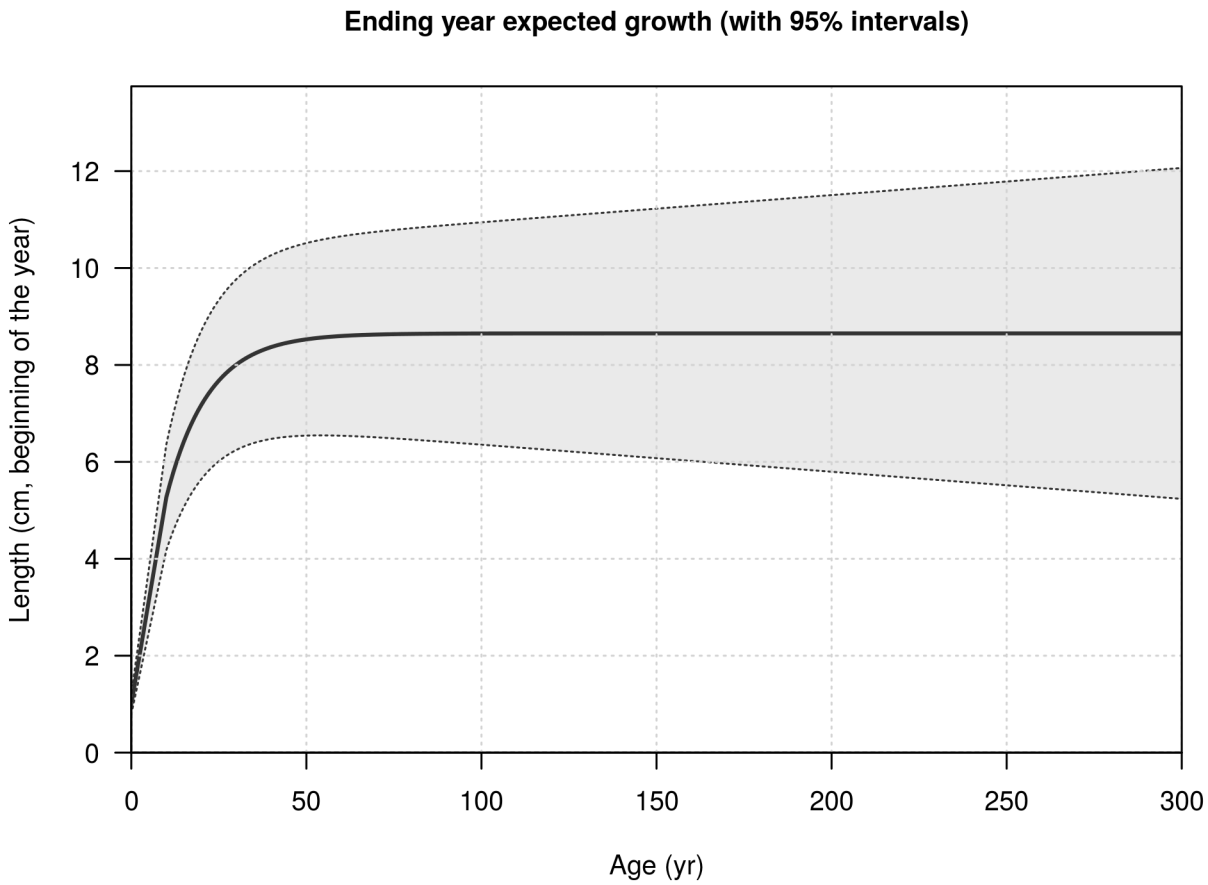

Figure 61: Length at age relationship from the assessment model for ocean quahog.

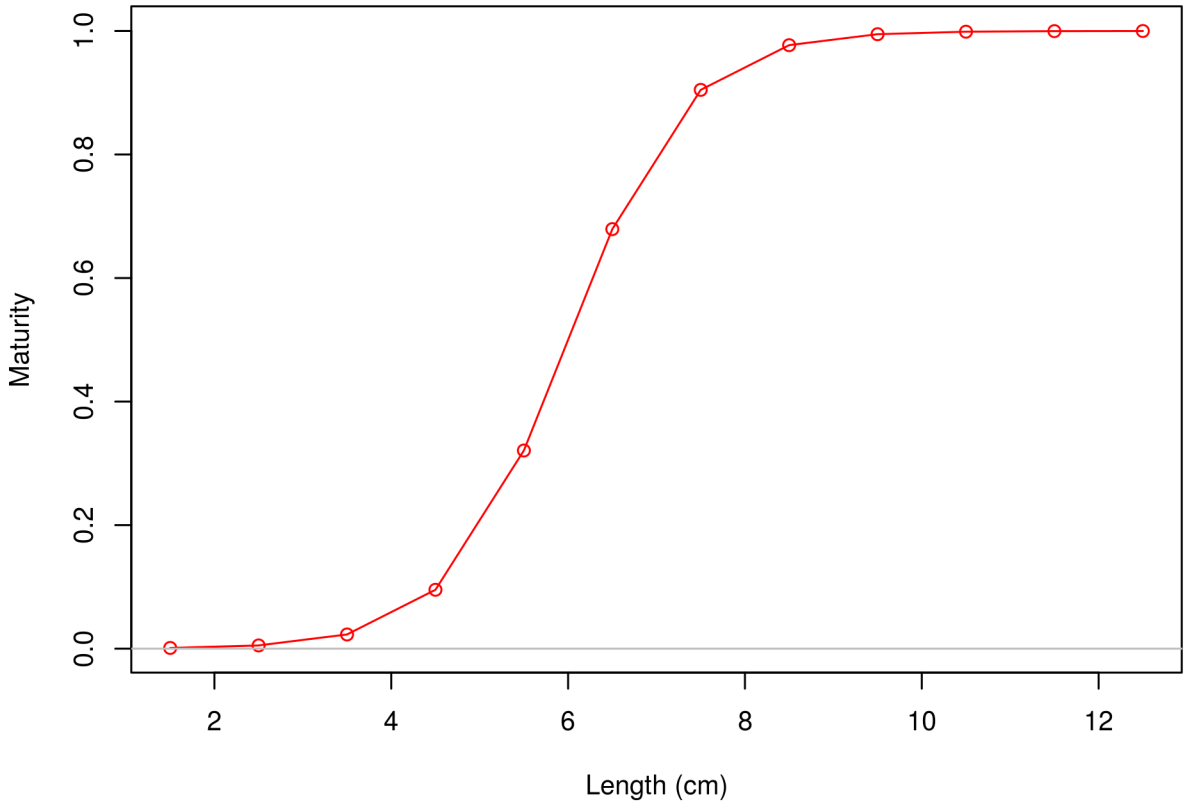

Figure 62: Maturity at age relationship in the assessment model for ocean quahog.

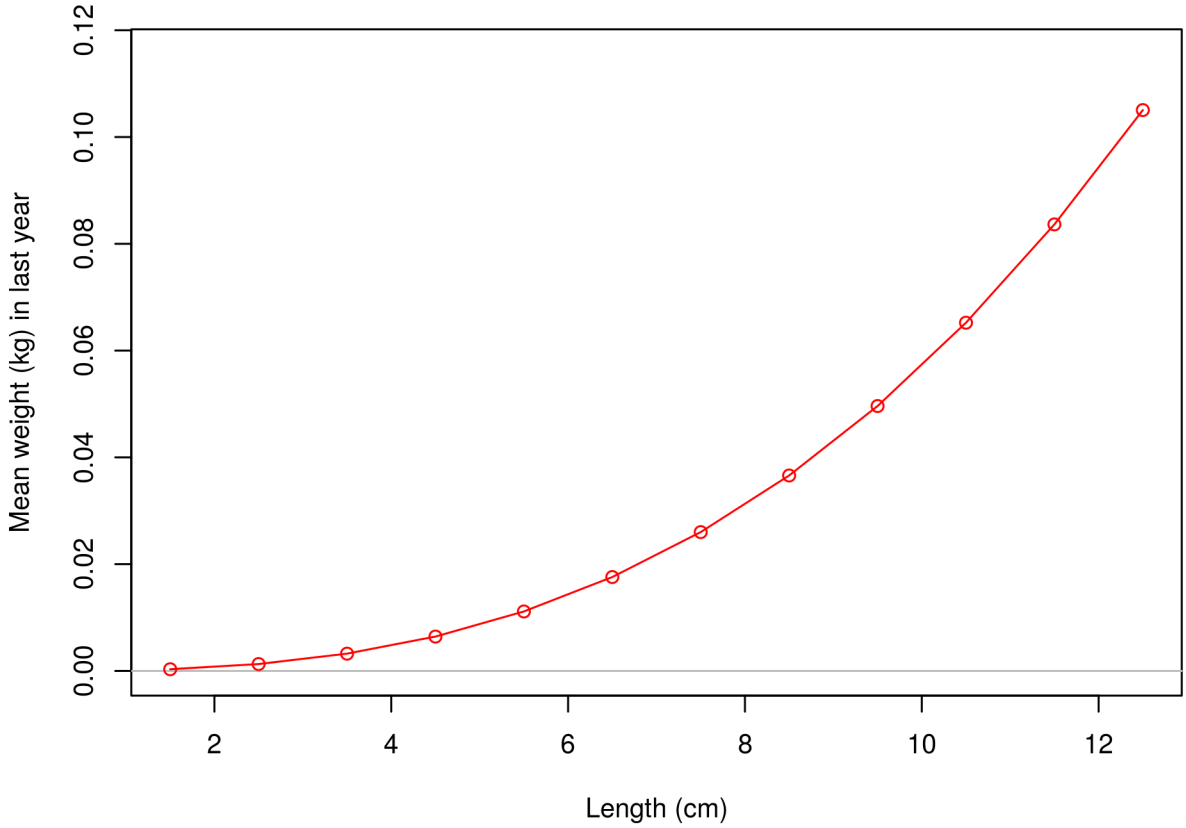

Figure 63: Weight at length relationship in the assessment model for ocean quahog.

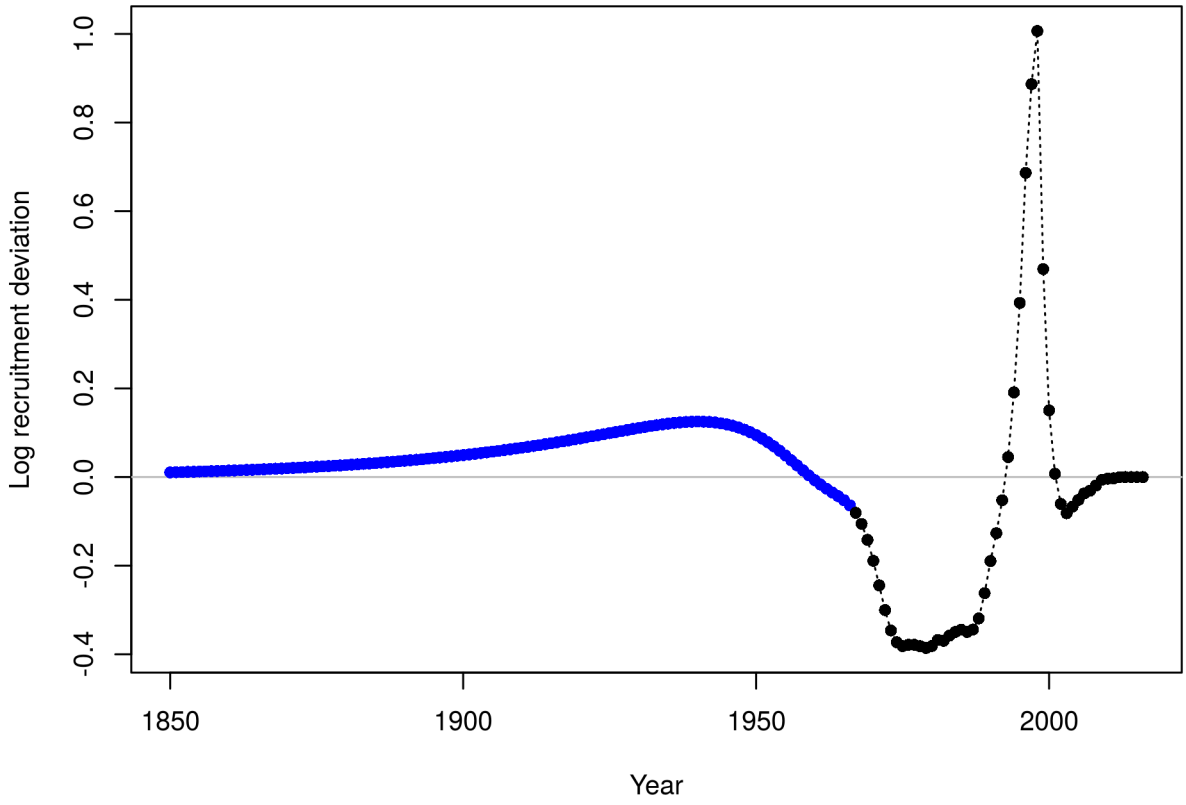

Figure 64: Recruitment deviations estimated in the basecase assessment model for ocean quahog.

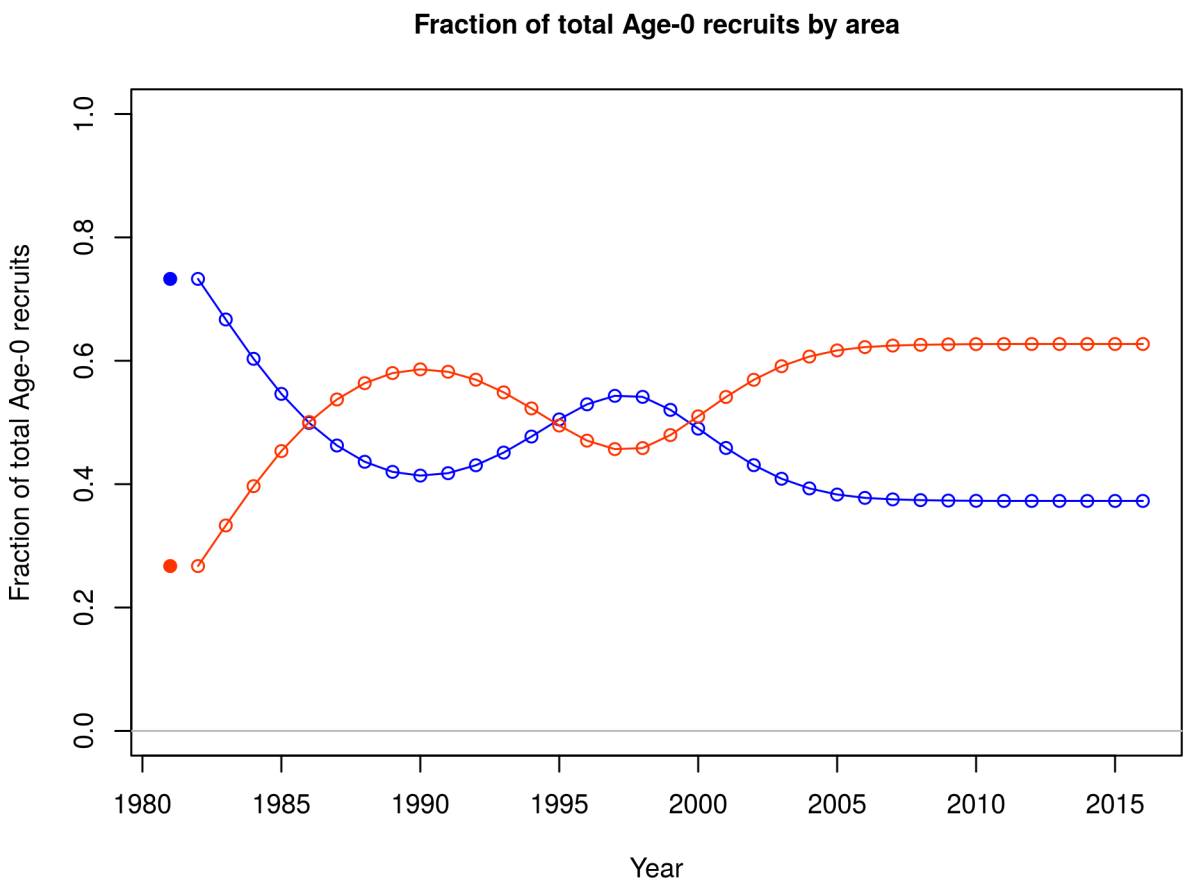

Figure 65: Proportion of total recruitment assigned to each area in the assessment model for ocean quahog. The southern area is blue and the northern area is red.

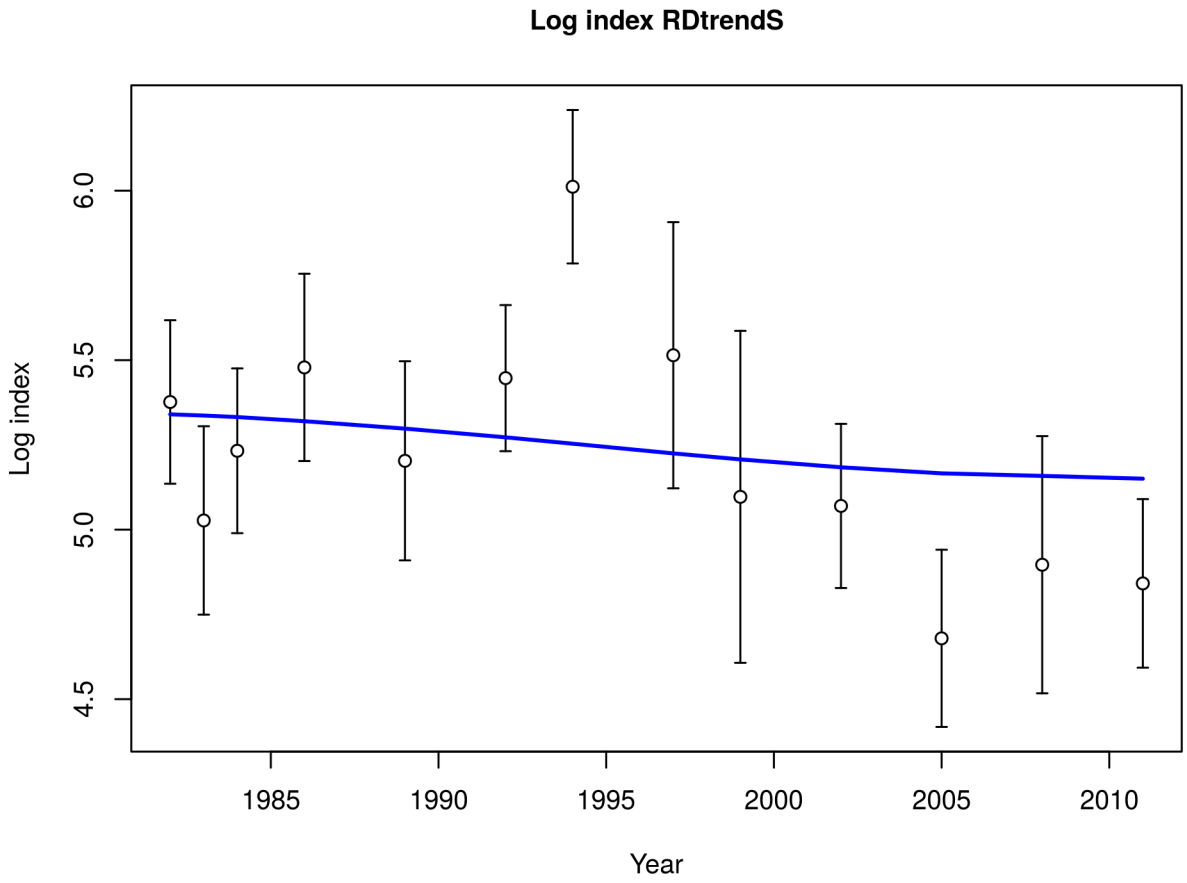

Figure 66: Fit to log RDtrend survey for ocean quahog in the southern area. Vertical lines are 95% confidence intervals.

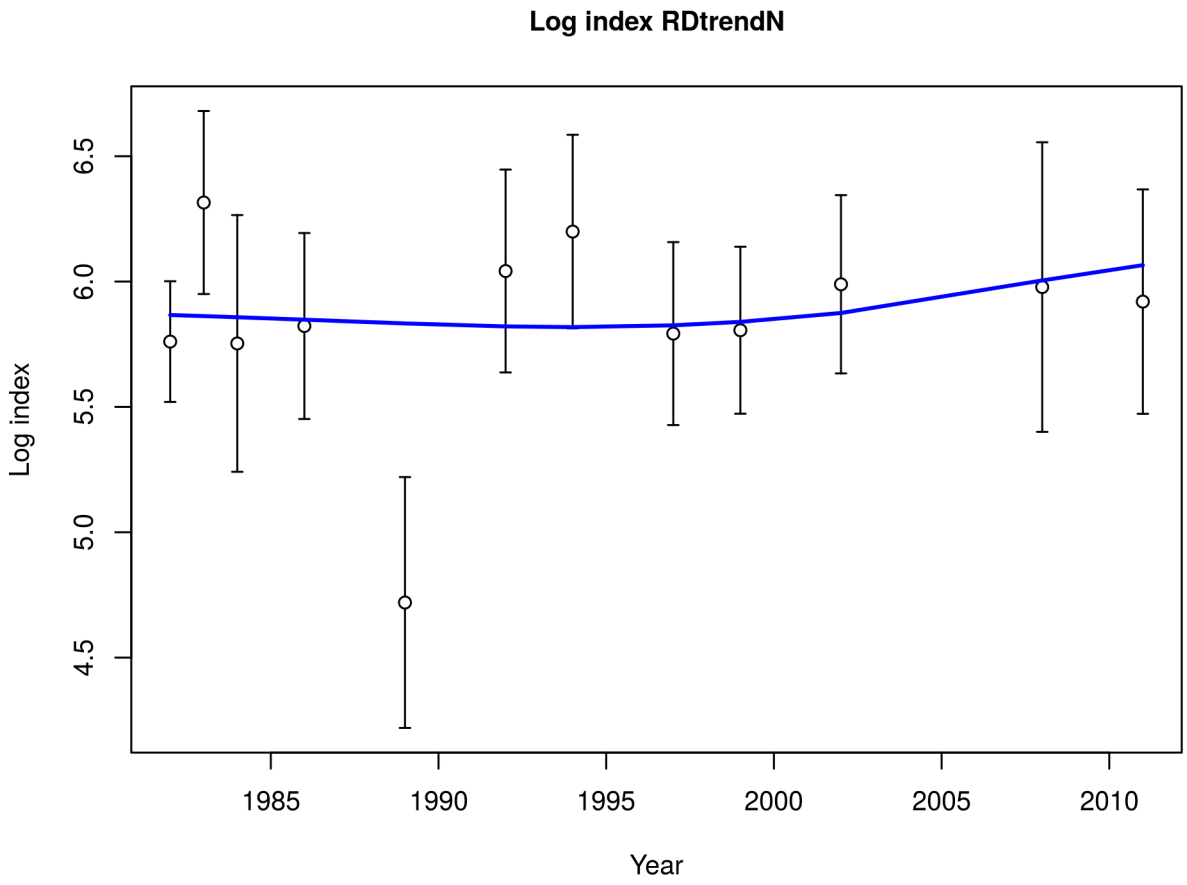

Figure 67: Fit to log RDtrend survey for ocean quahog in the northern area. Vertical lines are 95% confidence intervals.

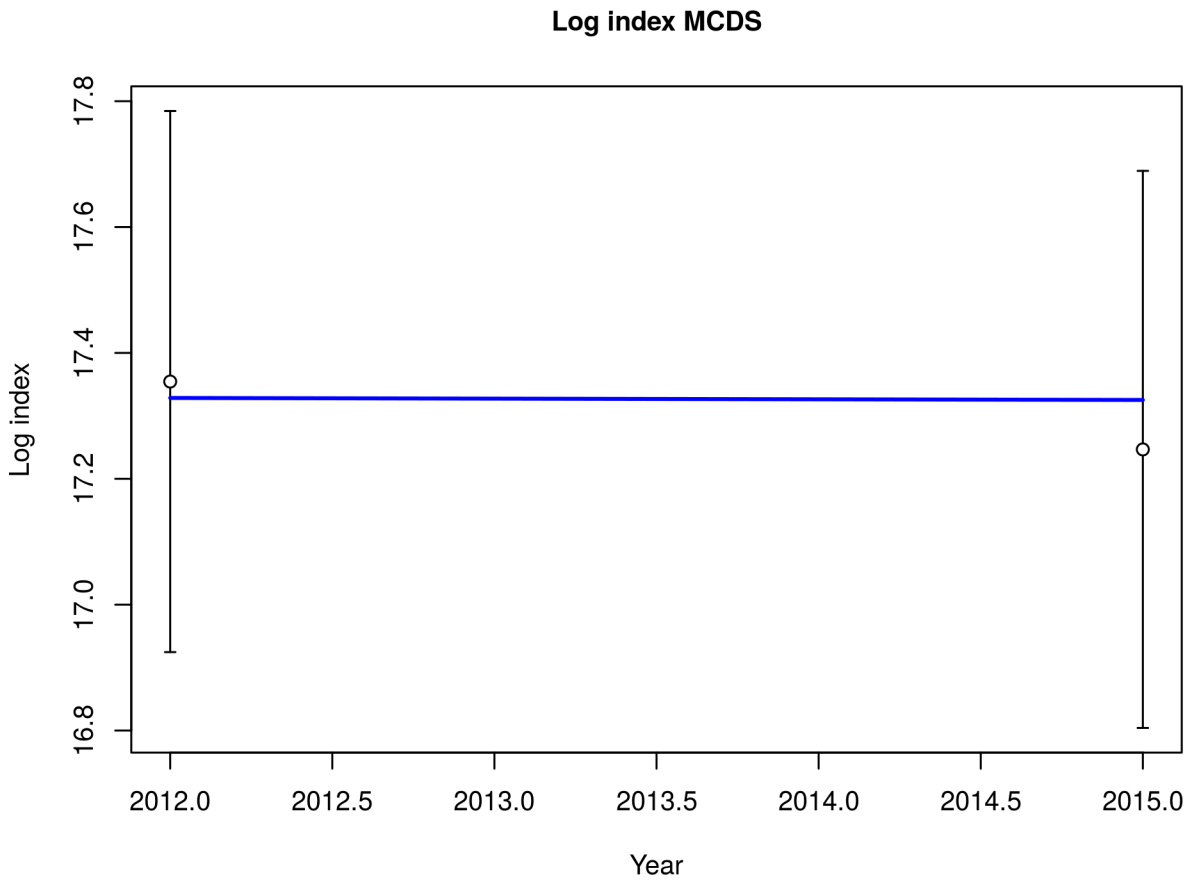

Figure 68: Fit to log MCD survey for ocean quahog for the southern area. Vertical lines are 95% confidence intervals.

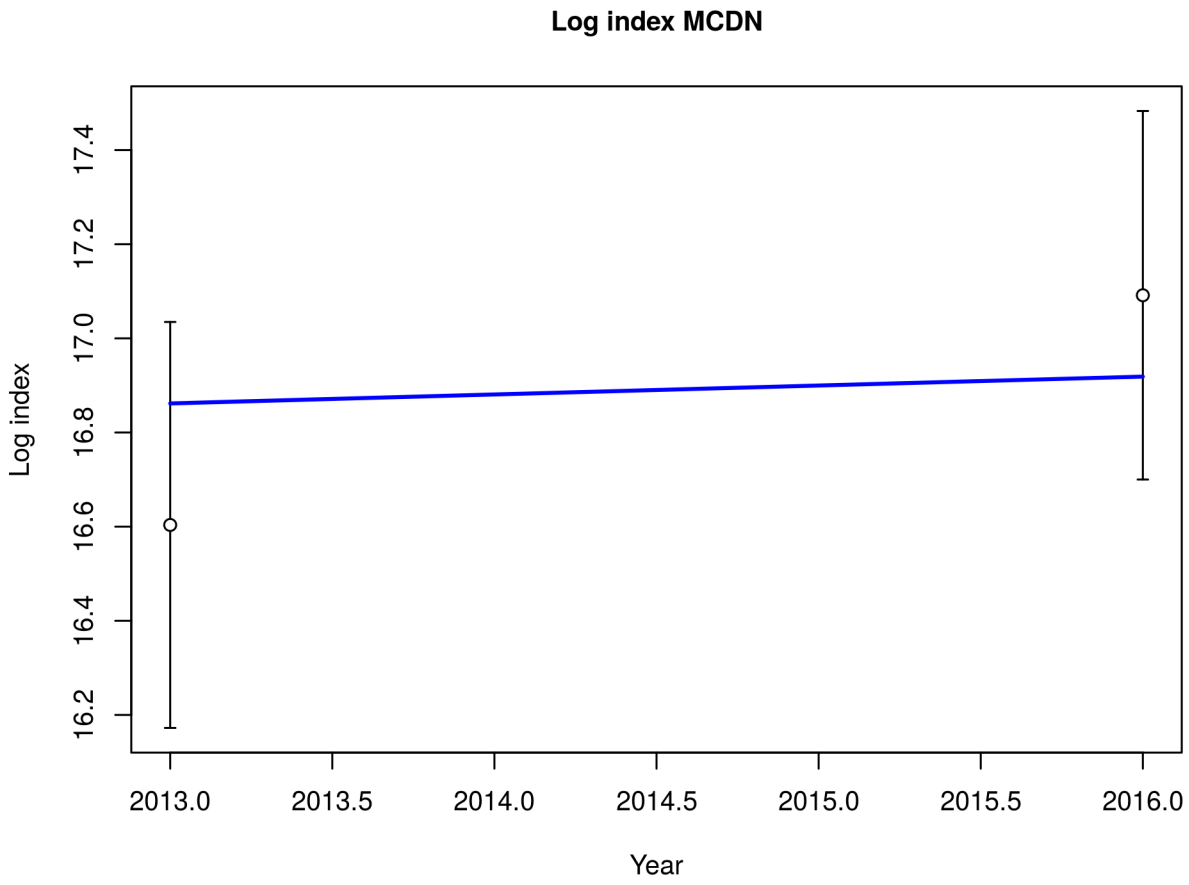

Figure 69: Fit to log MCD survey for ocean quahog for the northern area. Vertical lines are 95% confidence intervals.

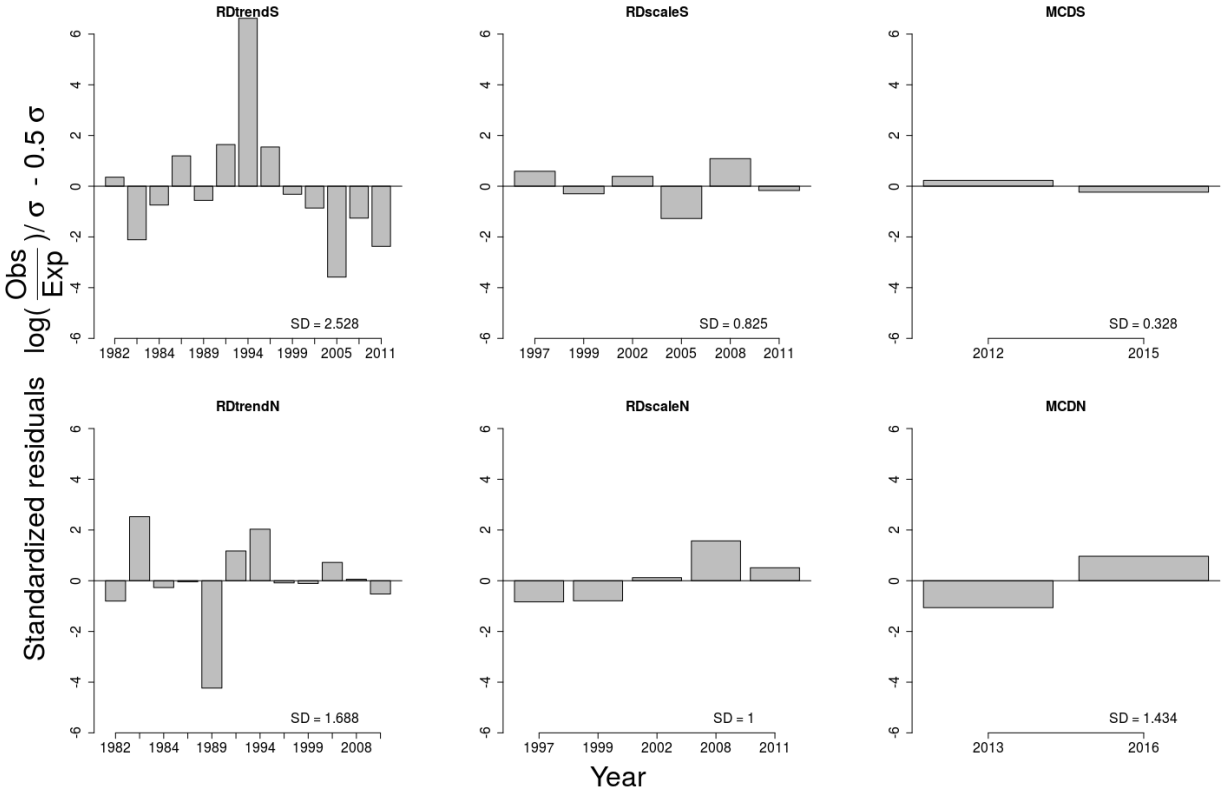

Figure 70: Residuals from the model fits to each survey index in the assessment model for ocean quahog by year. The standard deviation of the residuals over the time series is indicated above the horizontal axis.

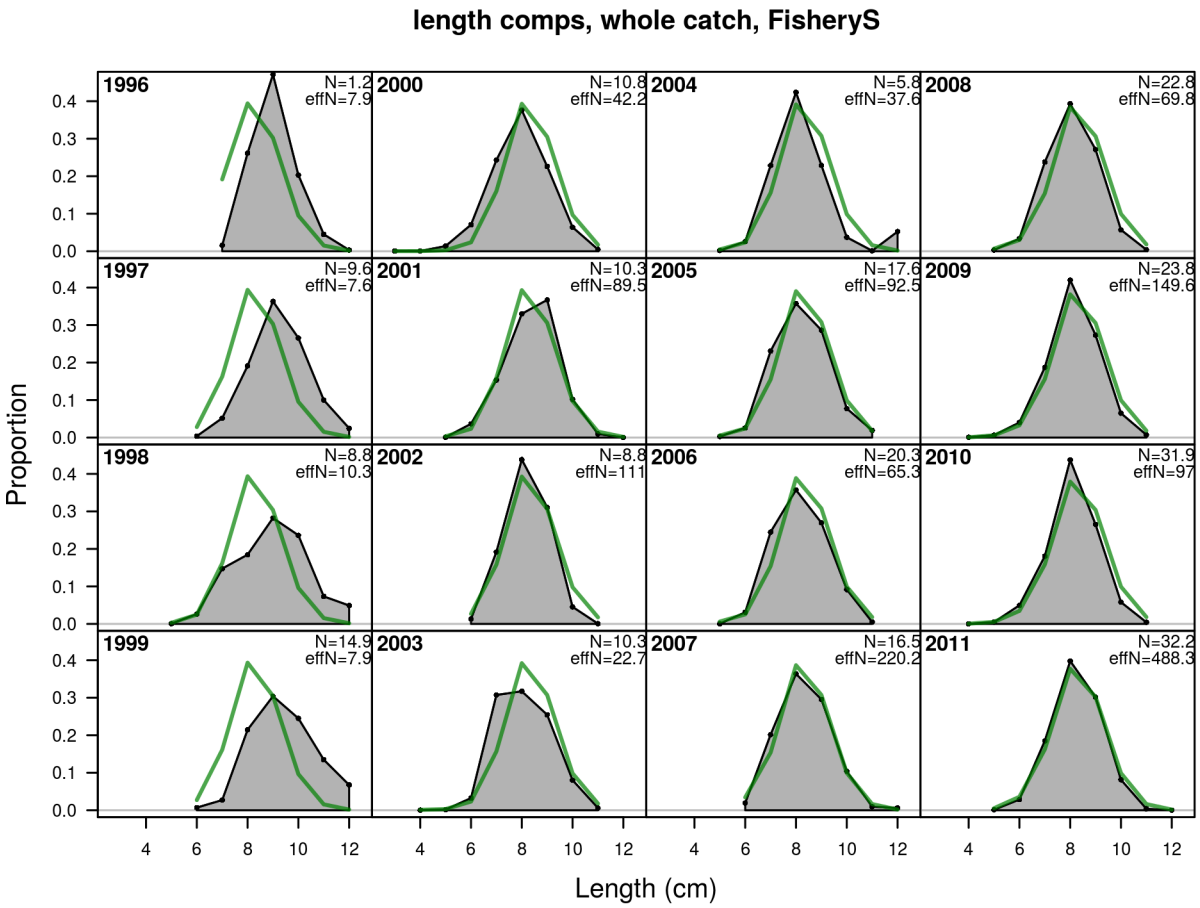

Figure 71: Model fit to length composition data from the commercial fishery in the southern area in the assessment model for ocean quahog.

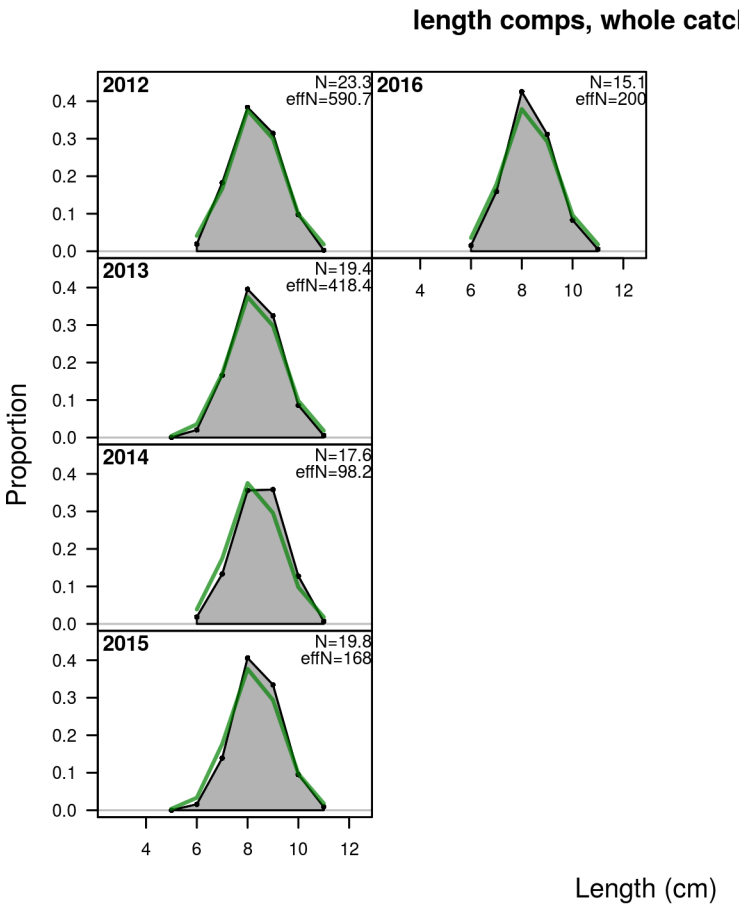

Figure 71 cont.

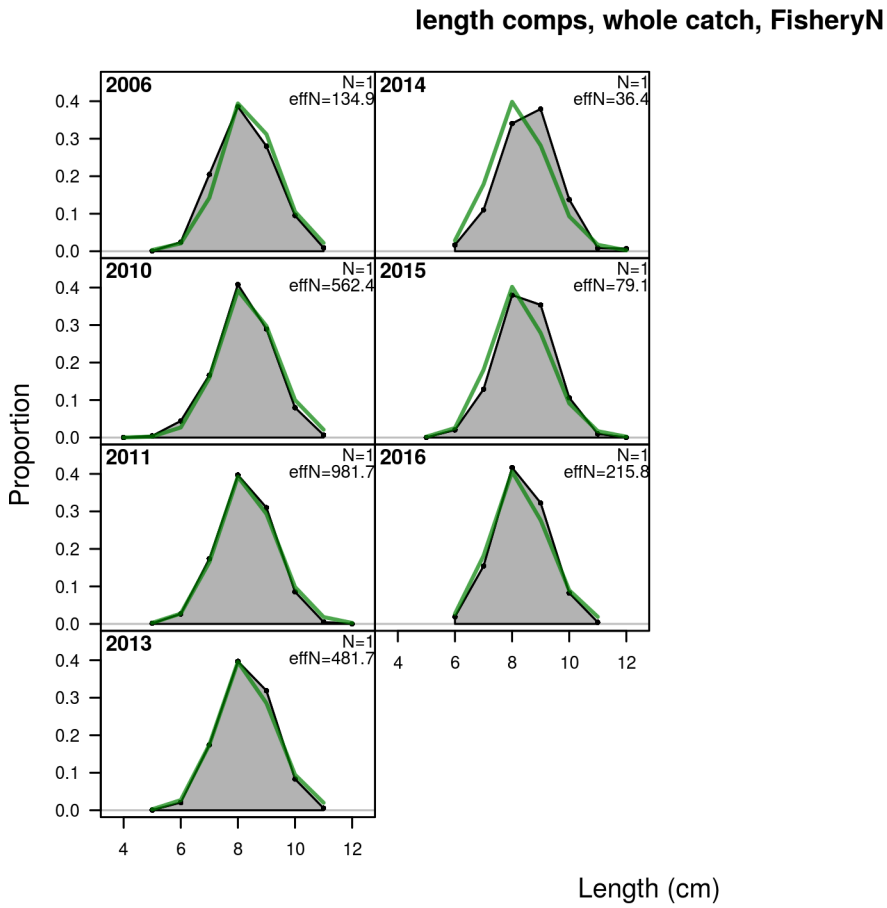

Figure 72: Model fit to length composition data from the commercial fishery in the northern area in the assessment model for ocean quahog.

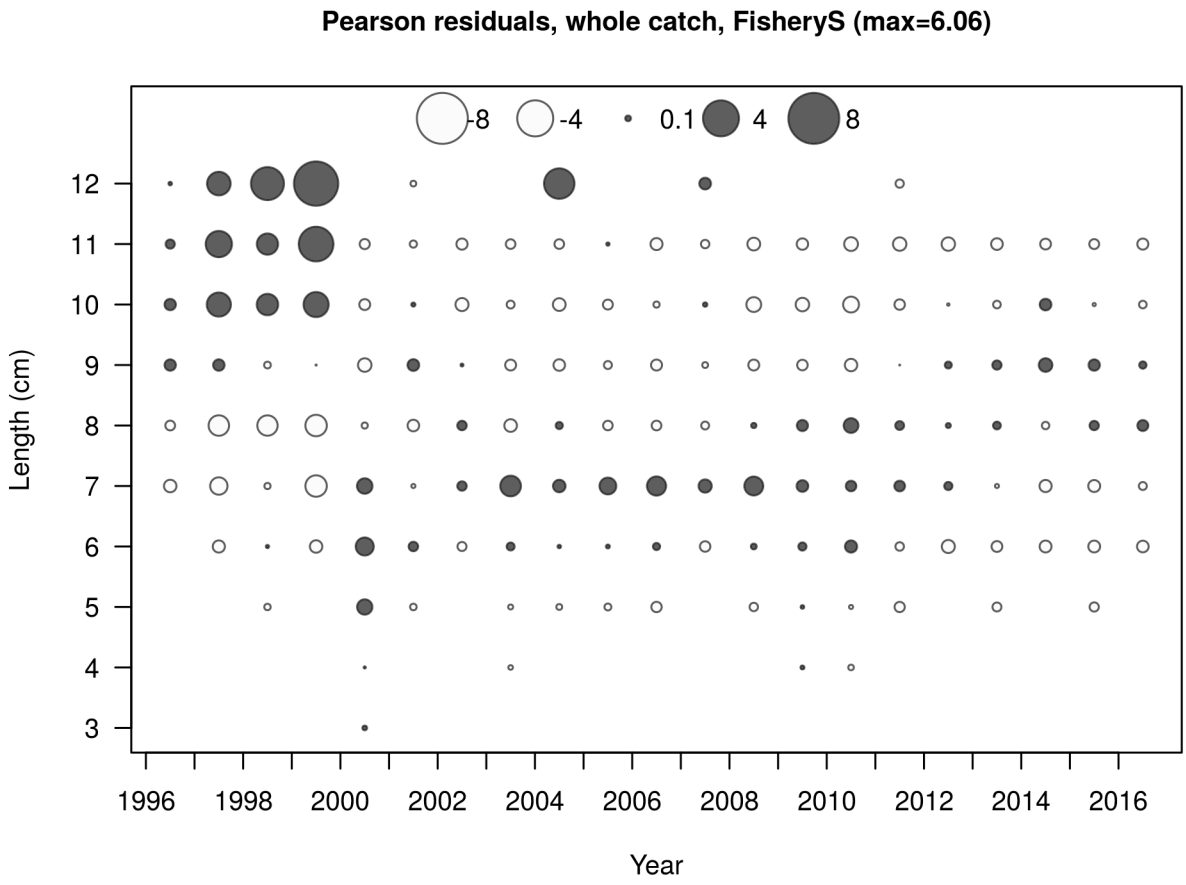

Figure 73: Pearson residuals from the fit to commercial length composition data in the assessment model for ocean quahog in the southern area. Closed bubbles are positive residuals (observed > expected) and open bubbles are negative residuals (observed < expected).

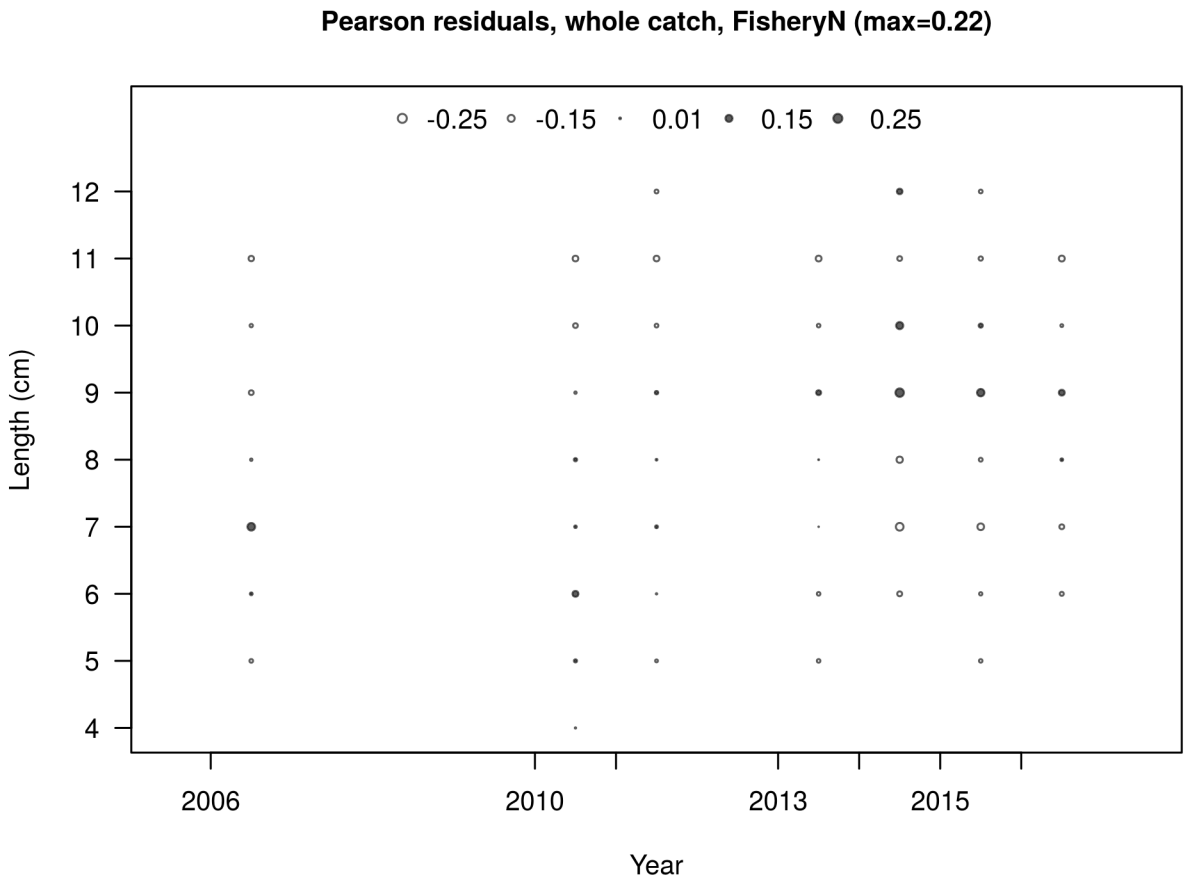

Figure 74: Pearson residuals from the fit to commercial length composition data in the assessment model for ocean quahog in the northern area. Closed bubbles are positive residuals (observed > expected) and open bubbles are negative residuals (observed < expected).

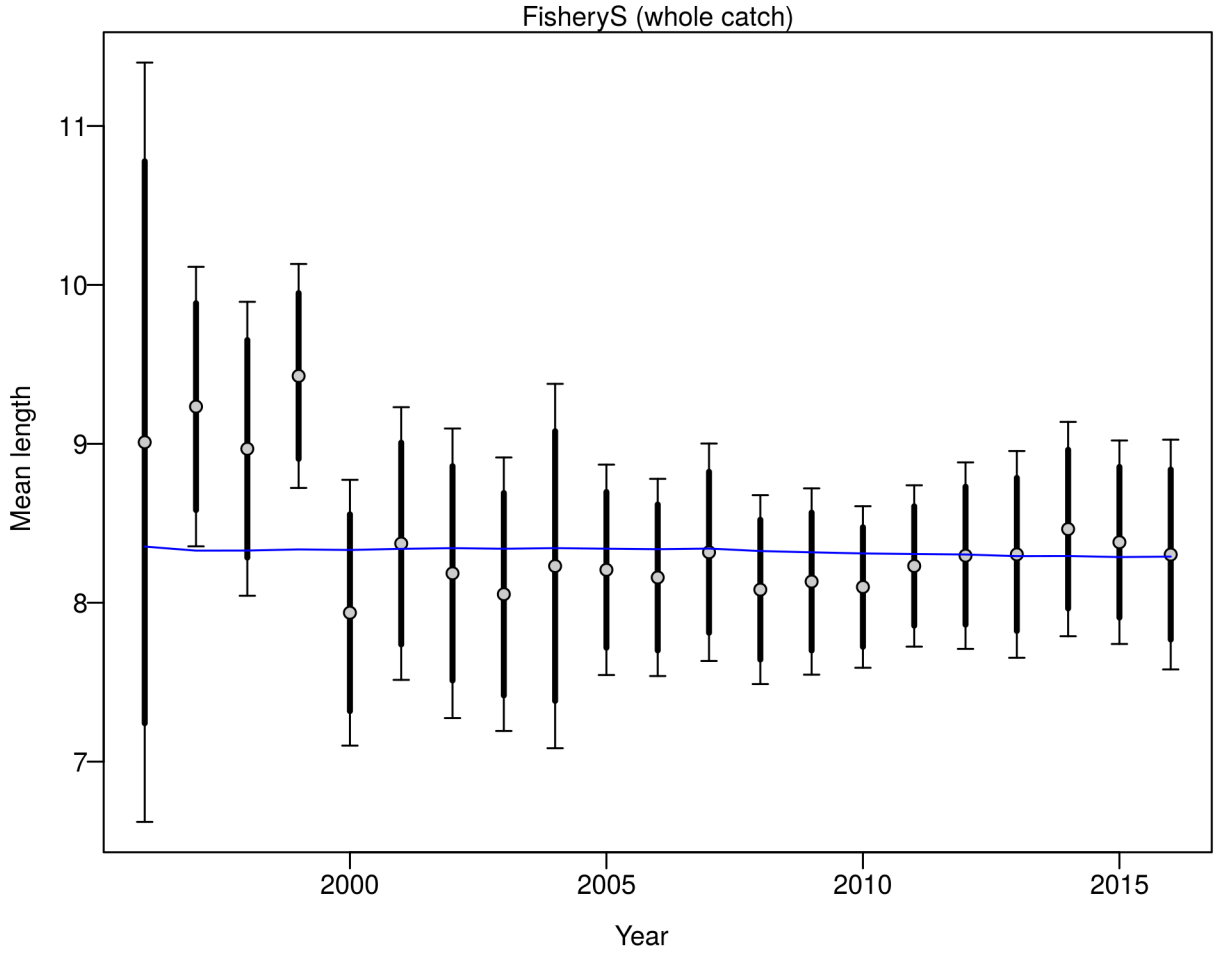

Figure 75: Observed mean length (cm) vs. the mean length predicted by the model based on fits to commercial length composition data in the assessment model for ocean quahog in the southern area.

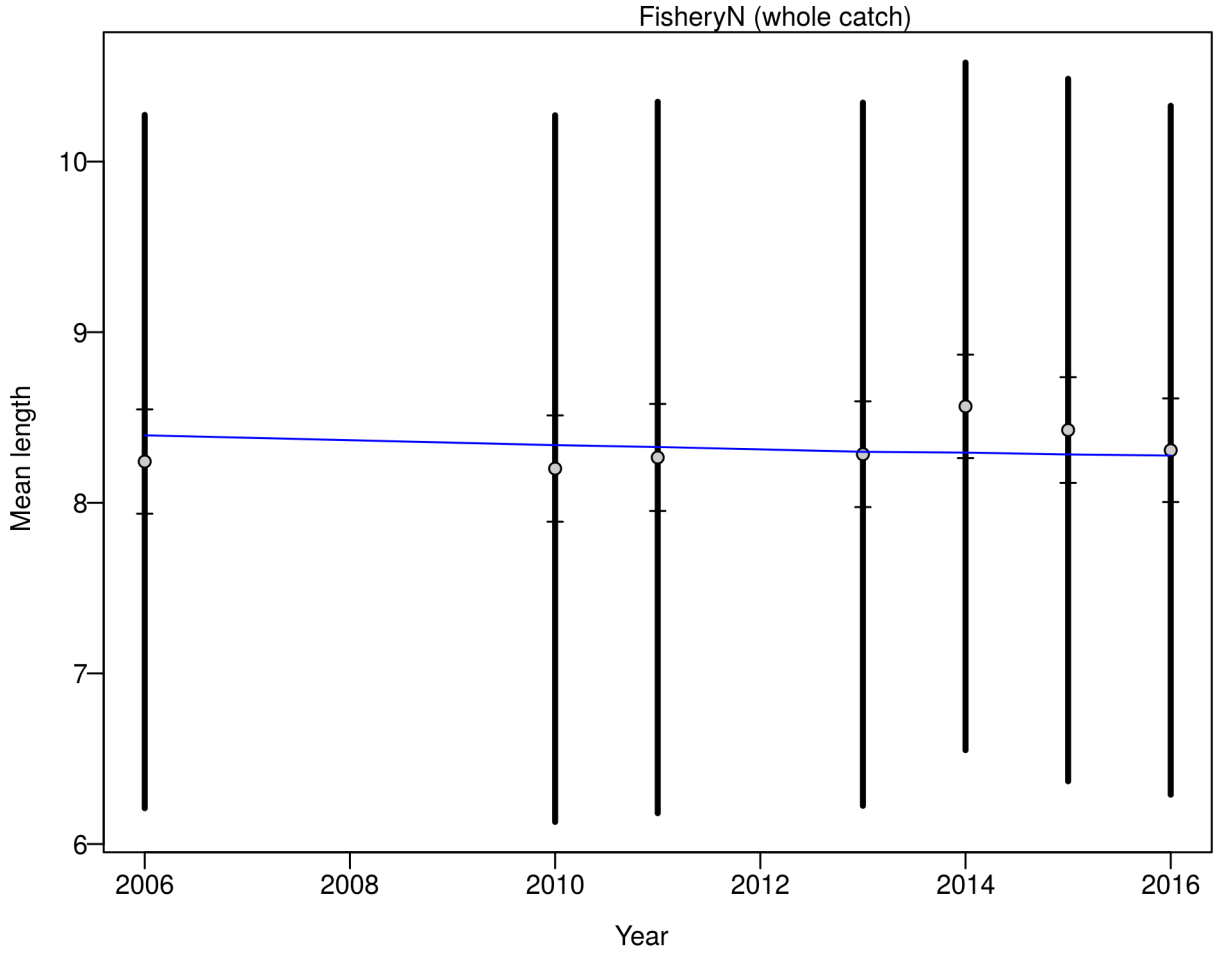

Figure 76: Observed mean length (cm) vs. the mean length predicted by the model based on fits to commercial length composition data in the assessment model for ocean quahog in the northern area.

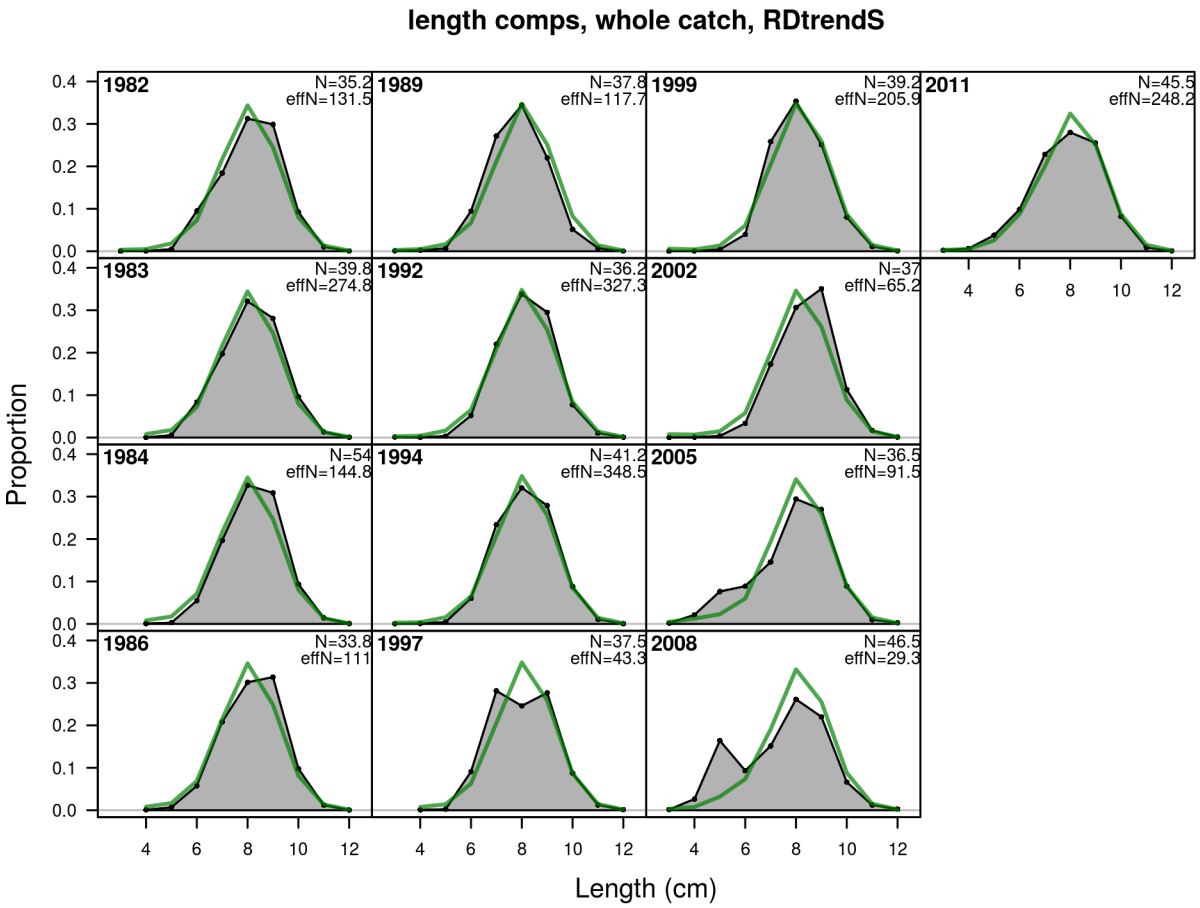

Figure 77: Model fit to length composition data from the NEFSC survey (RD) in the assessment model for ocean quahog in the southern area.

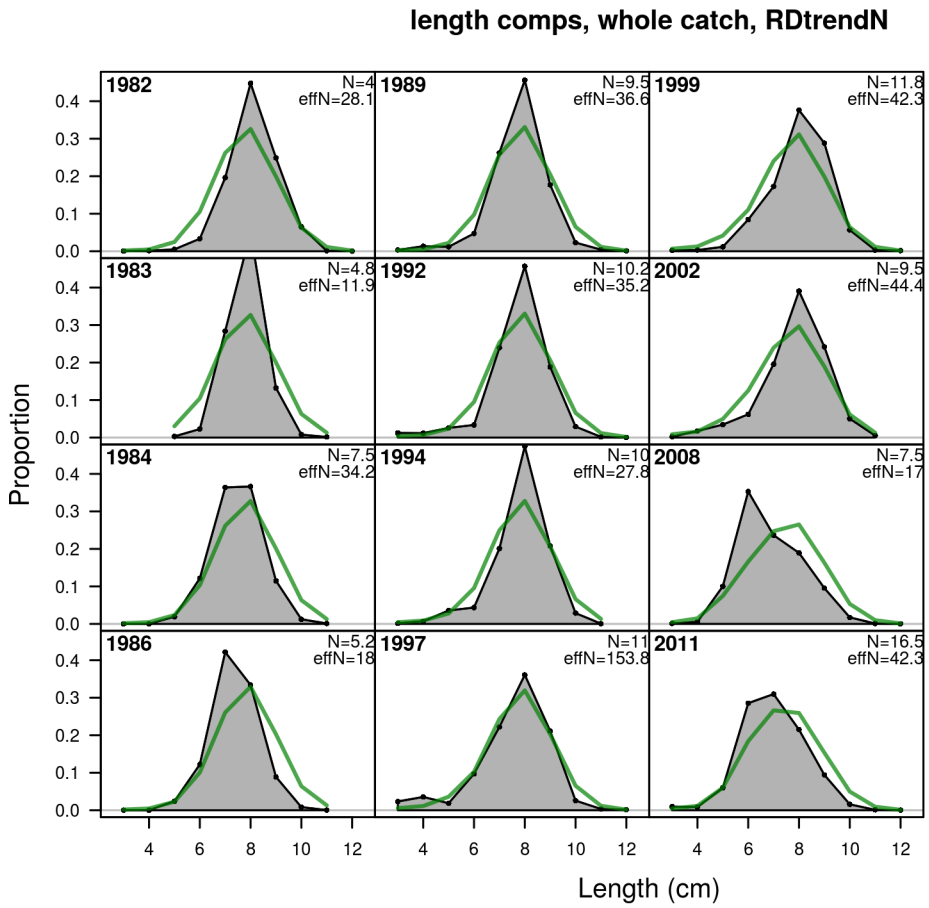

Figure 78: Model fit to length composition data from the NEFSC survey (RD) in the assessment model for ocean quahog in the northern area.

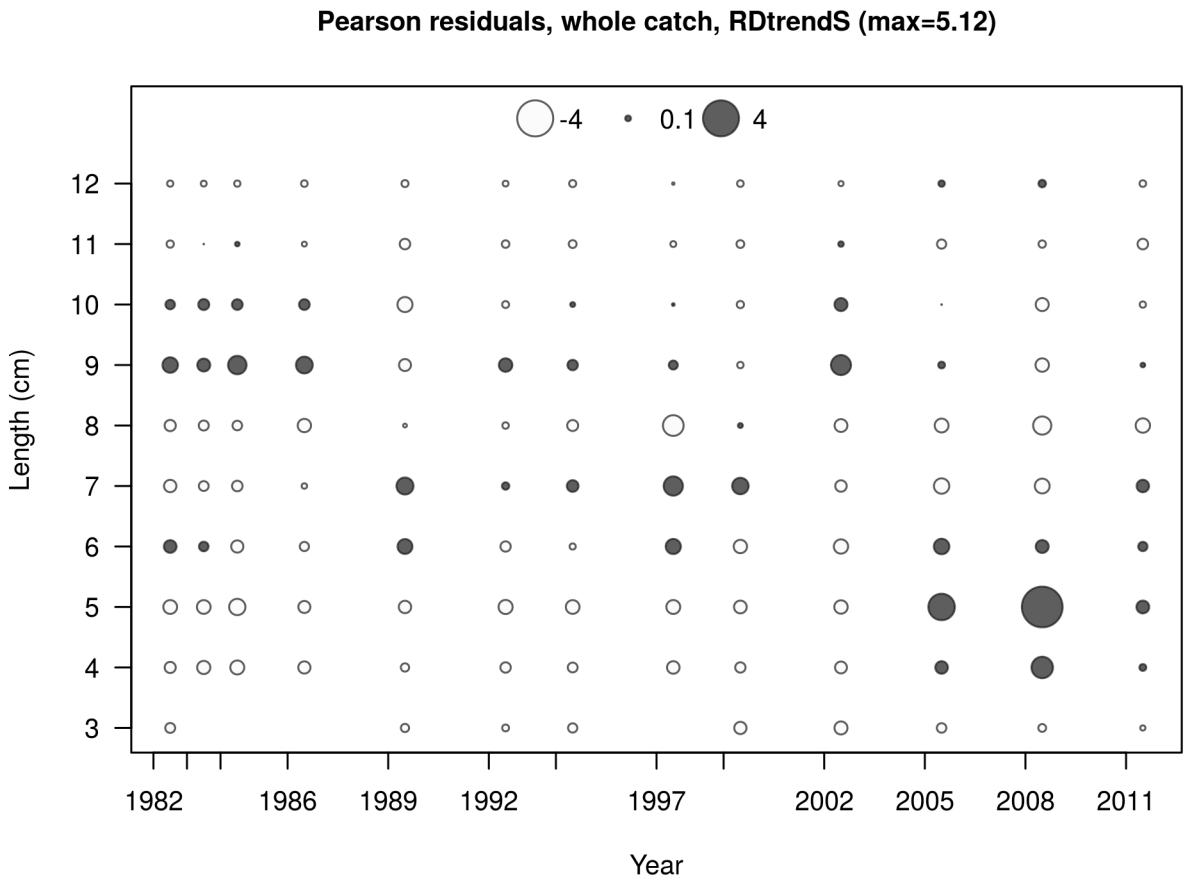

Figure 79: Pearson residuals from the fit to NEFSC survey (RD) length composition data in the assessment model for ocean quahog in the southern area. Closed bubbles are positive residuals (observed > expected) and open bubbles are negative residuals (observed < expected).

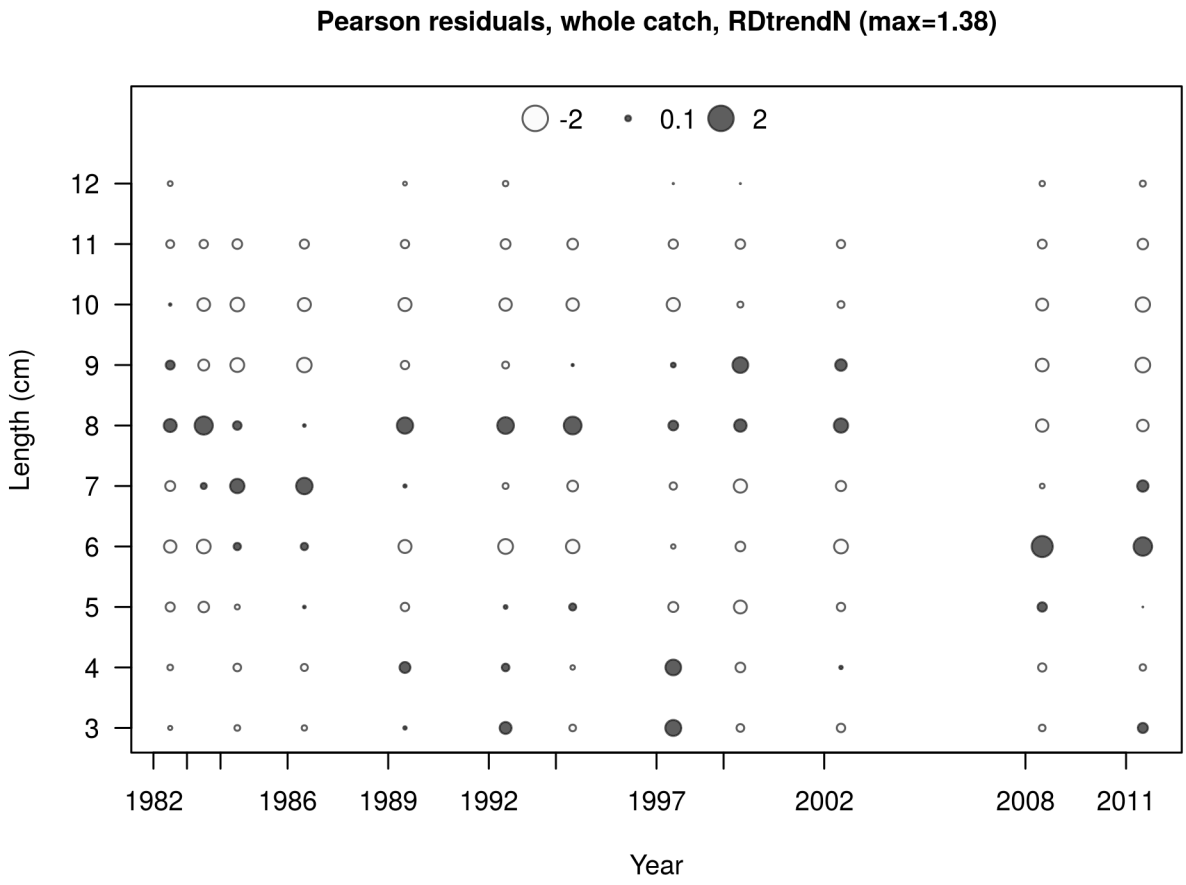

Figure 80: Pearson residuals from the fit to NEFSC survey (RD) length composition data in the assessment model for ocean quahog in the northern area. Closed bubbles are positive residuals (observed > expected) and open bubbles are negative residuals (observed < expected).

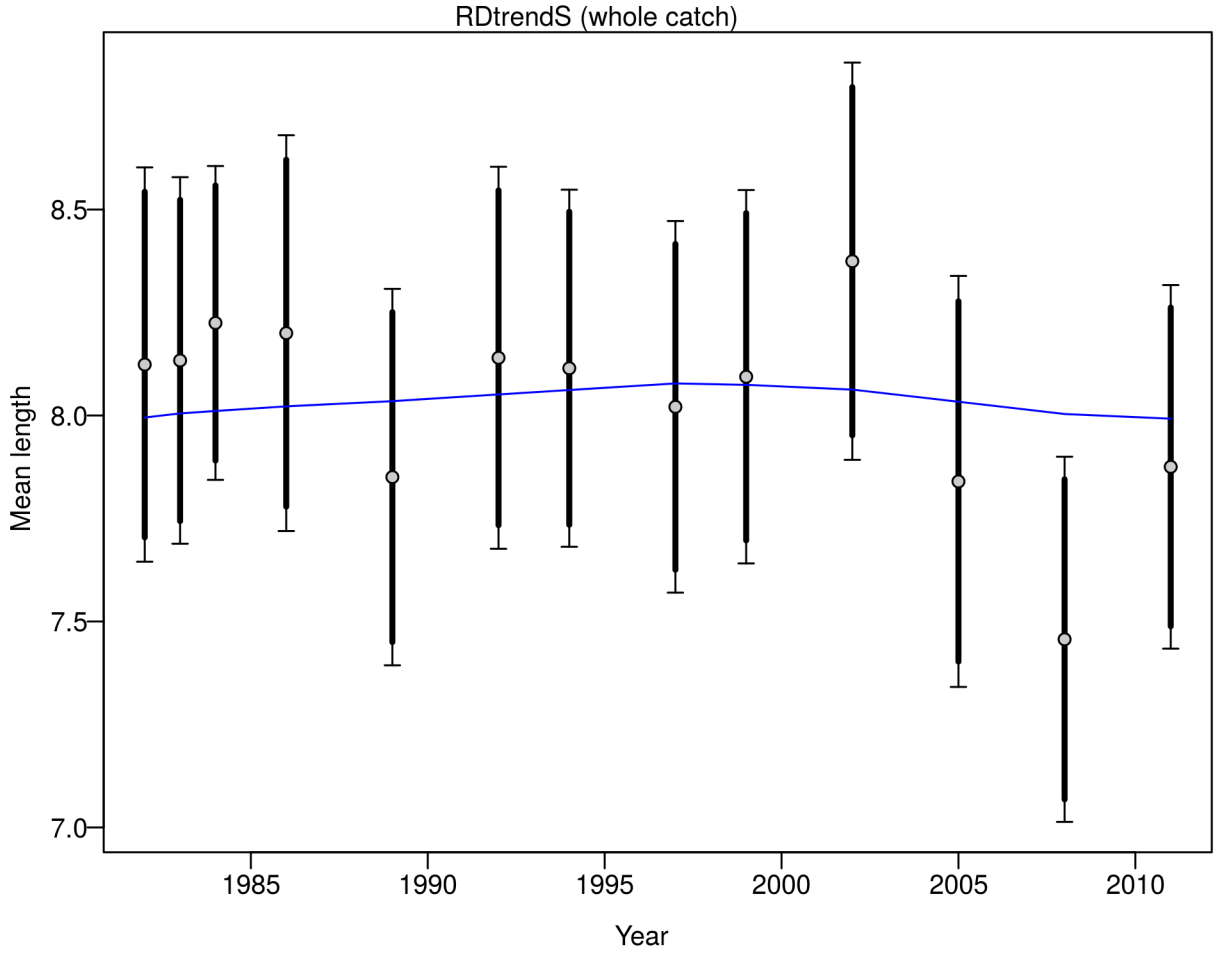

Figure 81: Observed mean length (cm) vs. the mean length predicted by the model based on fits to NEFSC survey (RD) length composition data in the assessment model for ocean quahog in the southern area.

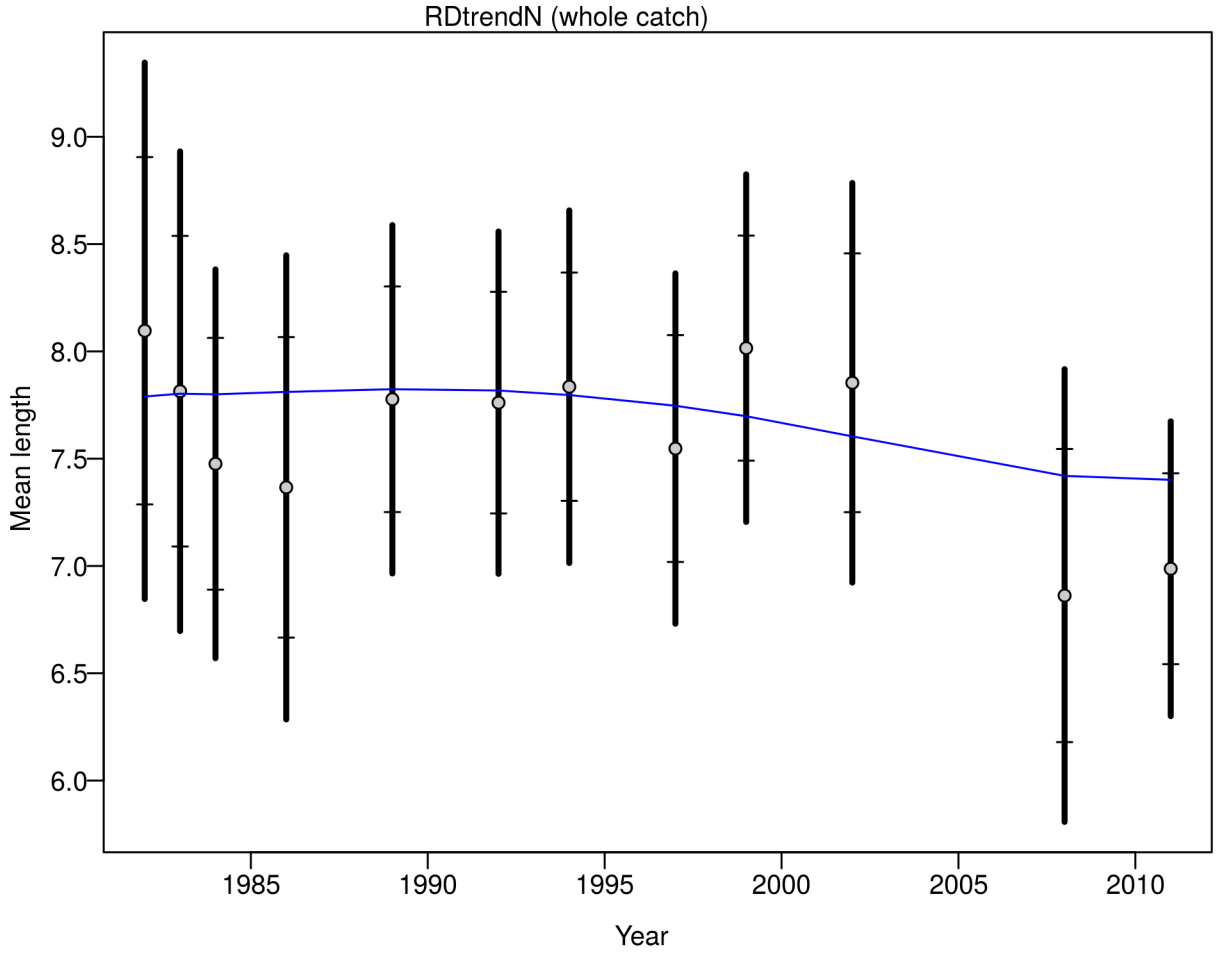

Figure 82: Observed mean length (cm) vs. the mean length predicted by the model based on fits to NEFSC survey (RD) length composition data in the assessment model for ocean quahog in the northern area.

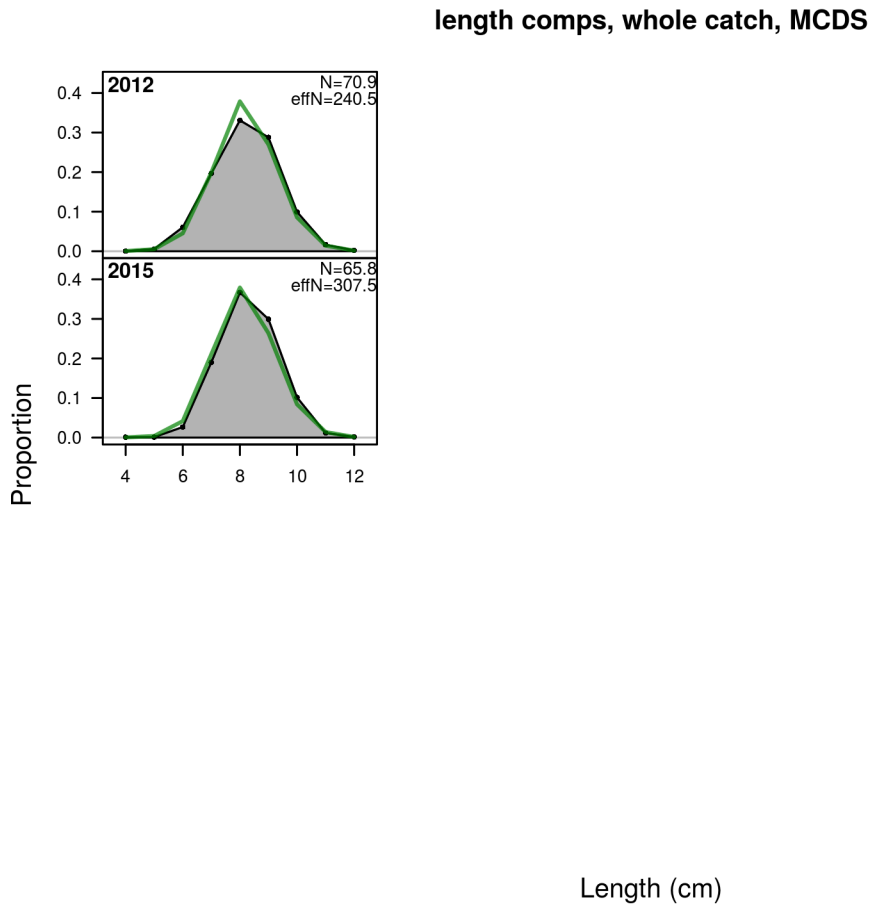

Figure 83: Model fit to length composition data from the NEFSC survey (MCD) in the assessment model for ocean quahog in the southern area.

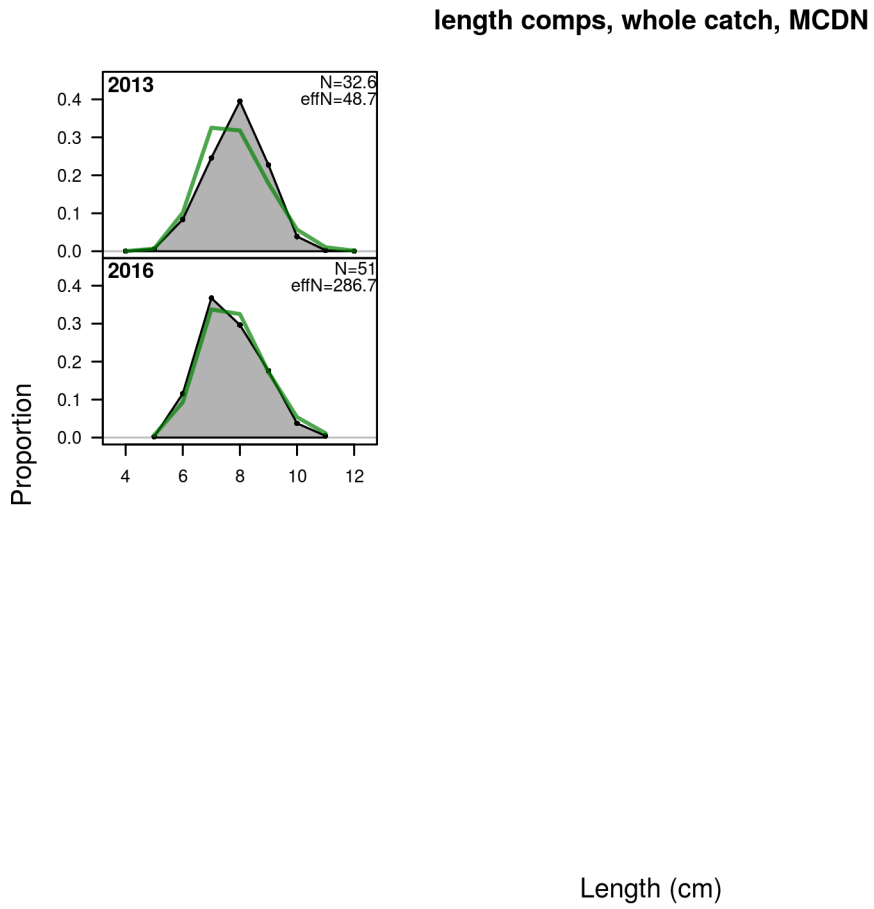

Figure 84: Model fit to length composition data from the NEFSC survey (MCD) in the assessment model for ocean quahog in the northern area.

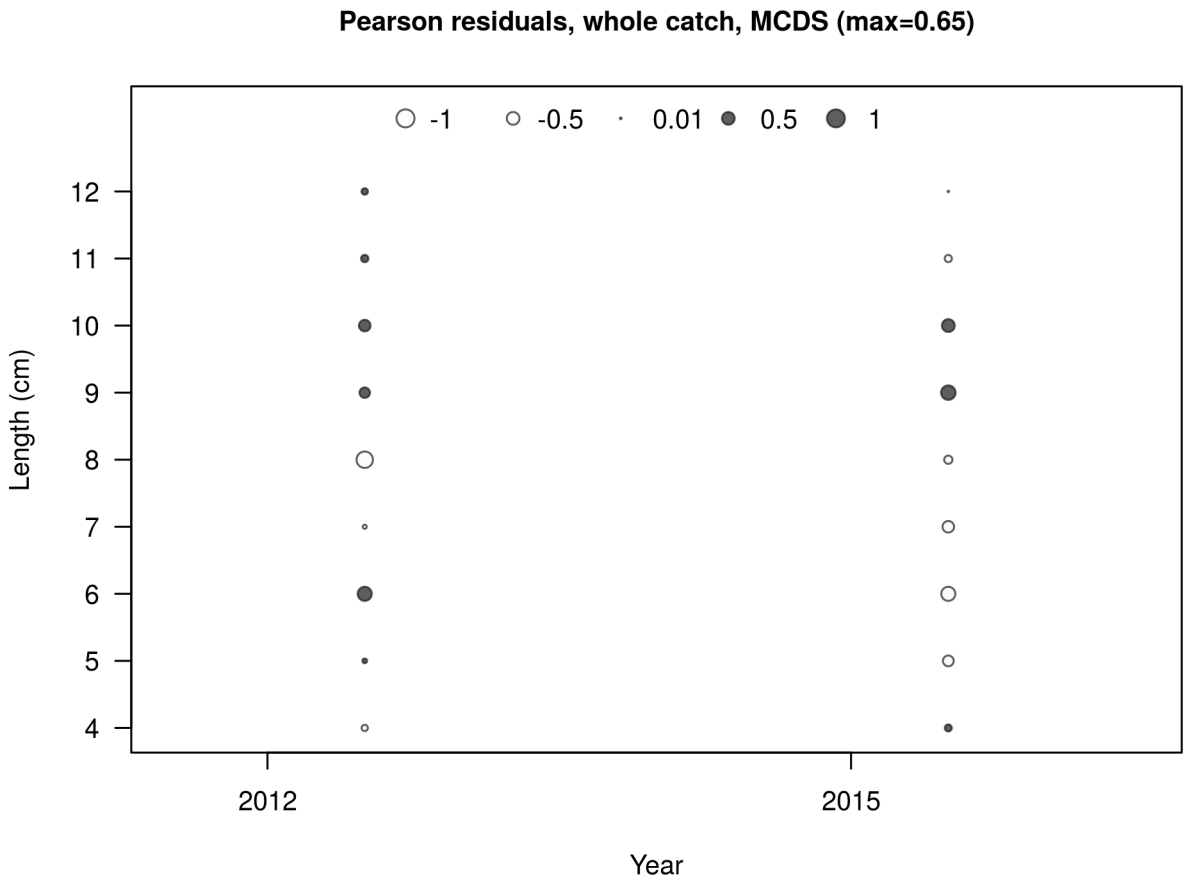

Figure 85: Pearson residuals from the fit to NEFSC survey (MCD) length composition data in the assessment model for ocean quahog in the southern area. Closed bubbles are positive residuals (observed > expected) and open bubbles are negative residuals (observed < expected).

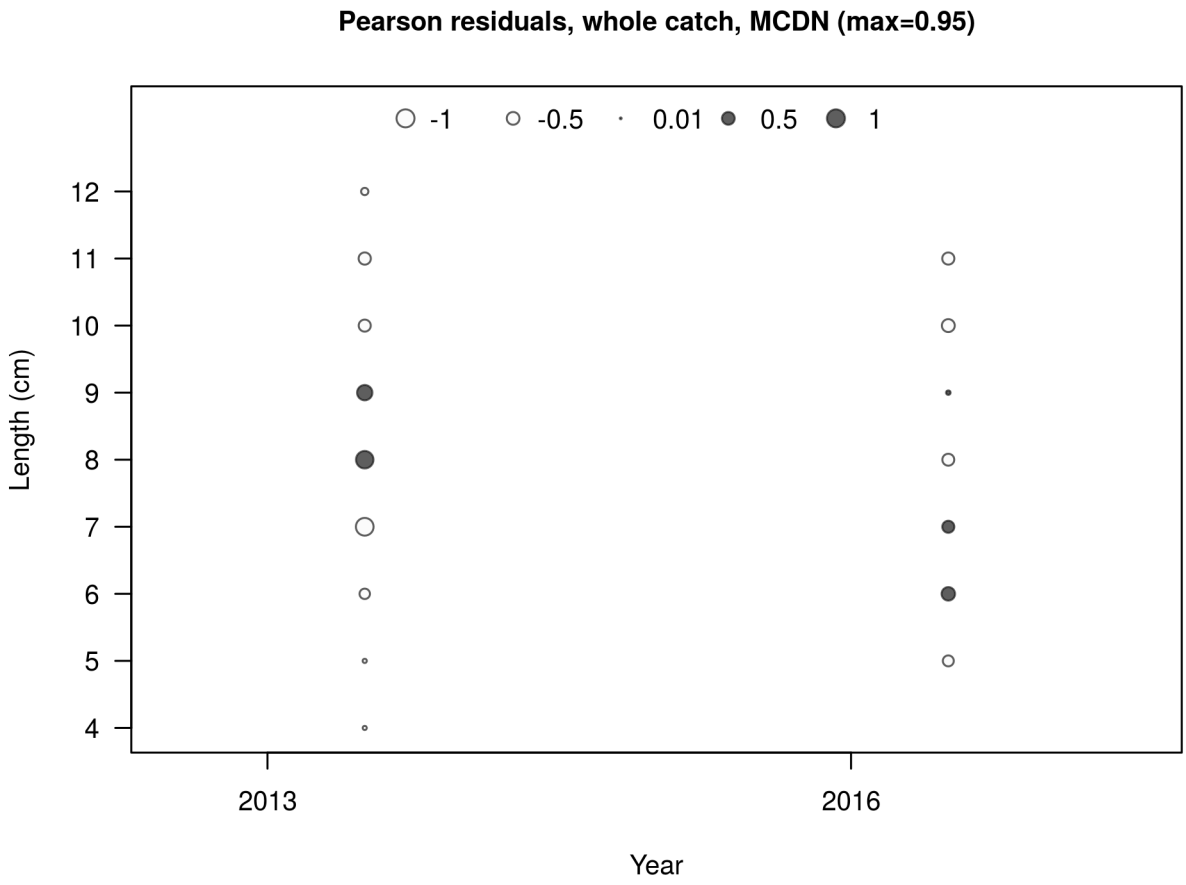

Figure 86: Pearson residuals from the fit to NEFSC survey (MCD) length composition data in the assessment model for ocean quahog in the northern area. Closed bubbles are positive residuals (observed > expected) and open bubbles are negative residuals (observed < expected).

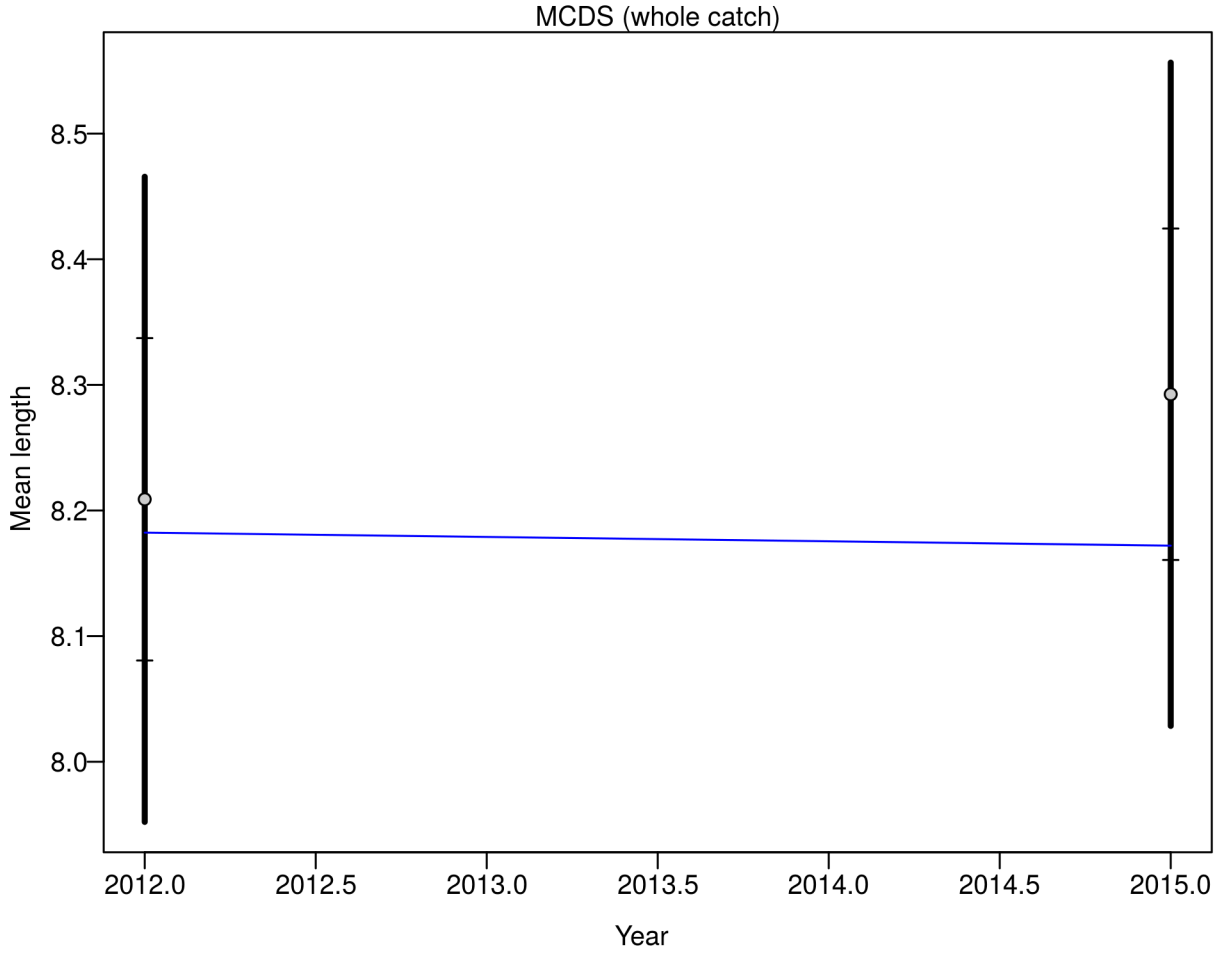

Figure 87: Observed mean length (cm) vs. the mean length predicted by the model based on fits to NEFSC survey (MCD) length composition data in the assessment model for ocean quahog in the southern area.

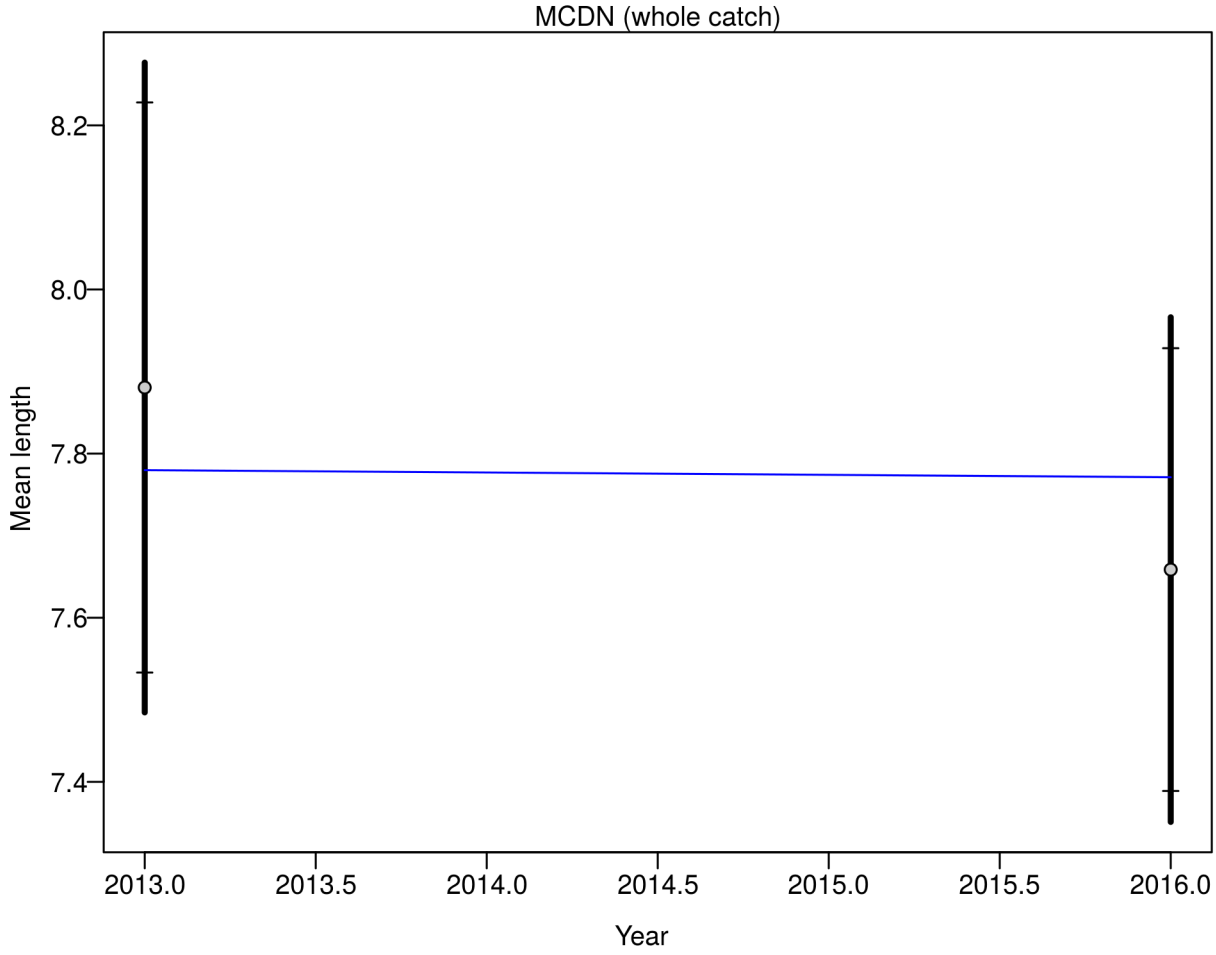

Figure 88: Observed mean length (cm) vs. the mean length predicted by the model based on fits to NEFSC survey (MCD) length composition data in the assessment model for ocean quahog in the northern area.

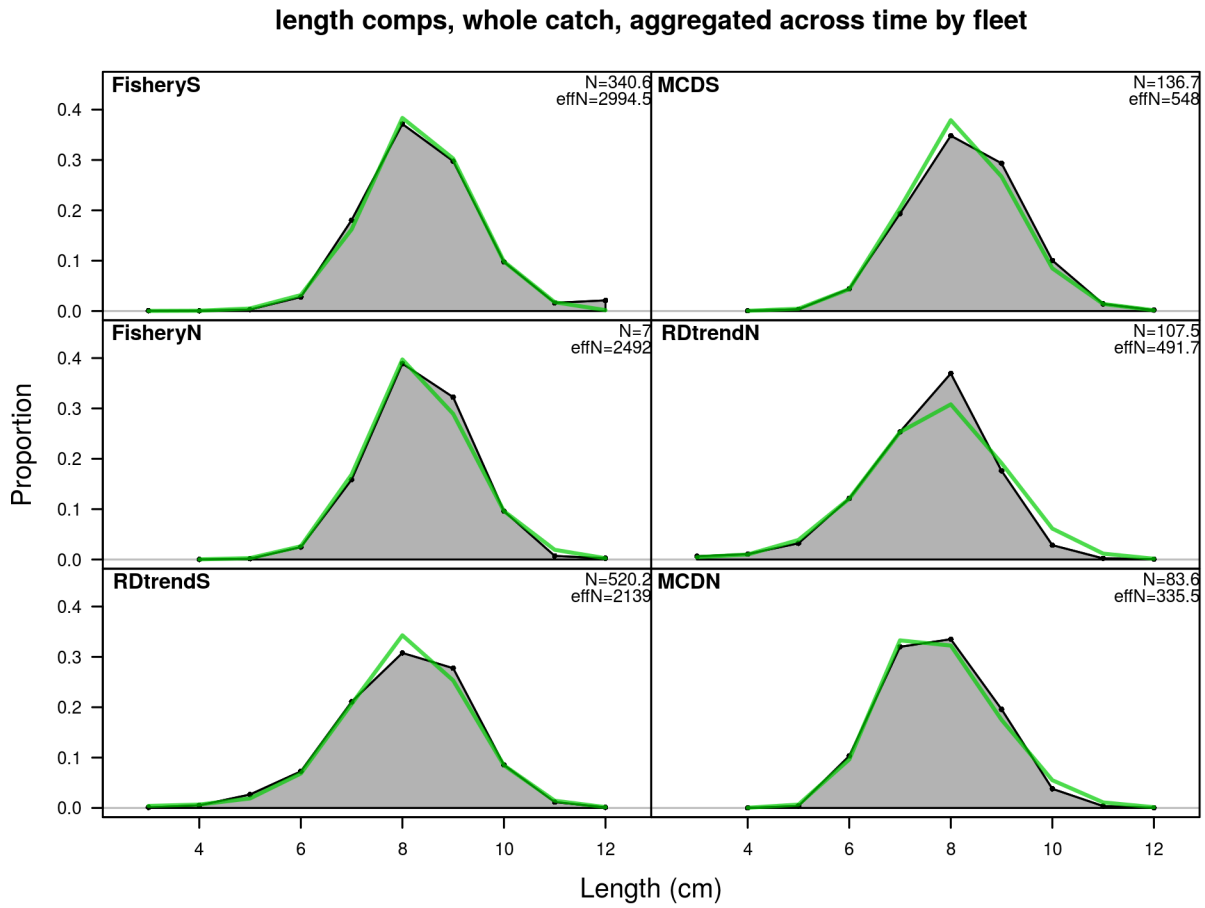

Figure 89: Model fit to length composition data from all sources aggregated across time, in the assessment model for ocean quahog.

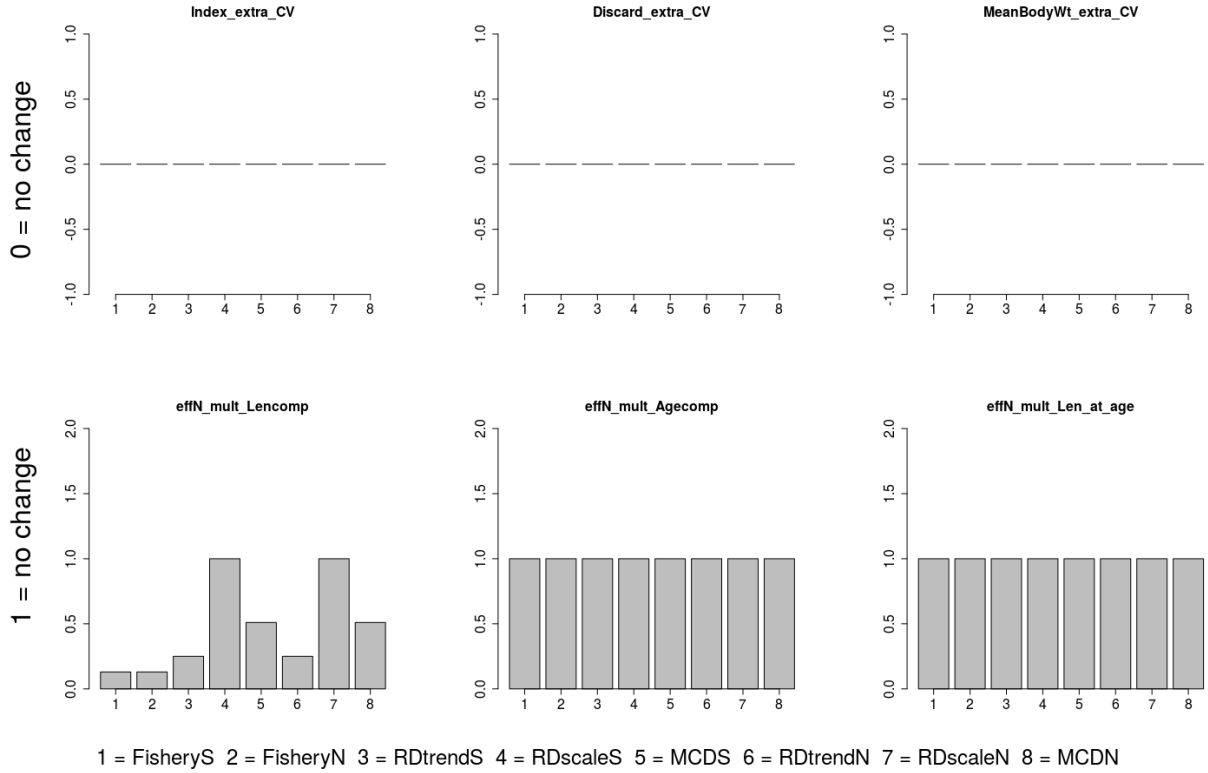

Figure 90: Adjustments made to variance components of model parameters in the assessment model for ocean quahog. The bar plots reflect data weighting decisions. In the top row deviations from 0 are the amount added to the standard deviation used initially. In the bottom row, the value shown in the bar plot is multiplied by the initial effective sample size associated with each composition component. Thus, a value of less than 1 represents a reduction in the relative weight of a component.

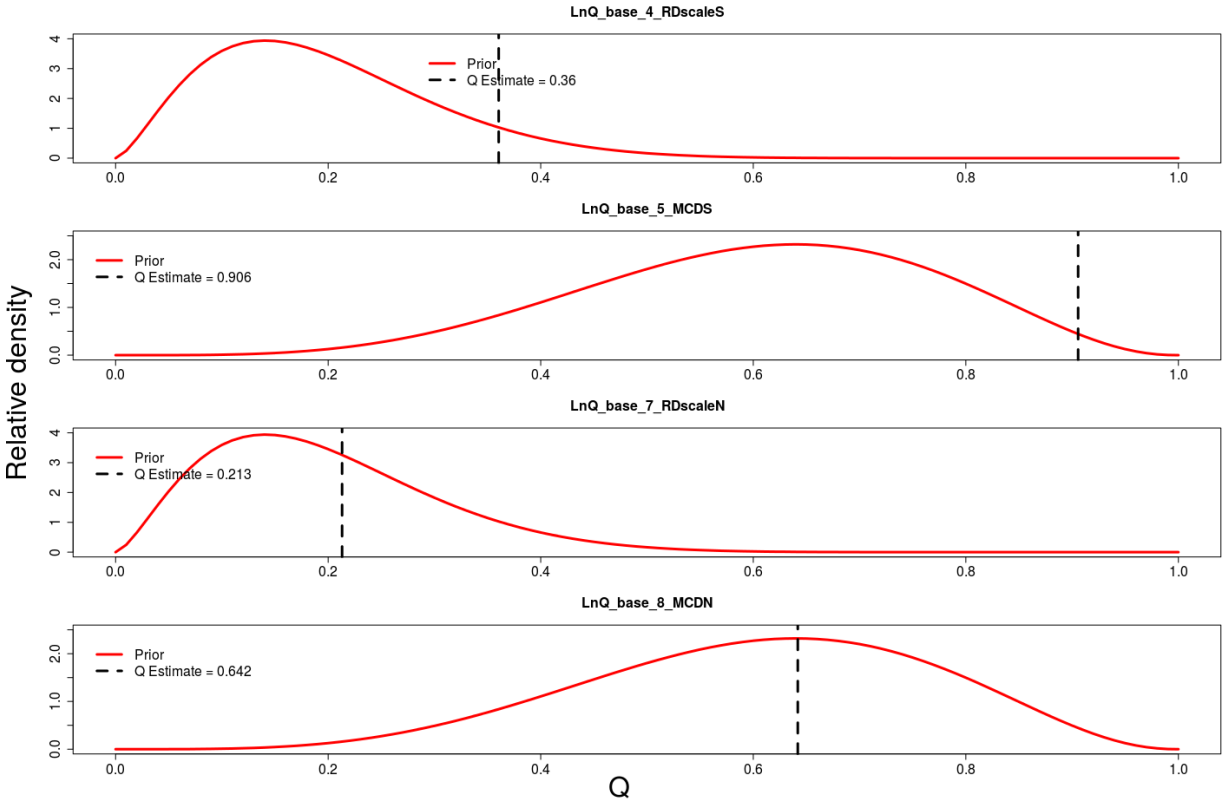

Figure 91: The prior distributions for catchability for each survey index and the model estimates that resulted from the basecase model for ocean quahog.

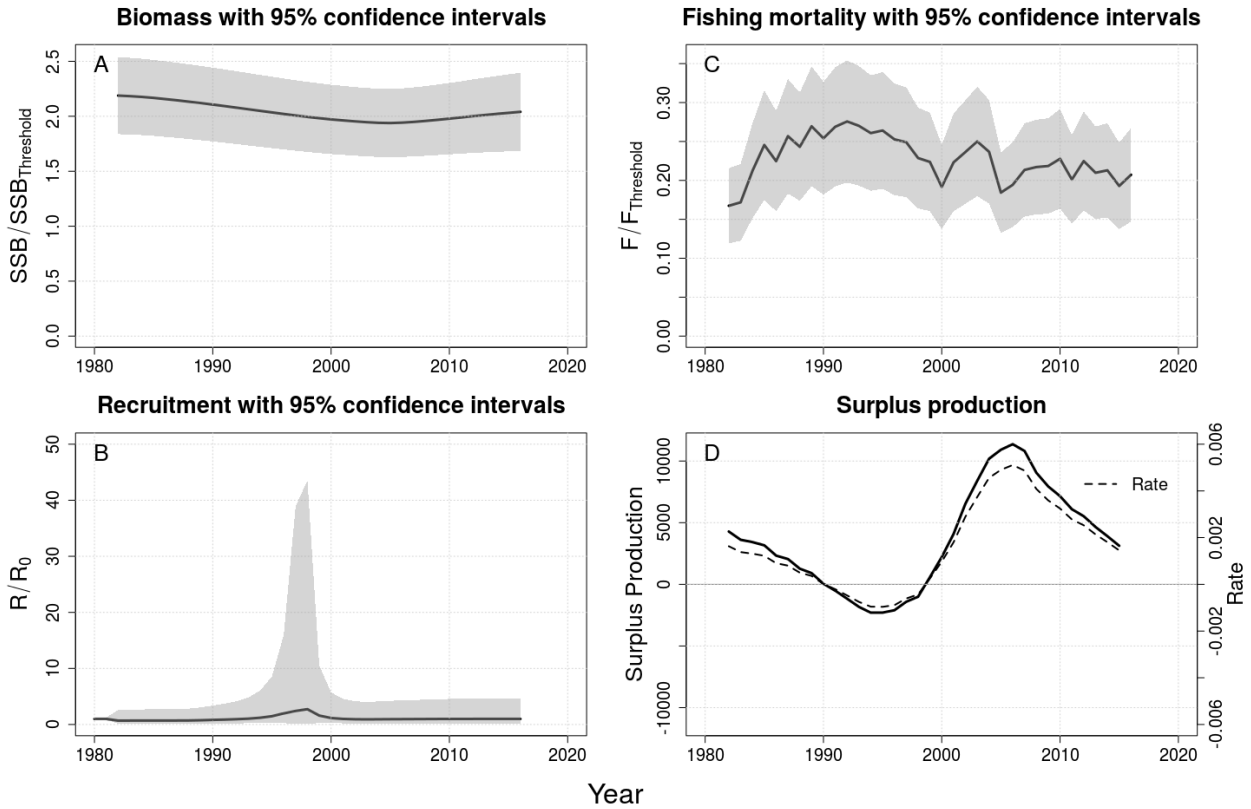

Figure 92: Trends and approximate 95% asymmetric confidence intervals for, (A) estimated SSB, (B) estimated recruitment, (C) estimated fully selected fishing mortality, and (D) surplus production with surplus production rate.

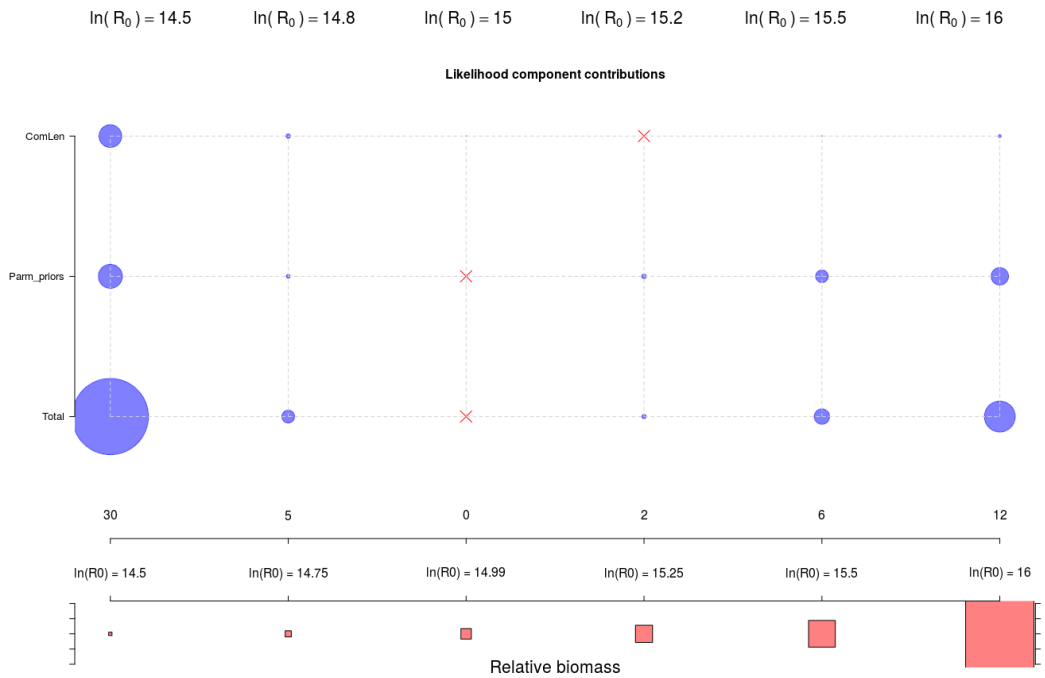

Figure 93: Likelihood profile over the virgin recruitment parameter (R0). A total of 5 model runs are depicted here. In each case, the R0 parameter was fixed at a different value. The columns of the large plot show how the component and total likelihoods change as the R0 parameter is varied. Each column of the large bubble plot represents one model run and the non-zero likelihood components in each run are shown in rows. For each row, the minimum likelihood component value was subtracted from each individual value, such that the minimum value in each row is represented by a red x. Bubbles are proportional to the values of each likelihood component in each run. The base value for R0 is the value at the model solution (middle column). The difference (in likelihood units) between each column and the minimum total likelihood is shown just above the x axis. Conflicts within the data are apparent when the minimum likelihood values (red x's) occur in different columns for each row. The red boxes show the relative difference in estimated terminal year biomass between runs.

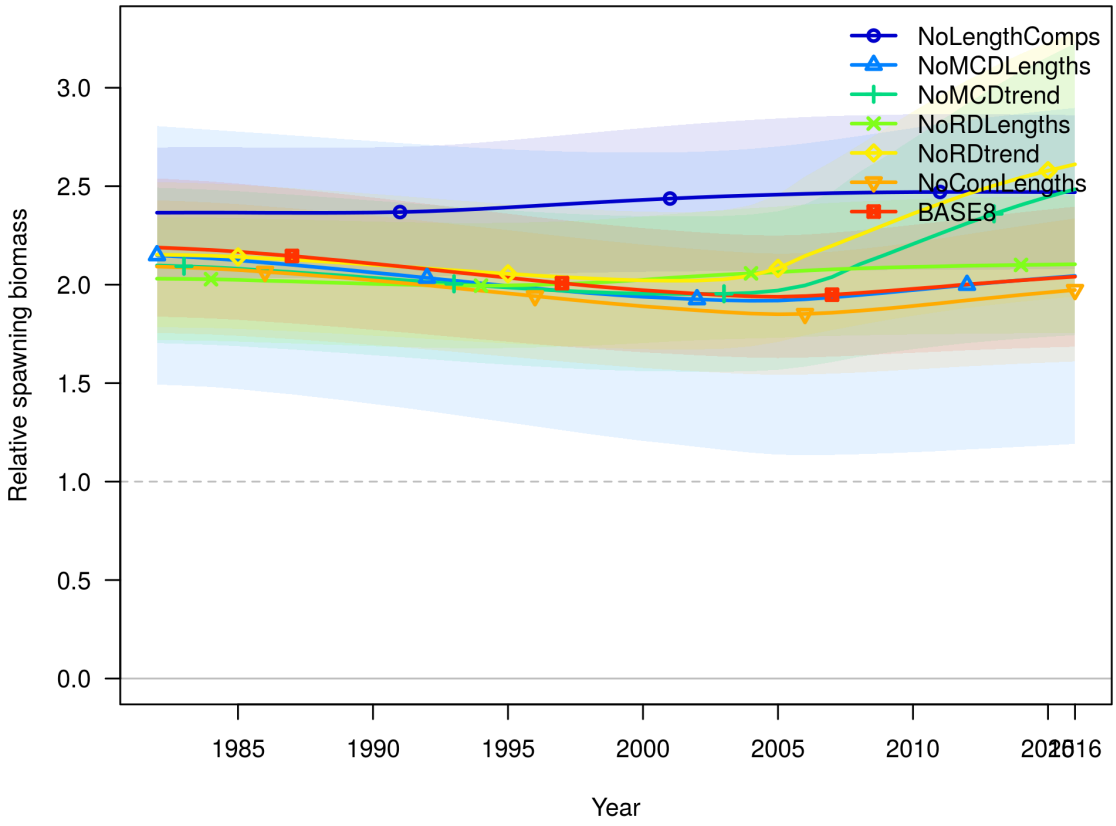

Figure 94: A comparison of the estimated biomass between the base run for ocean quahog (BASE8) and sensitivity runs in which different data were removed from the likelihood calculation (λ set to 0 for each component). The data removed were: all length composition data (NoLengthComps), lengths from the commercial fisheries (NoComLengths), lengths from the the MCD survey (NoMCDLengths), lengths from the RD survey (NoRDLengths), survey trend data from the MCD survey (NoMCDtrend), and survey trend data from the MCD survey (NoRDtrend).

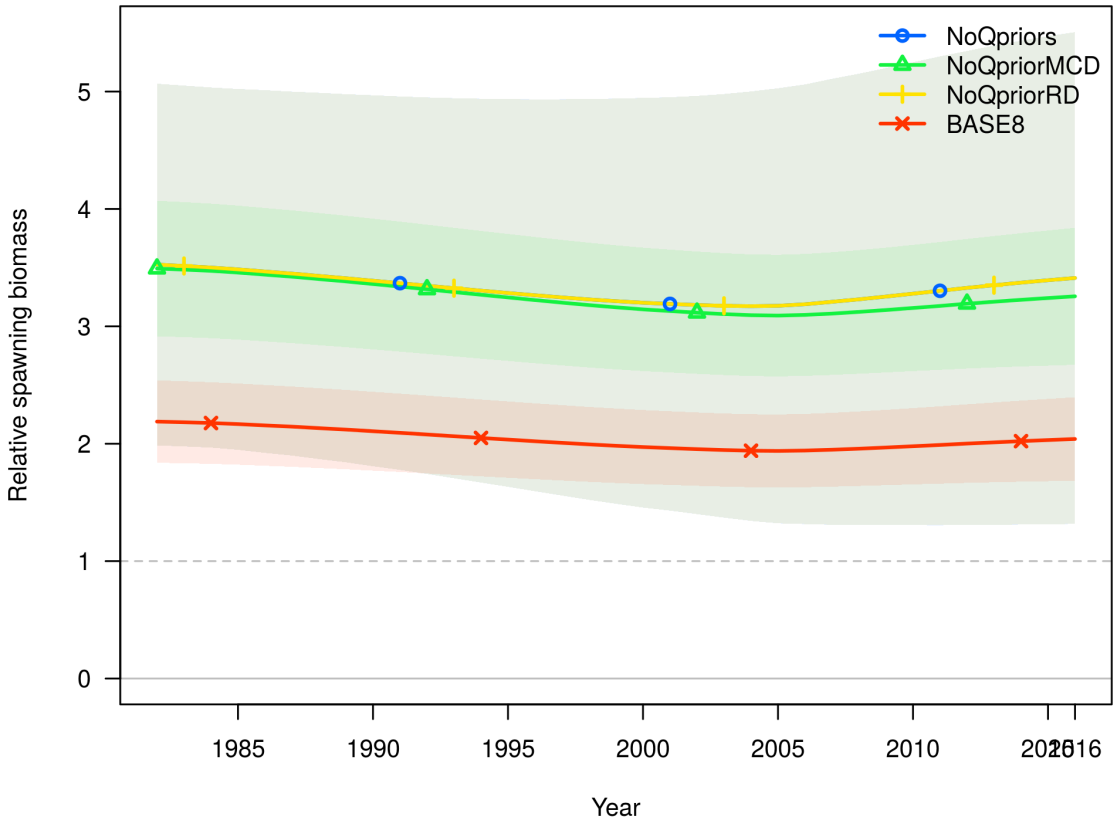

Figure 95: Biomass in model sensitivity runs for ocean quahog in which the priors for catchability from the surveys were not used compared to the base model (BASE8).

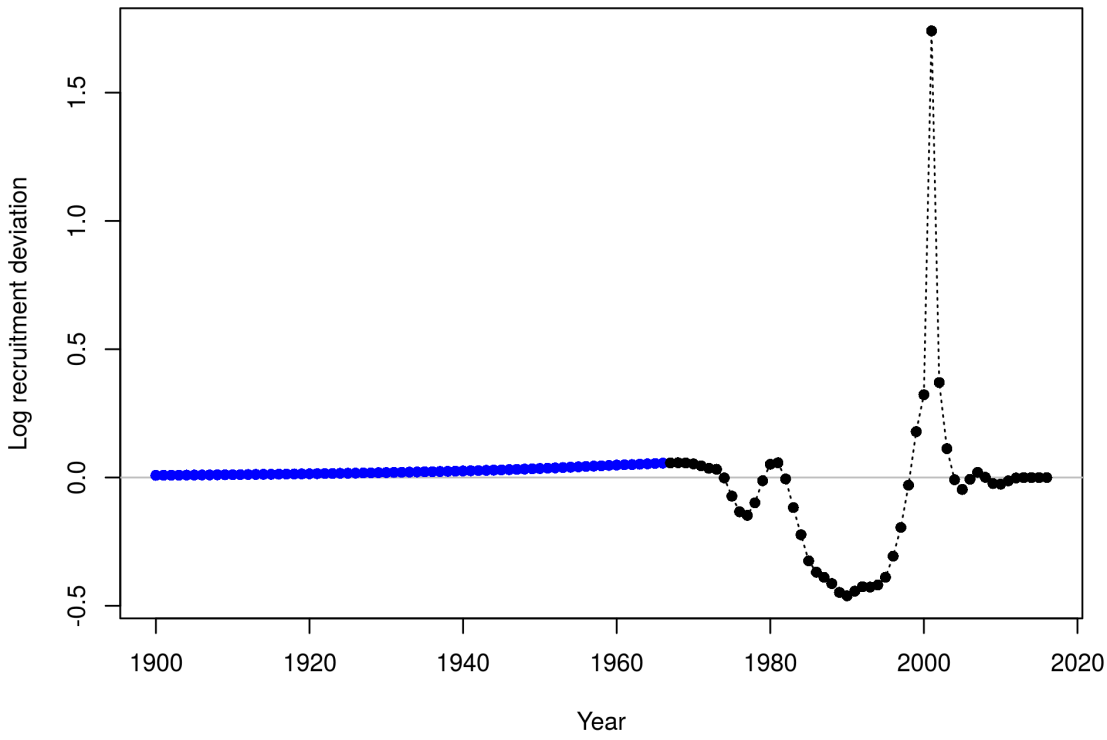

Figure 96: Recruitment deviations from a sensitivity run in which the recruitment variance was constrained relative to the base model.

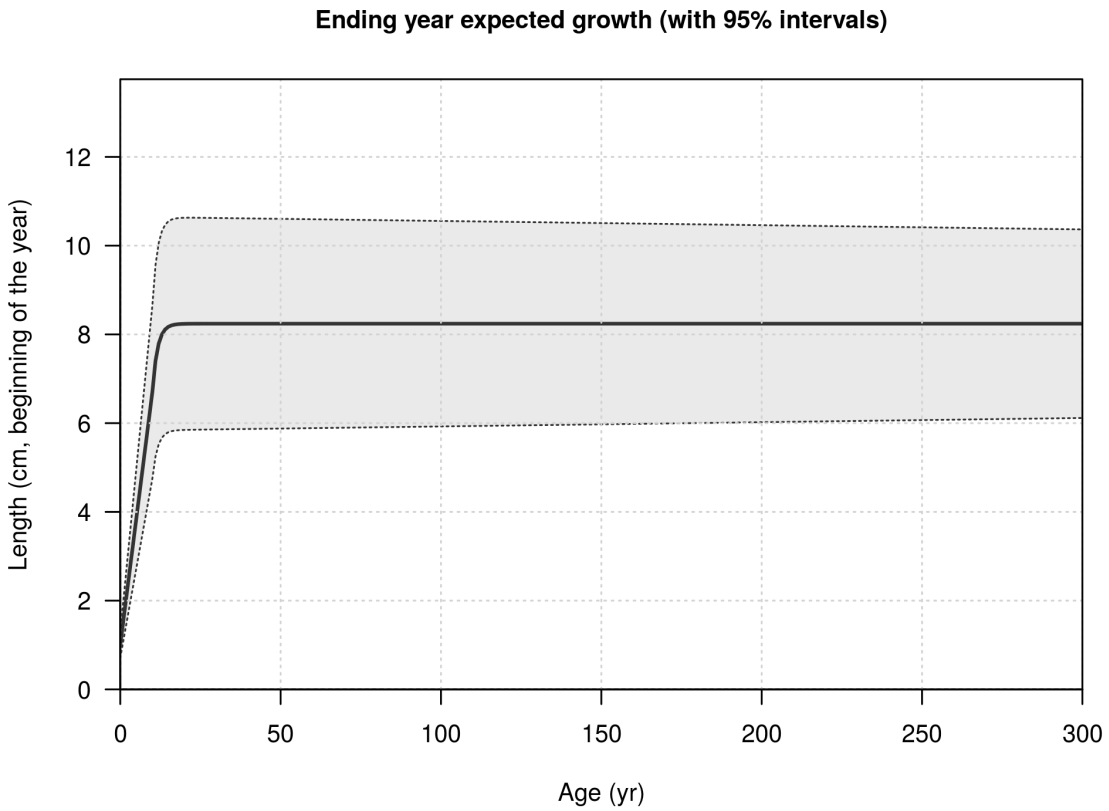

Figure 97: Growth curve from a sensitivity run in which the recruitment variance was constrained relative to the base model.

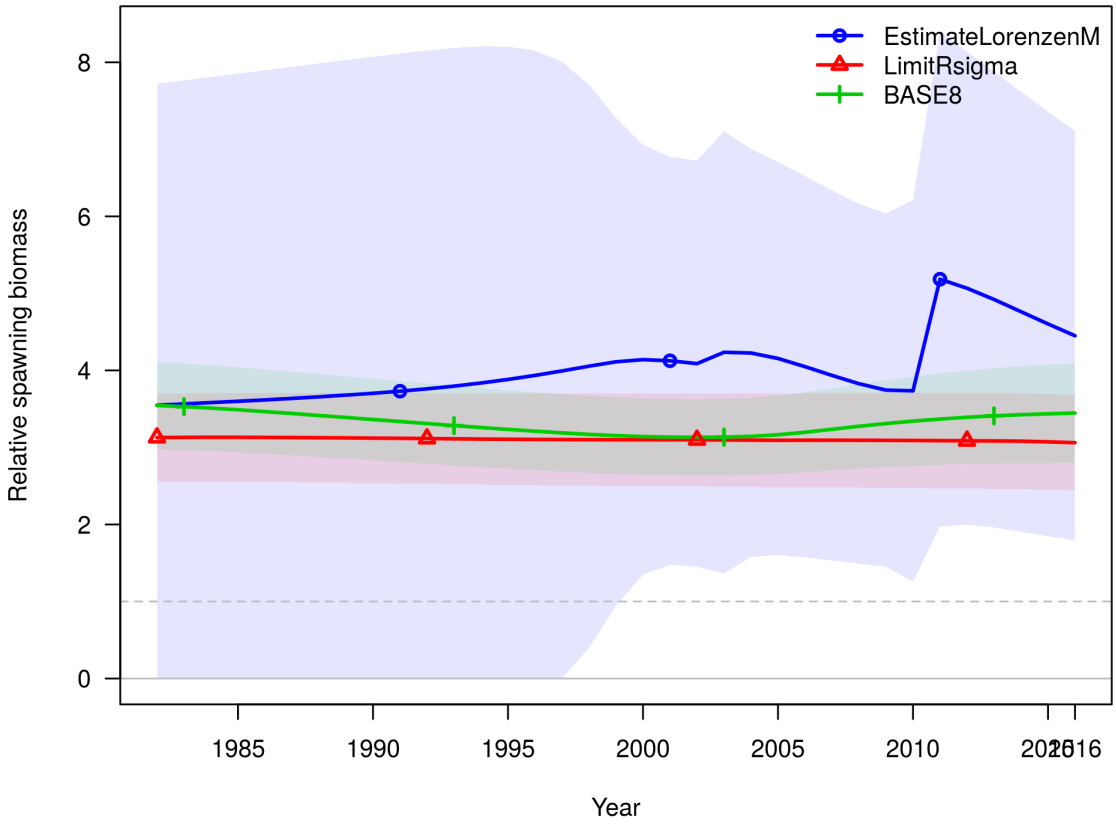

Figure 98: Biomass trends in model sensitivity runs for ocean quahog in which a Lorenzen M was estimated, and recruitment variance was tightly constrained, compared to the base model (BASE8).

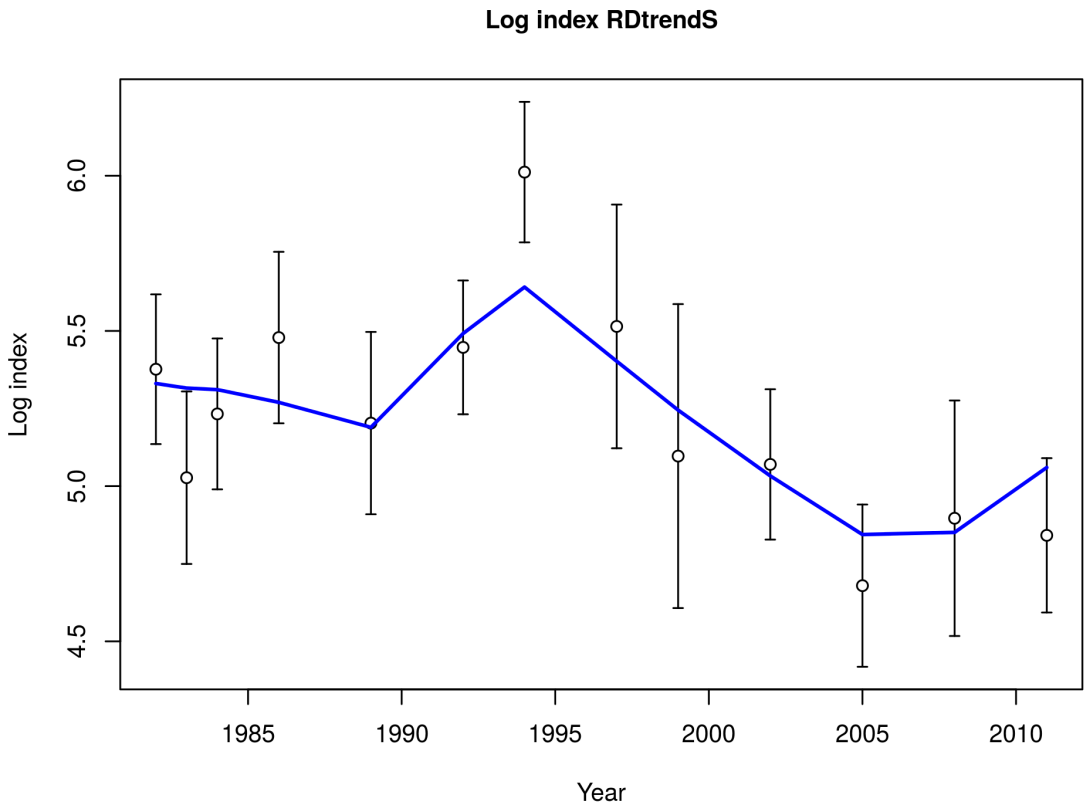

Figure 99: Fit to log index data on log scale for RDtrend survey for ocean quahog in the southern area from a sensitivity run in which a Lorenzen type natural mortality curve at age was estimated. Vertical lines are 95% confidence intervals.

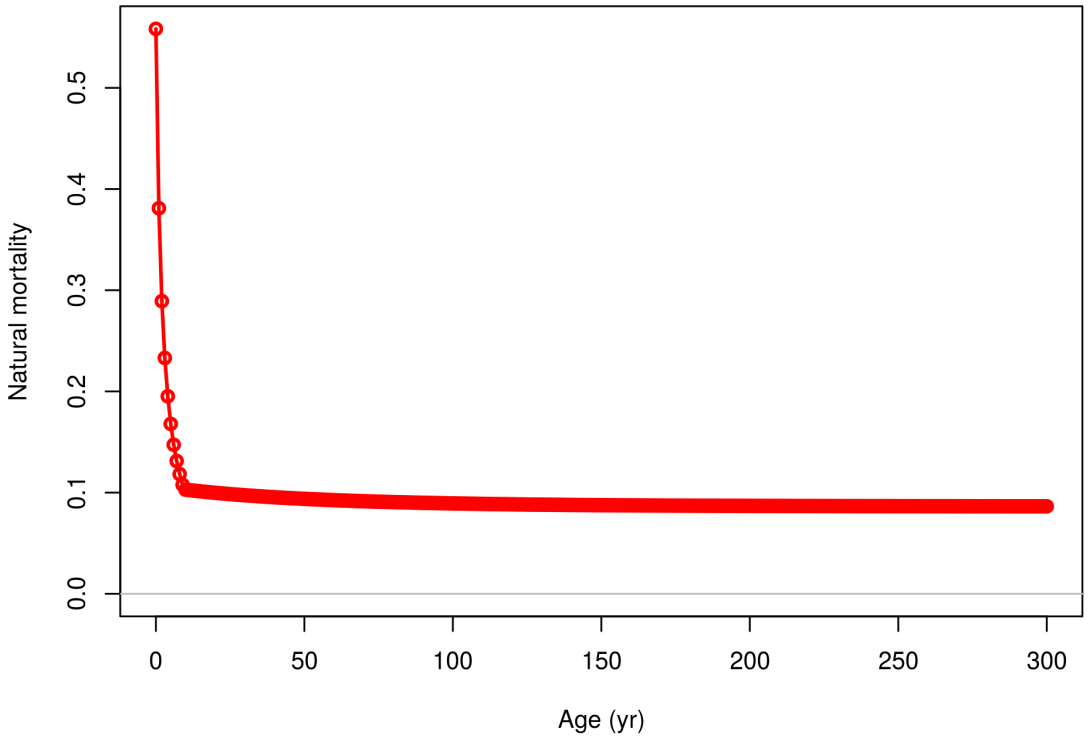

Figure 100: Natural mortality at age for ocean quahog from a sensitivity run in which a Lorenzen type natural mortality curve at age was estimated.

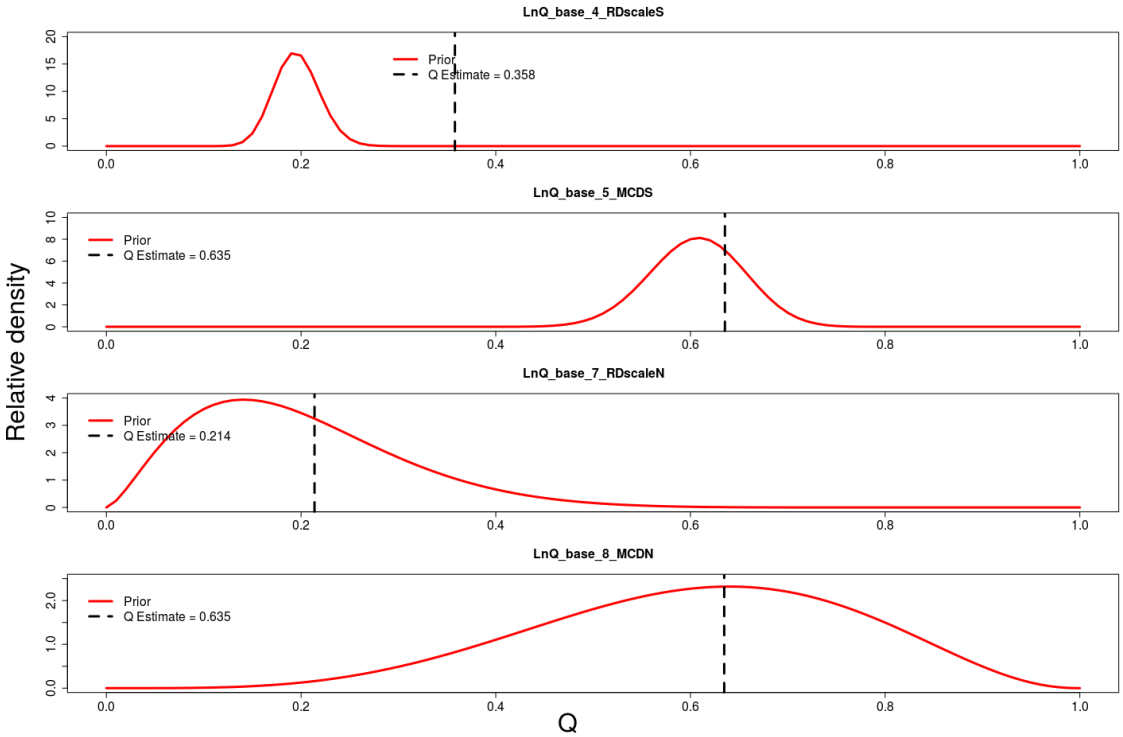

Figure 101: Estimated survey q with prior distributions for ocean quahog from a sensitivity run in which the variance of the prior distributions for survey q in the southern area was reduced, and the variance adjustments to the composition data for the southern area were reduced.

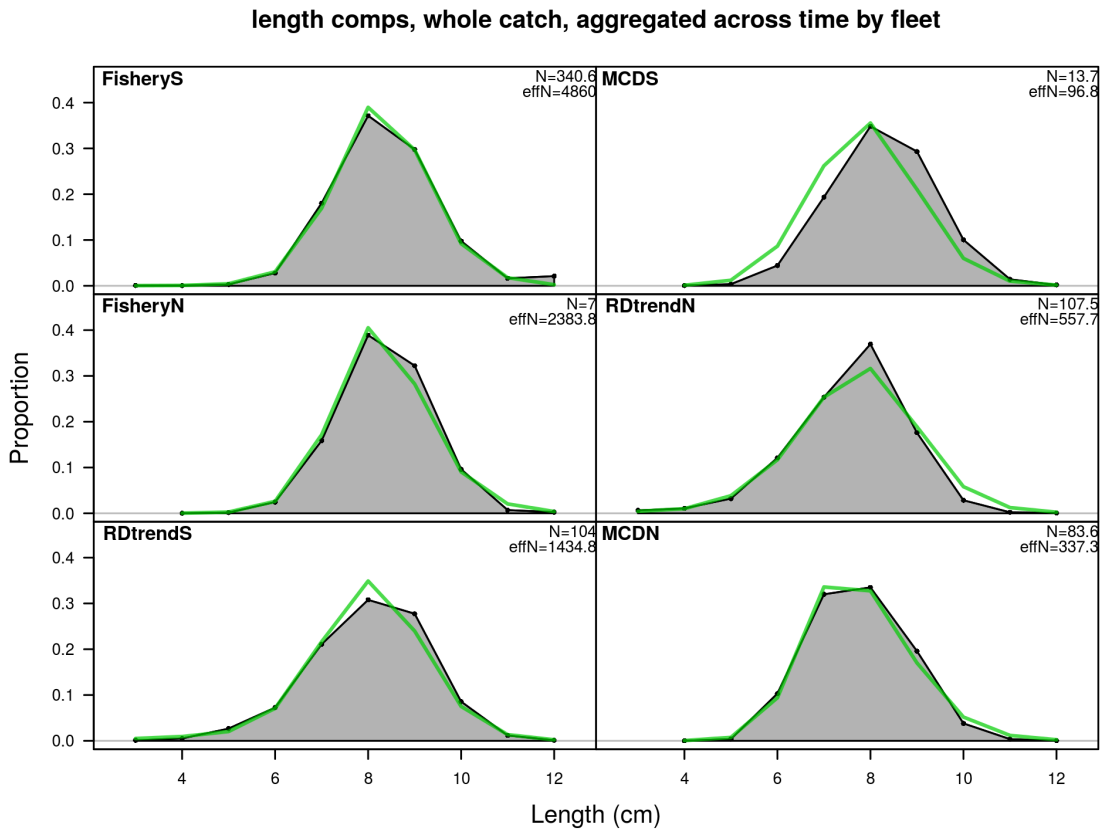

Figure 102: Model fit to length composition data from all sources aggregated across time for ocean quahog from a sensitivity run in which the variance of the prior distributions for survey q in the southern area was reduced, and the variance adjustments to the composition data for the southern area were reduced.

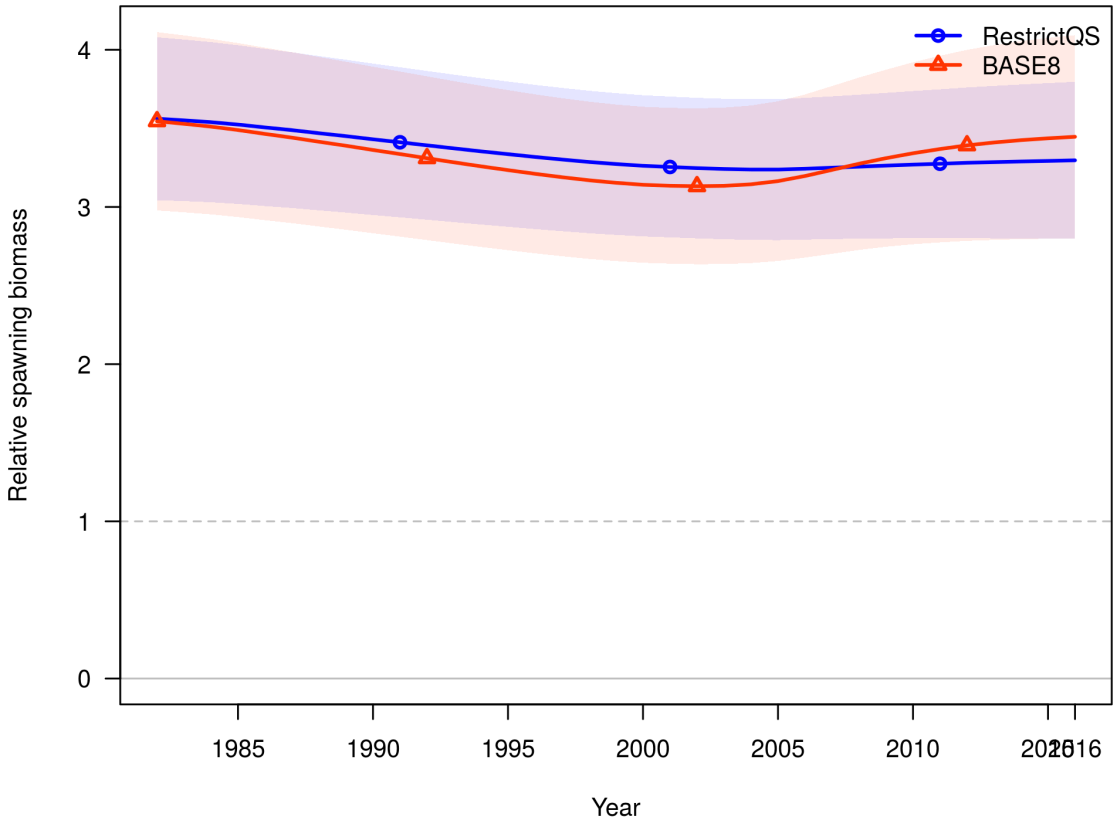

Figure 103: Biomass trends in model sensitivity runs for ocean quahog in which the variance of the prior distributions for survey q in the southern area was reduced, and the variance adjustments to the composition data for the southern area were reduced, compared to the base model (BASE8).

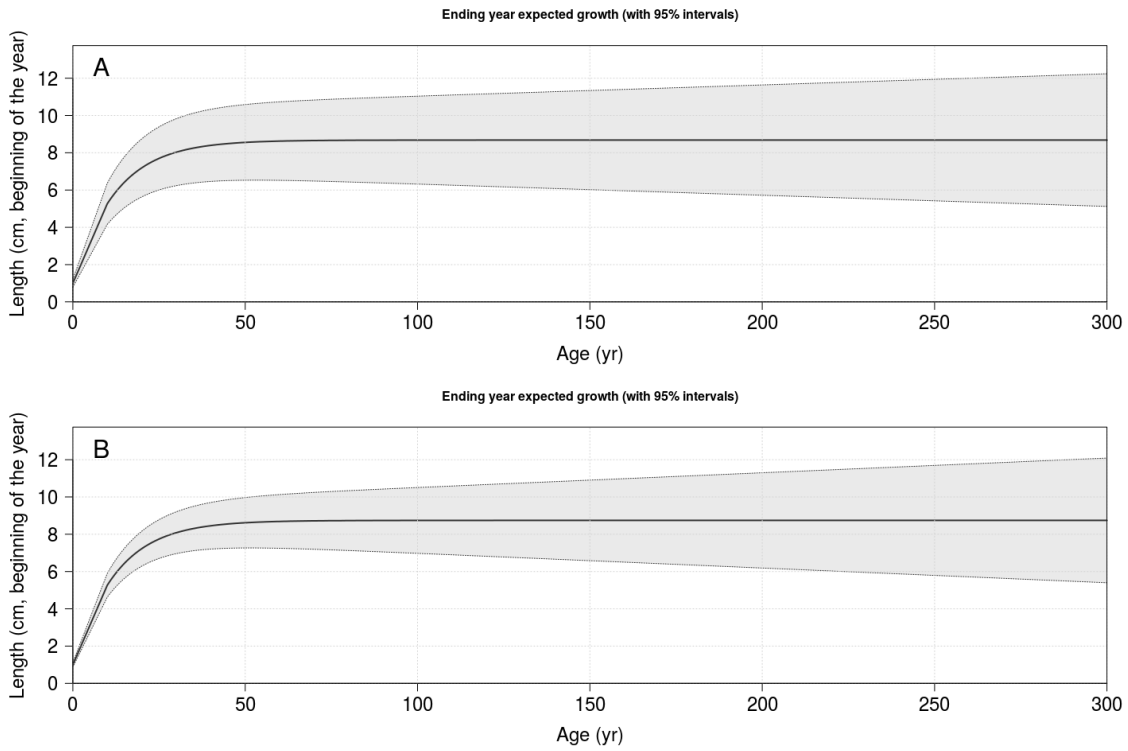

Figure 104: Length at age relationship by area from a sensitivity run for ocean quahog in which growth was allowed to vary by area, although the K parameter was fixed at the same value for each area.

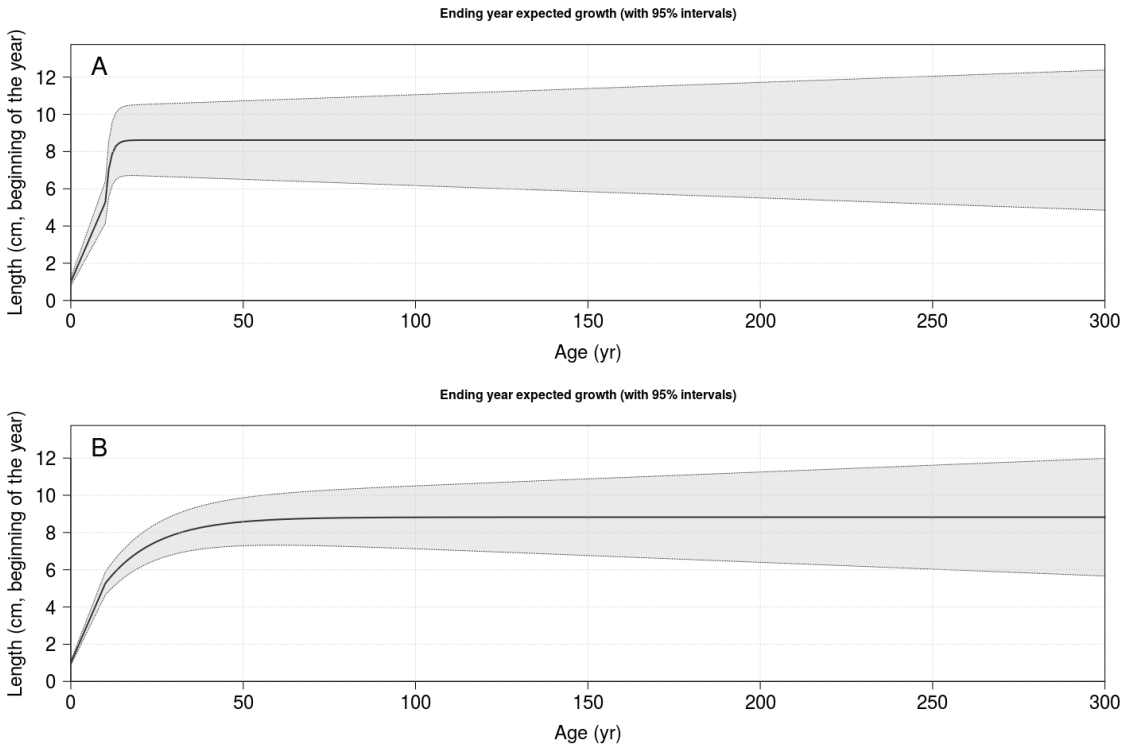

Figure 105: Length at age relationship by area from a sensitivity run for ocean quahog in which growth was allowed to vary freely by area.

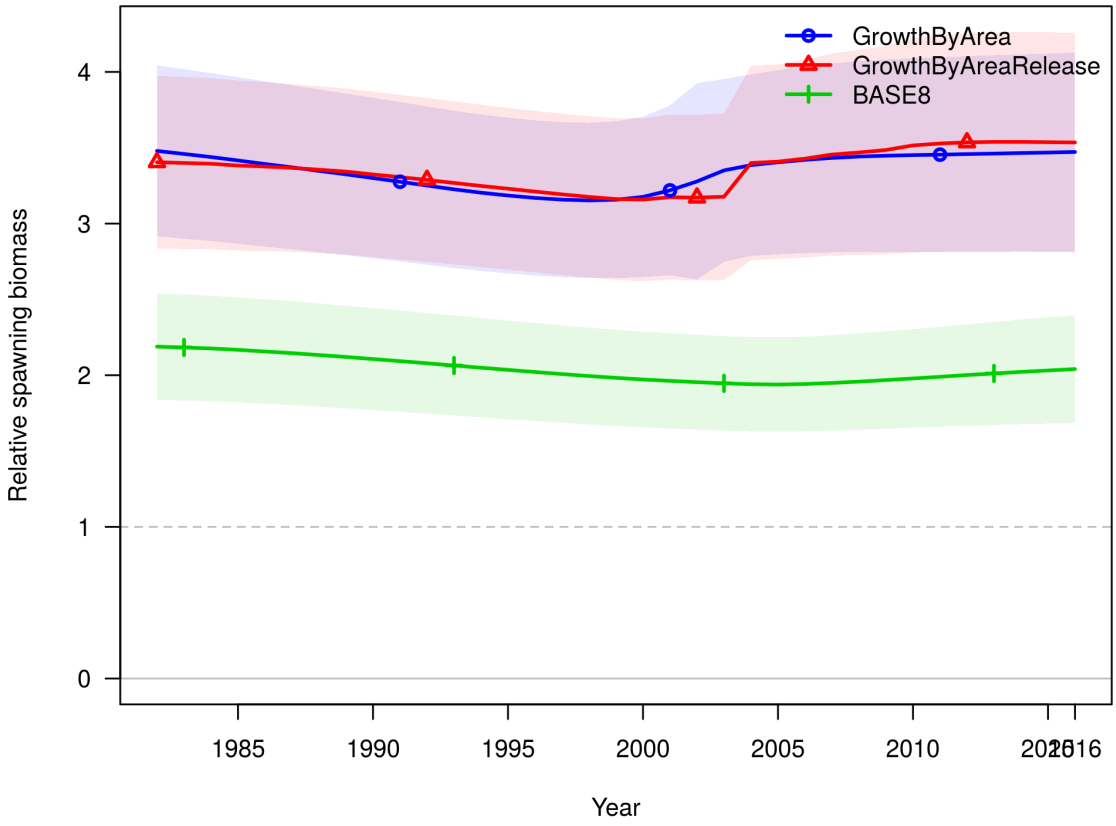

Figure 106: Biomass trends in model sensitivity runs for ocean quahog in which growth was allowed to vary by area with the K parameter fixed at the same value for each area (GrowthByArea), and where growth was allowed to vary freely by area (GrowthByAreaRelease), compared to the base model (BASE8).

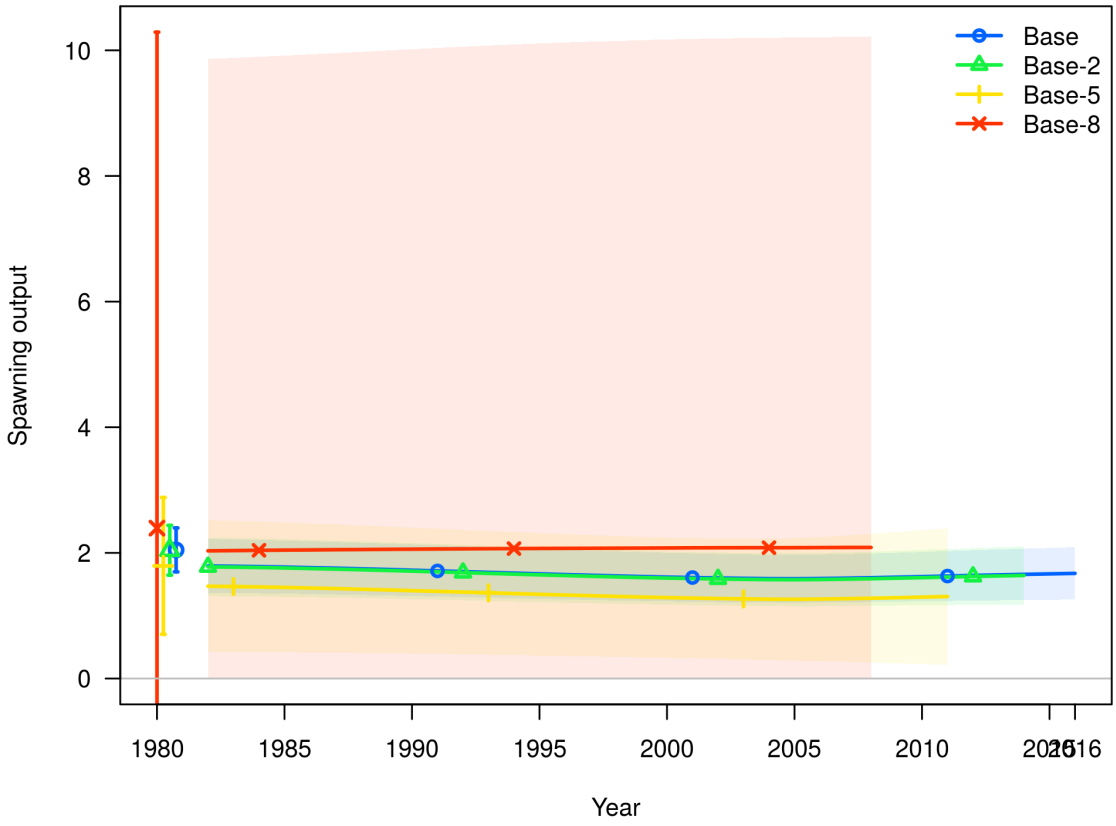

Figure 107: Biomass scale and uncertainty from 4 retrospective runs of the model for ocean quahog. The y axis is the proportional number of spawning clams in all areas. The biomass scale changes slightly, and uncertainty increases substantially, as survey data are removed.

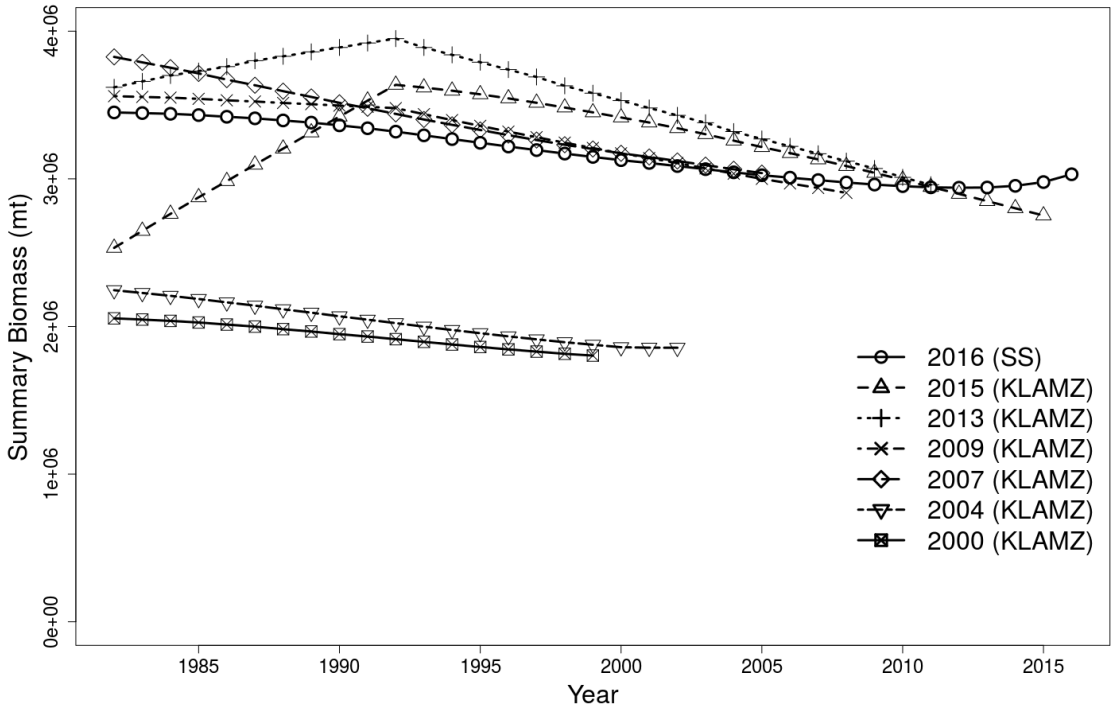

Figure 108: Historical retrospective plot showing the biomass trajectory from each of the previous ocean quahog assessments as well as the KLAMZ model run from Appendix 6 (2015) and the current SS base model (2016). All biomasses shown are "summary", which corresponds to all animals older than 20 years in SS and all animals longer than 50 mm in all other models.

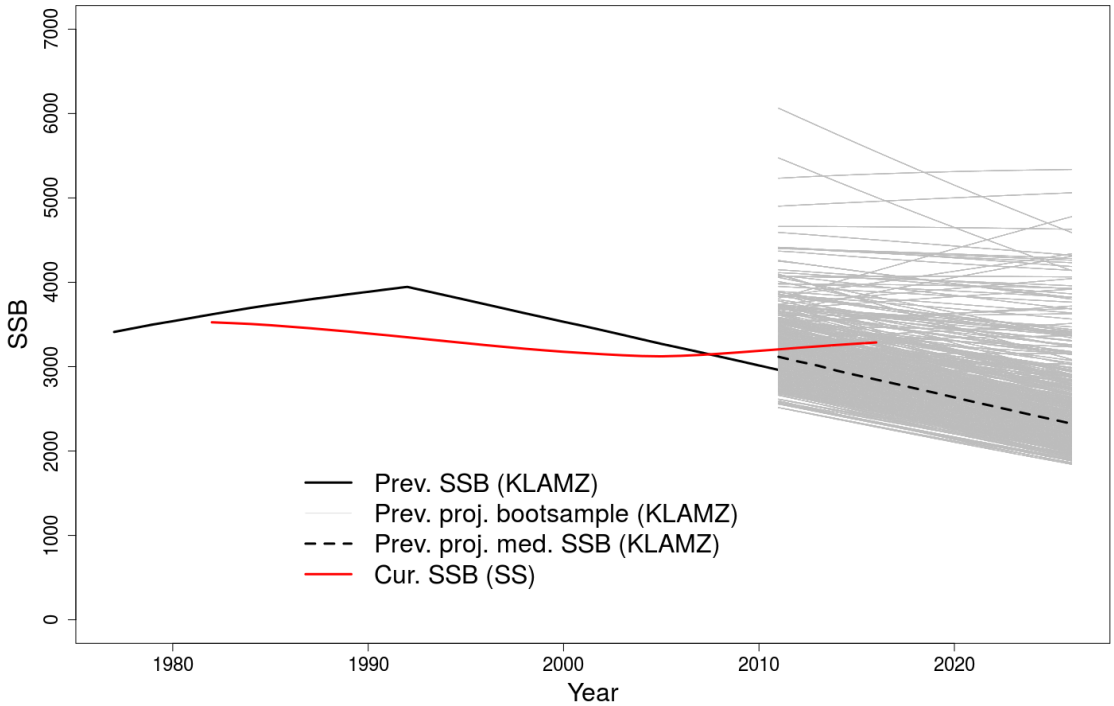

Figure 109: Point estimates of SSB, bootstrap projections, and median projected SSB from the previous assessment, compared to the current point estimates of SSB.

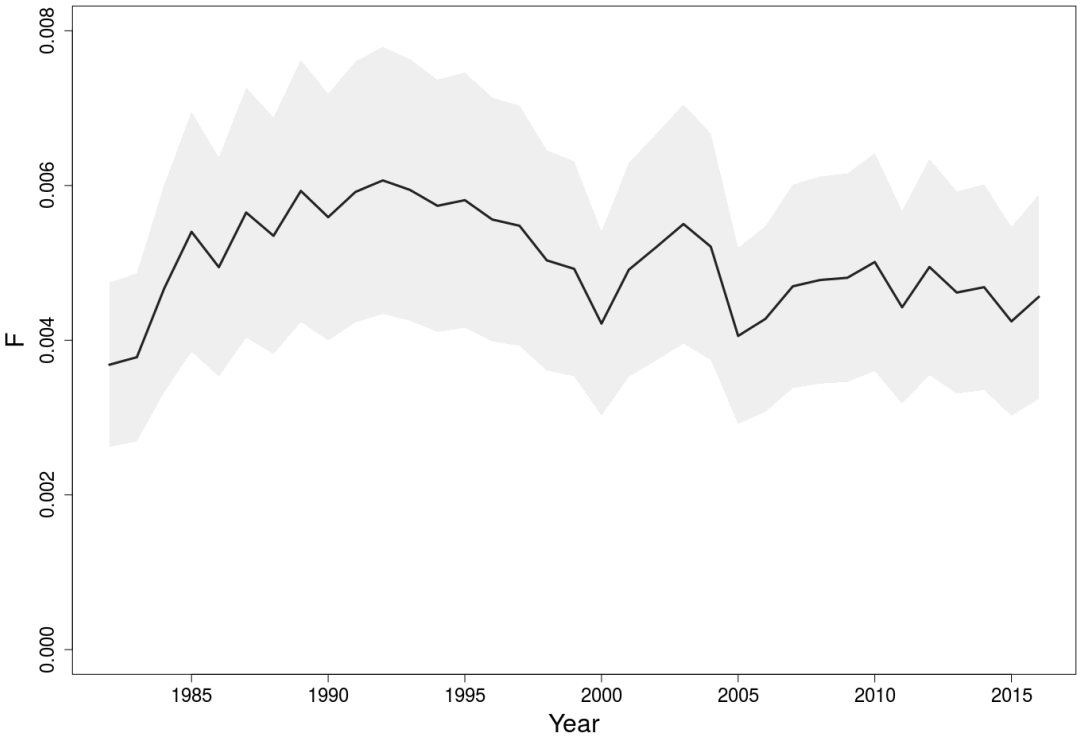

Figure 110: Fishing mortality estimates from the ocean quahog assessment base model, including lower and upper 95% confidence bounds.

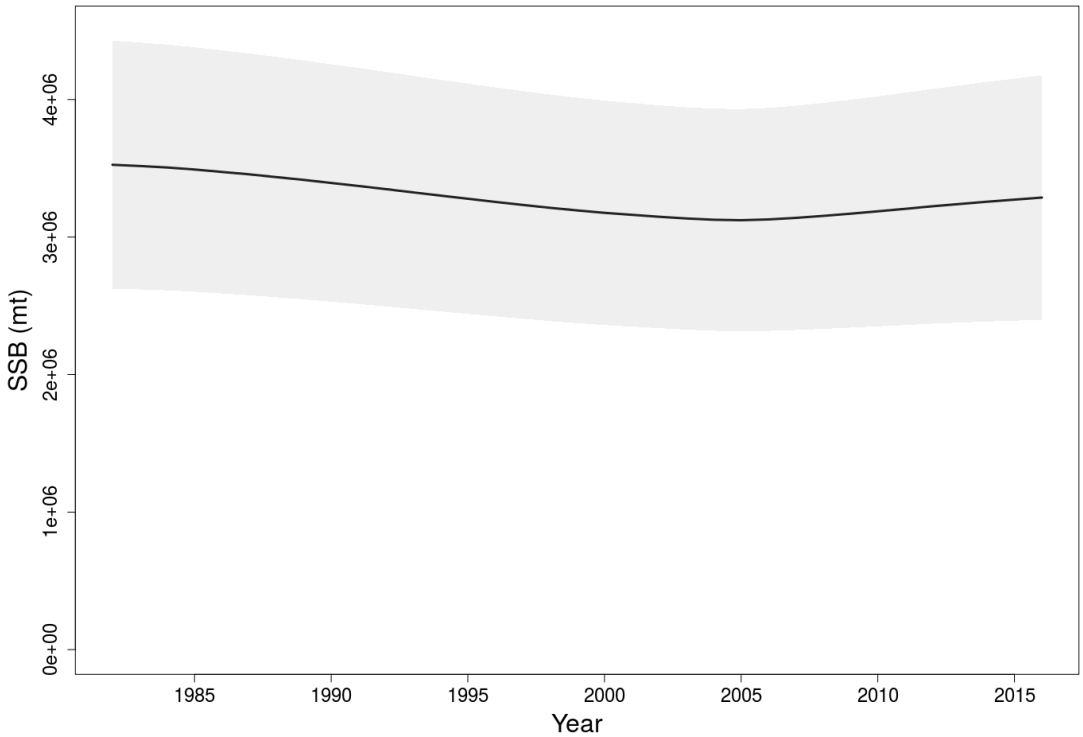

Figure 111: Spawning stock biomass estimates from the ocean quahog assessment base model in '000 mt, including lower and upper 95% confidence bounds.

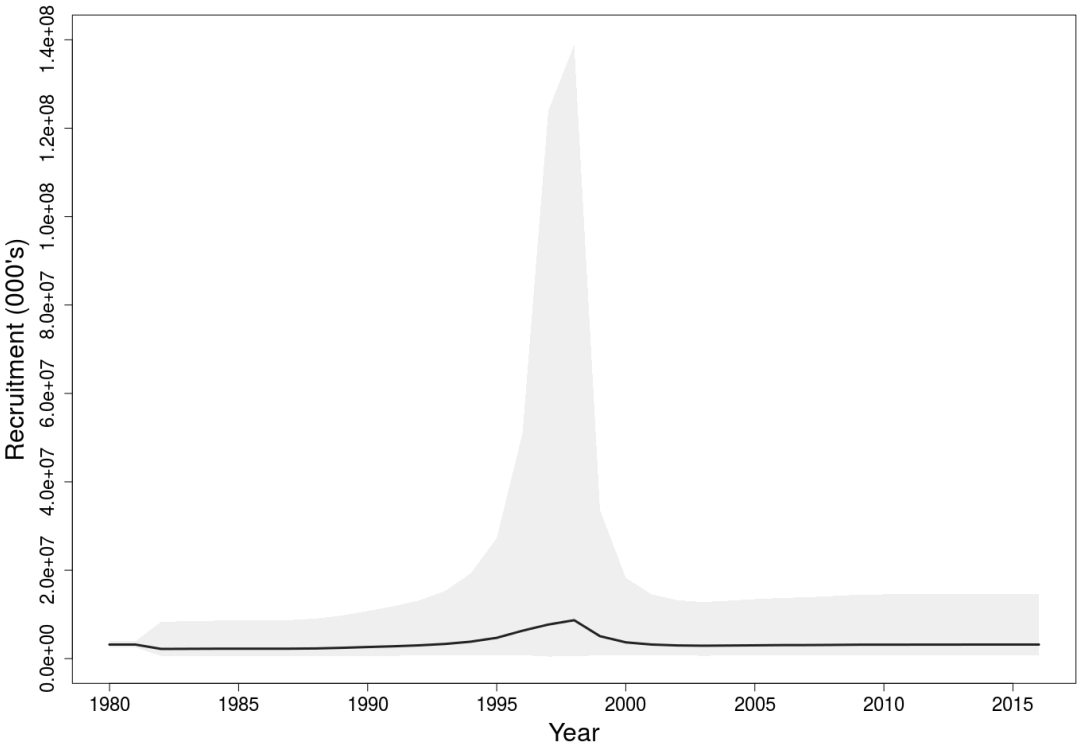

Figure 112: Recruitment estimates from the ocean quahog assessment base model, including lower and upper 95% confidence bounds.

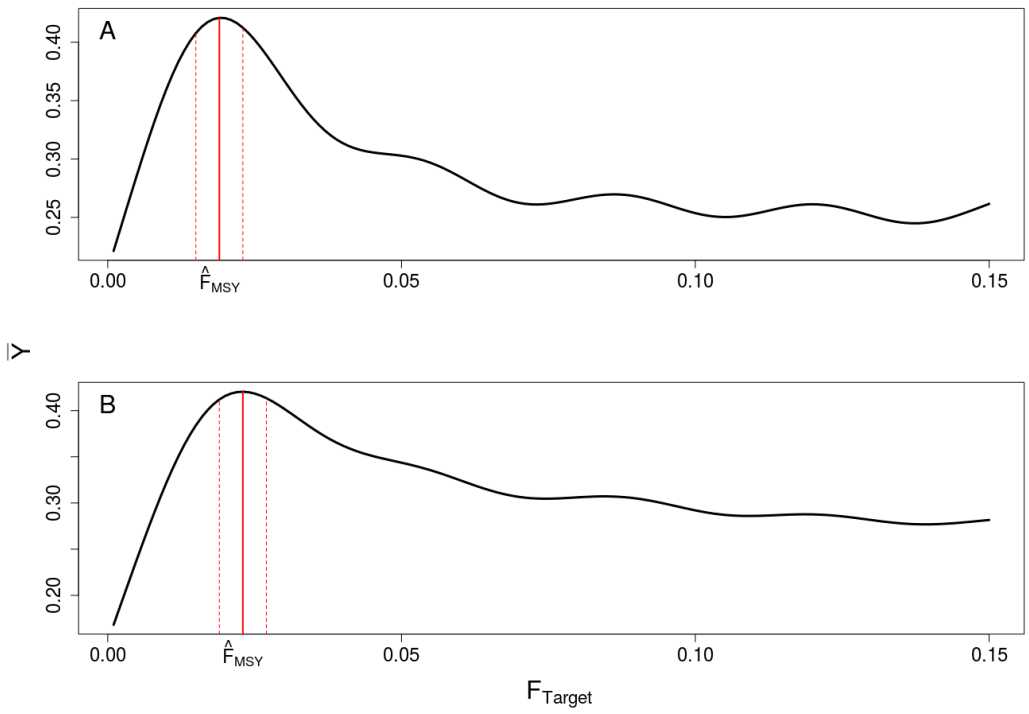

Figure 113: $F_{MSYproxy}$ from the MSE. The average yield over 1000 years fit to a GAM over the F_{Target} from each simulation run. Maximum average yield was achieved at the F_{Target} that is designated as $\hat{F}_{MSY}$ and a solid red vertical line. The dashed red vertical lines show the F_{Target} closest to the 95% quantiles of average yield to either side of $\hat{F}_{MSY}$. Panel A shows the results for simulations where growth was Von Bertalanffy and panel B shows the results from simulations using Tanaka growth.

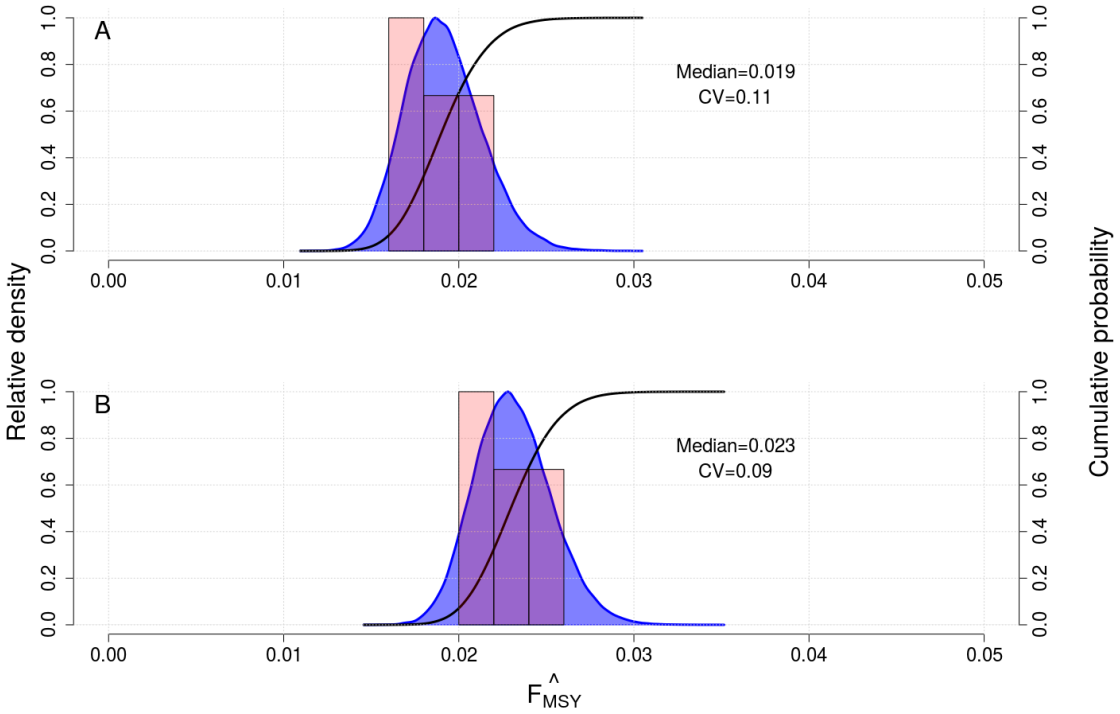

Figure 114: A lognormal distribution with mean, $\hat{F}_{MSY}$ and variance based on all of the F_{Target} that resulted in average yield between the bounds formed by the 95% quantiles to either side of $\hat{F}_{MSY}$ (see Figure 113) in the MSE. A frequency histogram of the F_{Target} values used to produce each distribution is superimposed over each plot. Panel A shows the results for simulations where growth was Von Bertalanffy and panel B shows the results from simulations using Tanaka growth.

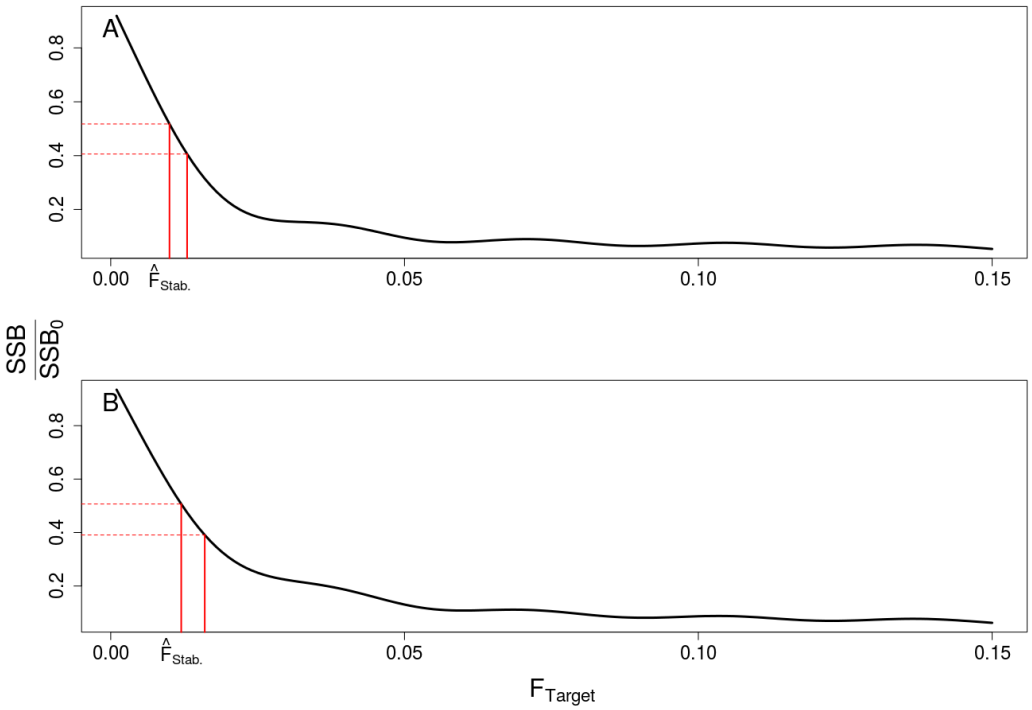

Figure 115: $F_{Stab.proxy}$ from the MSE. The average biomass over 1000 years fit to a GAM over the F_{Target} from each simulation run. Average biomass closest to $SSB_{Target} = \frac{1}{2}SSB_0$ was achieved at the F_{Target} that is designated as $\hat{F}_{Stab.}$ and a solid red vertical line. The second solid red vertical lines show the F_{Target} closest to the $SSB_{Theshold} = \frac{2}{5}SSB_0$. Panel A shows the results for simulations where growth was Von Bertalanffy and panel B shows the results from simulations using Tanaka growth.

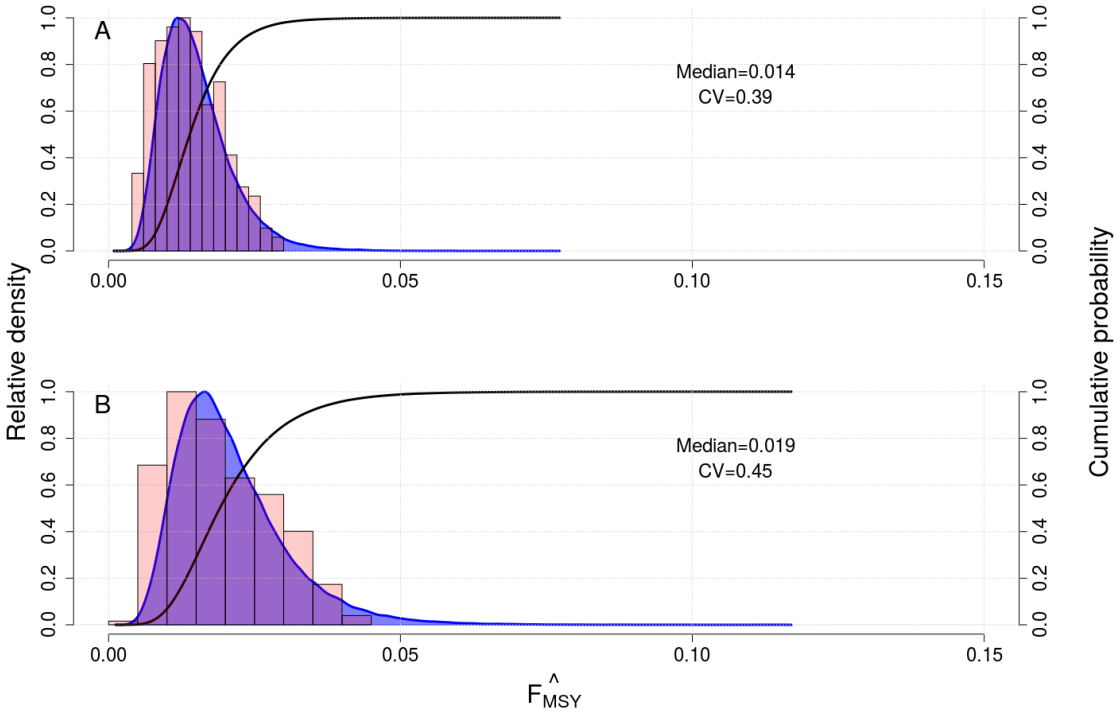

Figure 116: A lognormal distribution with mean, $\hat{F}_{Stab.}$ and variance based on all of the F_{Target} that resulted in average biomass between the bounds formed by $\frac{2}{5}SSB_0$ and $\frac{1}{2}SSB_0$ (see Figure 115) in the MSE. A frequency histogram of the F_{Target} values used to produce each distribution is superimposed over each plot. Panel A shows the results for simulations where growth was Von Bertalanffy and panel B shows the results from simulations using Tanaka growth.

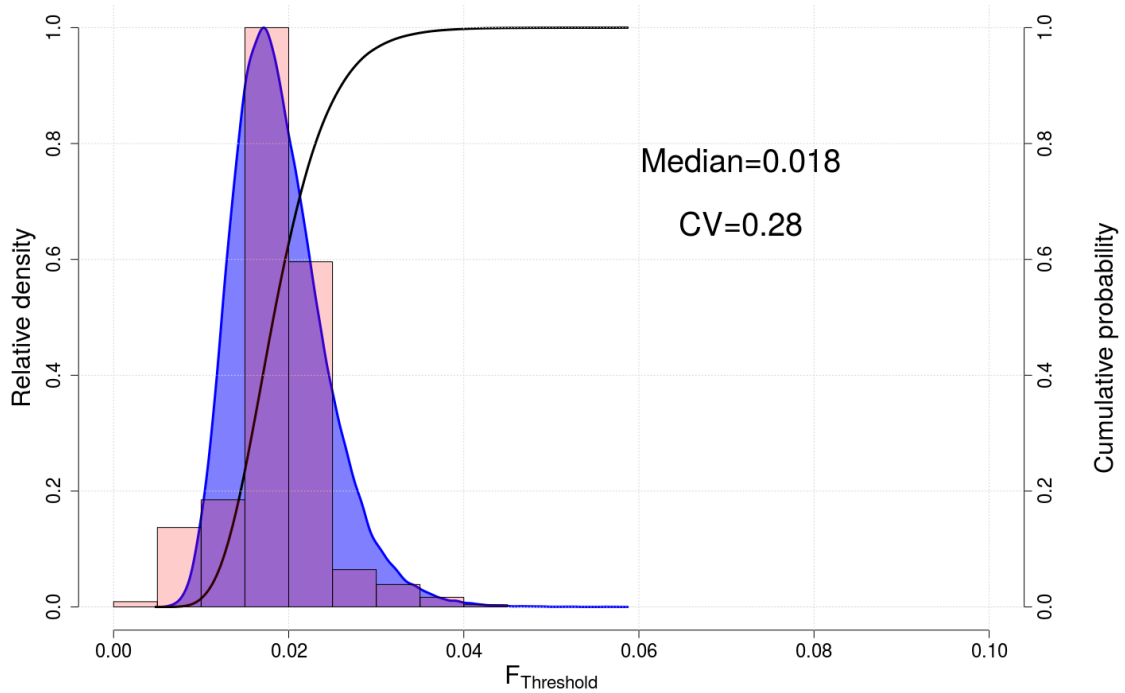

Figure 117: A lognormal distribution with mean and variance based on all of the F_{Target} that resulted in average biomass between the bounds formed by $\frac{2}{5}SSB_0$ and $\frac{1}{2}SSB_0$, or average yield between the bounds formed by the 95% quantiles to either side of $\hat{F}_{MSY}$ (see Figures 113 - 115). A frequency histogram of the F_{Target} values used to produce the distribution is superimposed over the plot. This is the preferred $F_{Threshold}$ used to determine stock status for ocean quahog.

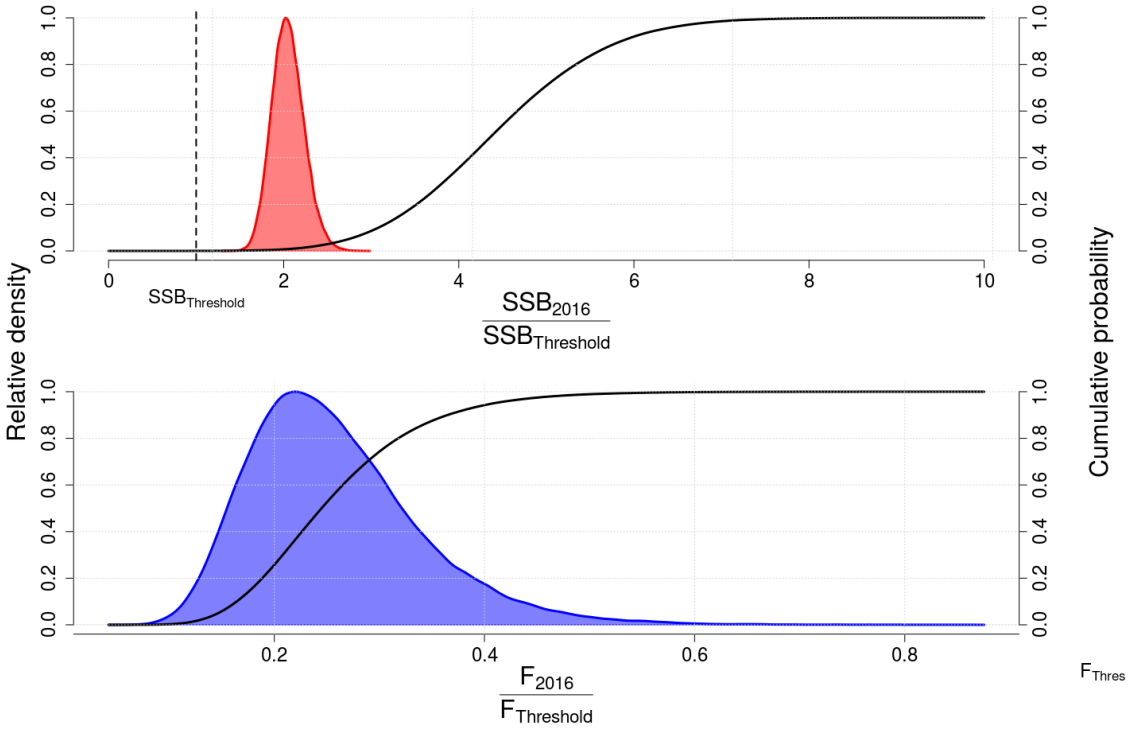

Figure 118: Probability distributions of $\frac{SSB_{2016}}{SSB_{Threshold}}$ and $\frac{F_{2016}}{F_{Threshold}}$, using the recommended reference points. The probability of overfished status during 2016 is equal to the area of the red, upper curve that is less than $SSB_{Threshold}$. The probability of overfishing status during 2016 is equal to the area of the blue, lower curve that is greater than $F_{Threshold}$. The probability of overfished and overfishing status can be approximated by the elevation (y axis scale) at which the solid line representing the cumulative probability distribution crosses the dashed vertical line representing the reference point in each plot. The probability distributions presented in this figure account for the positive correlation between the reference points ($SSB_{Threshold} = 0.4 * SSB_0$ and $F_{Threshold} = F^* \frac{F_{MSY}}{F^*_{Max}}$) and the fishing mortality and spawning biomass estimates in 2016, as well as the uncertainty in the estimation of both the point estimates and their respective reference points.

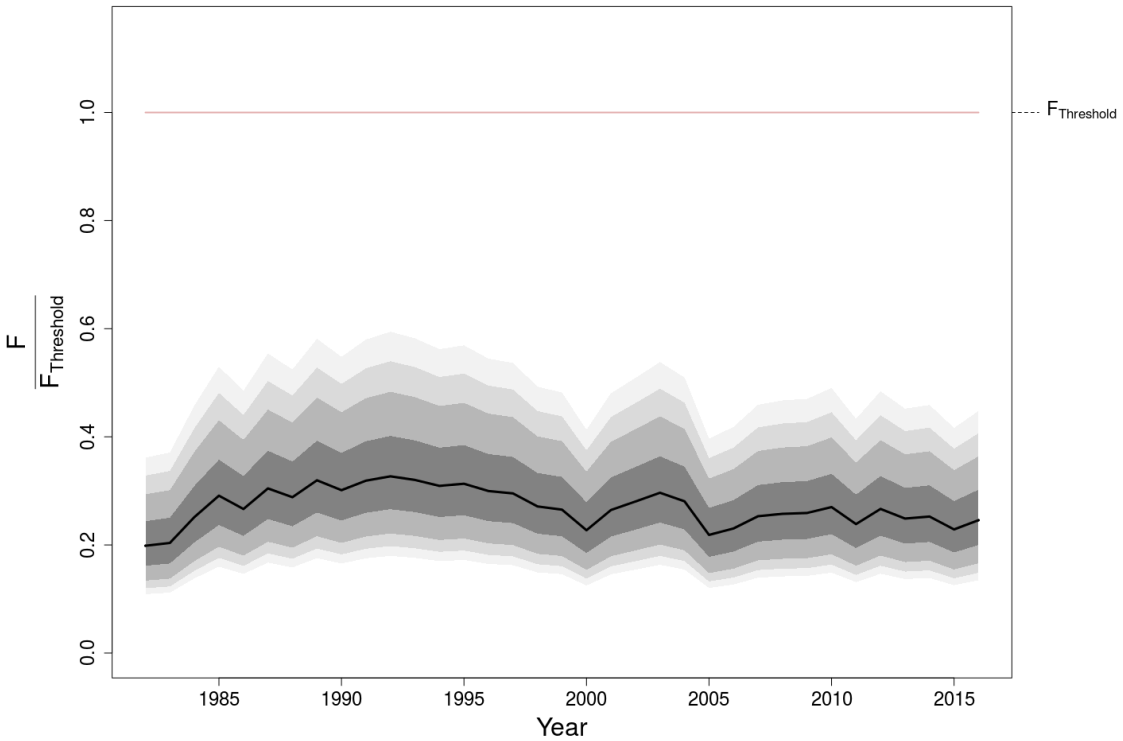

Figure 119: The time series of the ratio of fishing mortality estimates to the recommended F threshold, with the 95% confidence interval. The confidence interval accounts for the correlation between F and $F_{Threshold}$. Overfishing would occur if the ratio exceed 1.0.

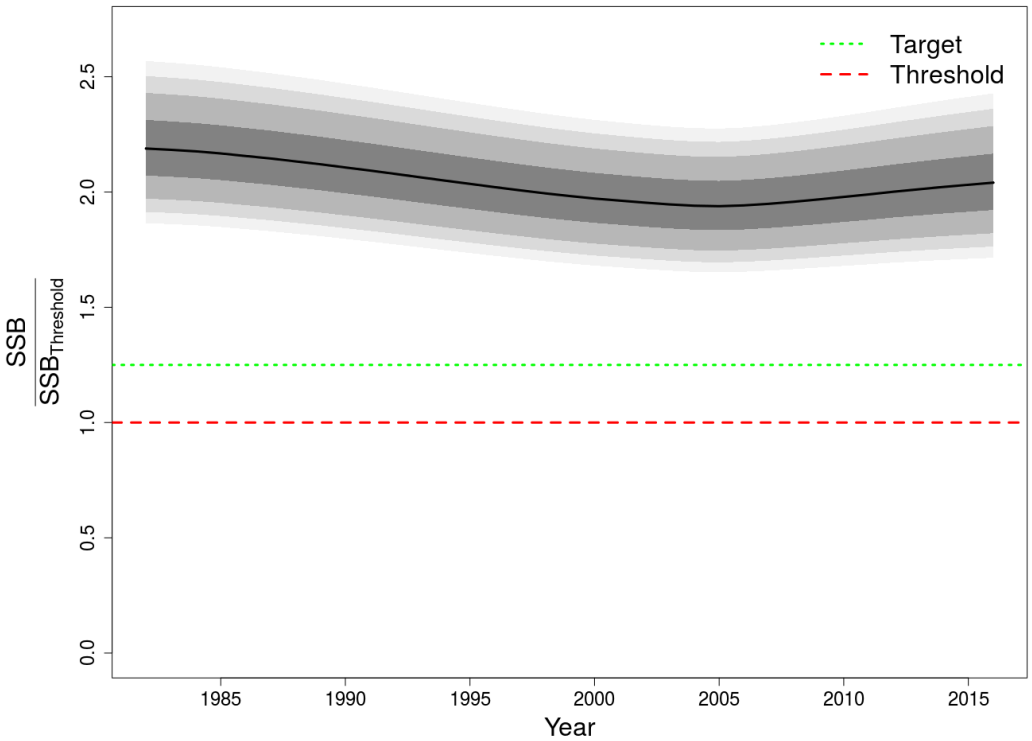

Figure 120: The time series of the ratio of spawning biomass estimates to the unfished spawning biomass (SSB_0), with the 95, 90, 80 and 50% confidence intervals. The confidence interval accounts for the correlation between SSB and SSB_0. Overfished status would occur if the ratio went below 1.0.

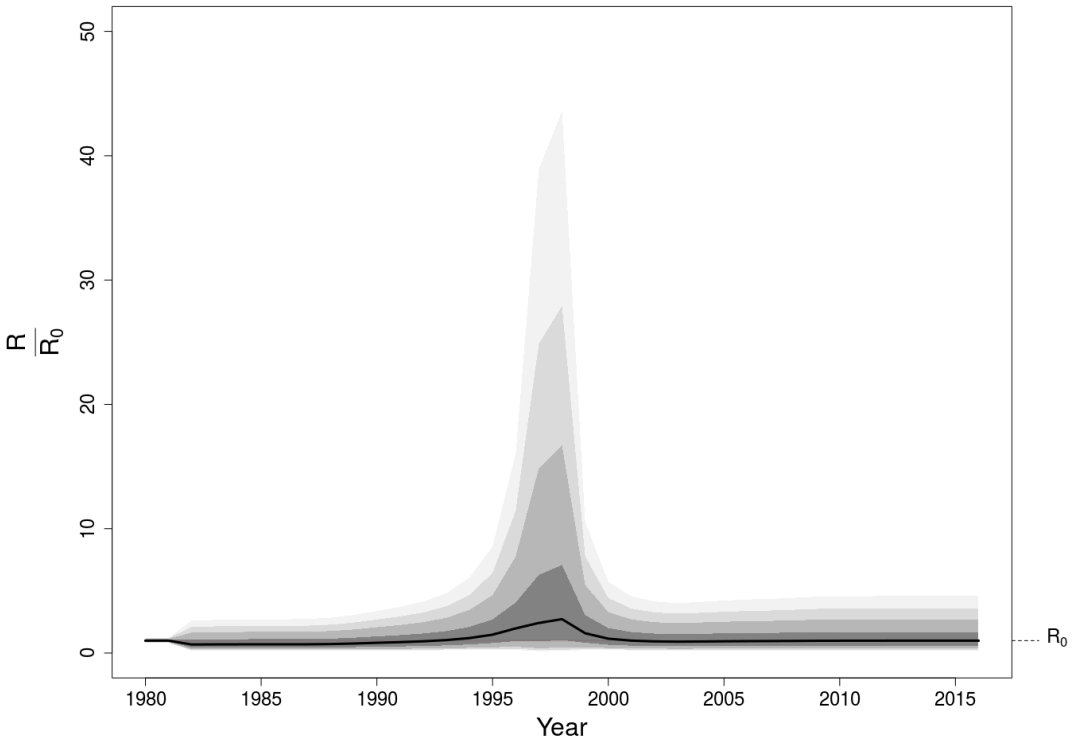

Figure 121: The time series of the ratio of recruitment estimates to the equilibrium recruitment (R_0), with the 95, 90, 80 and 50% confidence intervals.

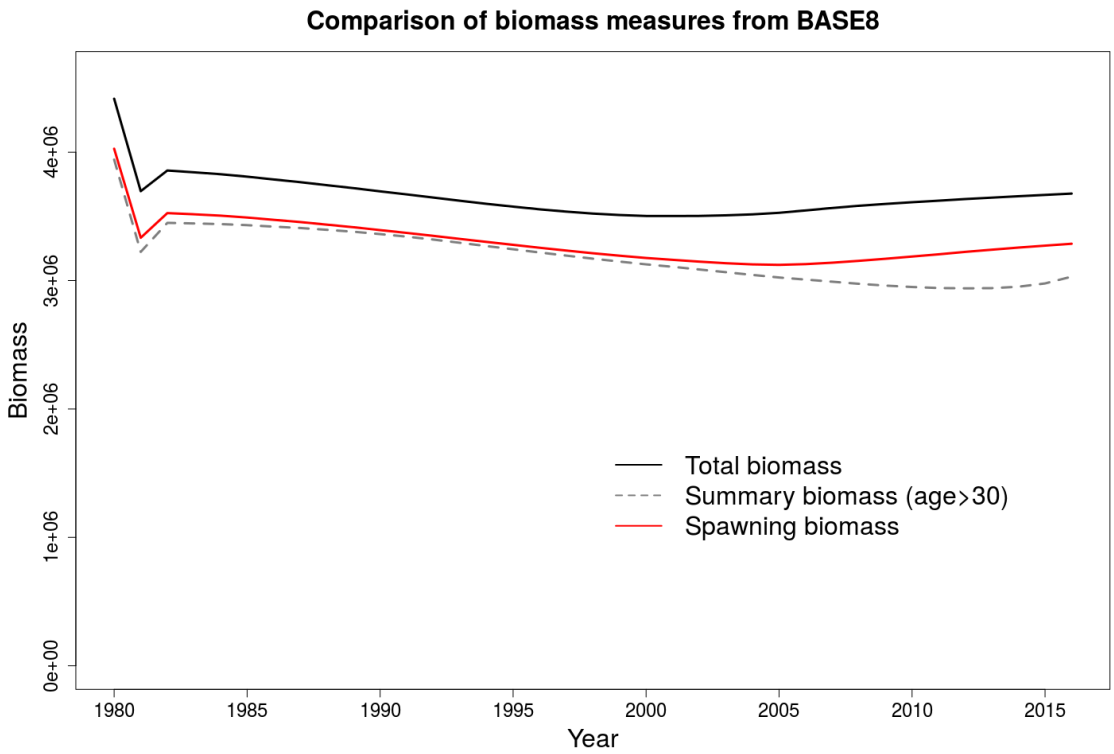

Figure 122: A comparison of different measures of biomass.

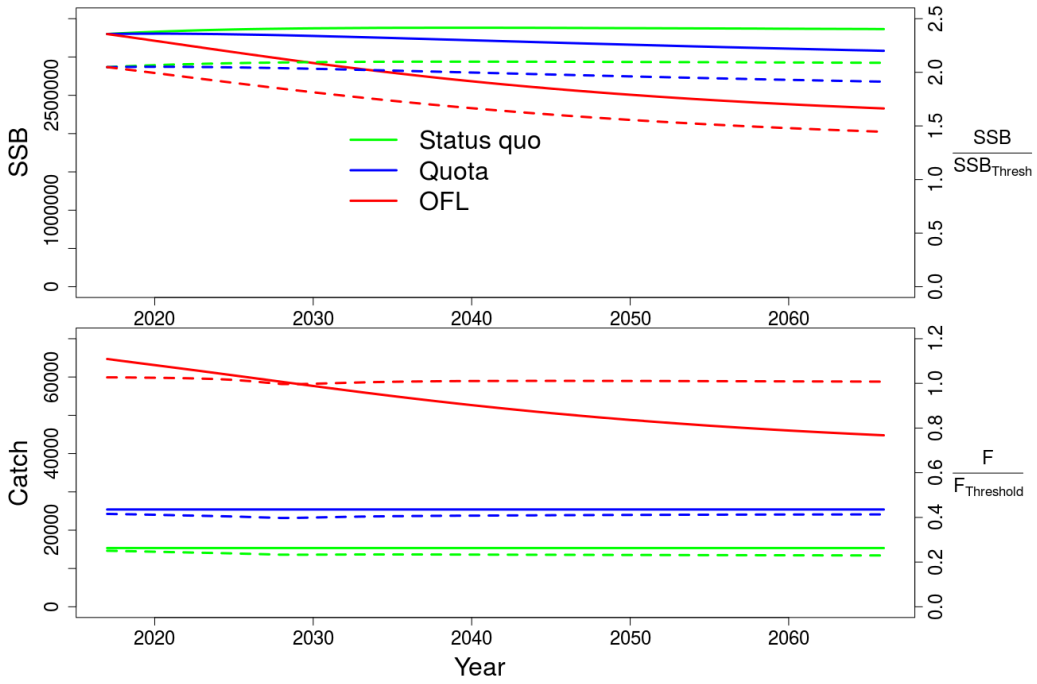

Figure 123: Projections using three different catch scenarios. The upper plot shows the biomass trends over time (solid lines) and the ratio of biomass to biomass threshold (dashed lines). The lower plot shows the landings (solid lines) and the ratio of F to $F_{Threshold}$. In all plots the status quo catch scenario is green, the quota catch scenario is blue and the OFL scenario is red.

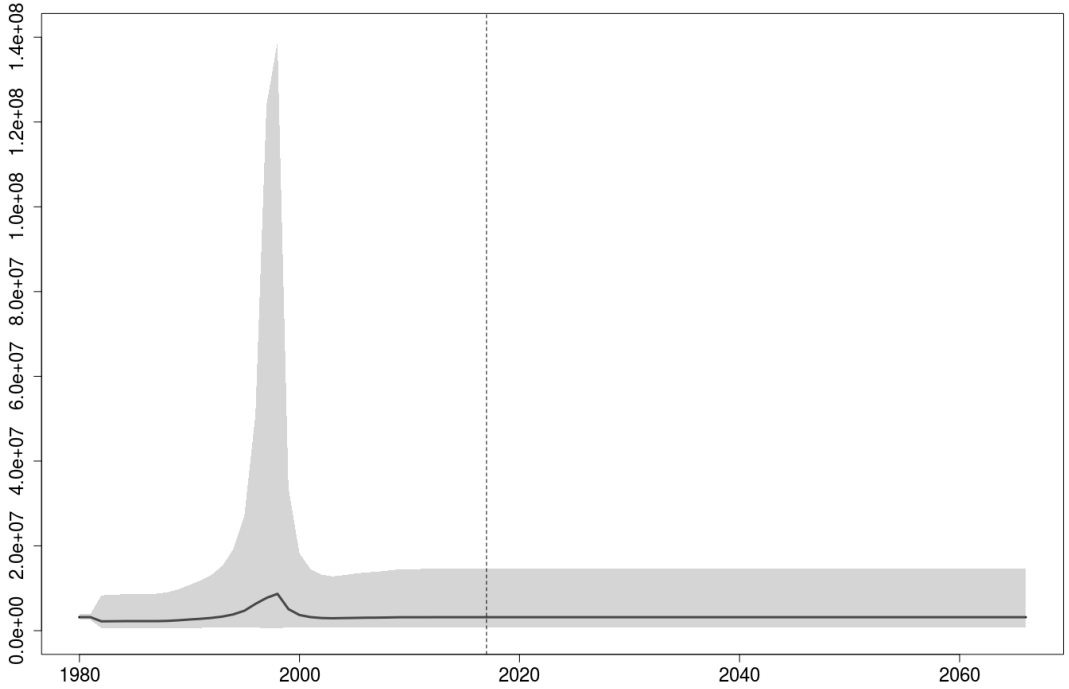

Figure 124: Forecast and time series recruitment estimates. Projections begin at the vertical dashed line.

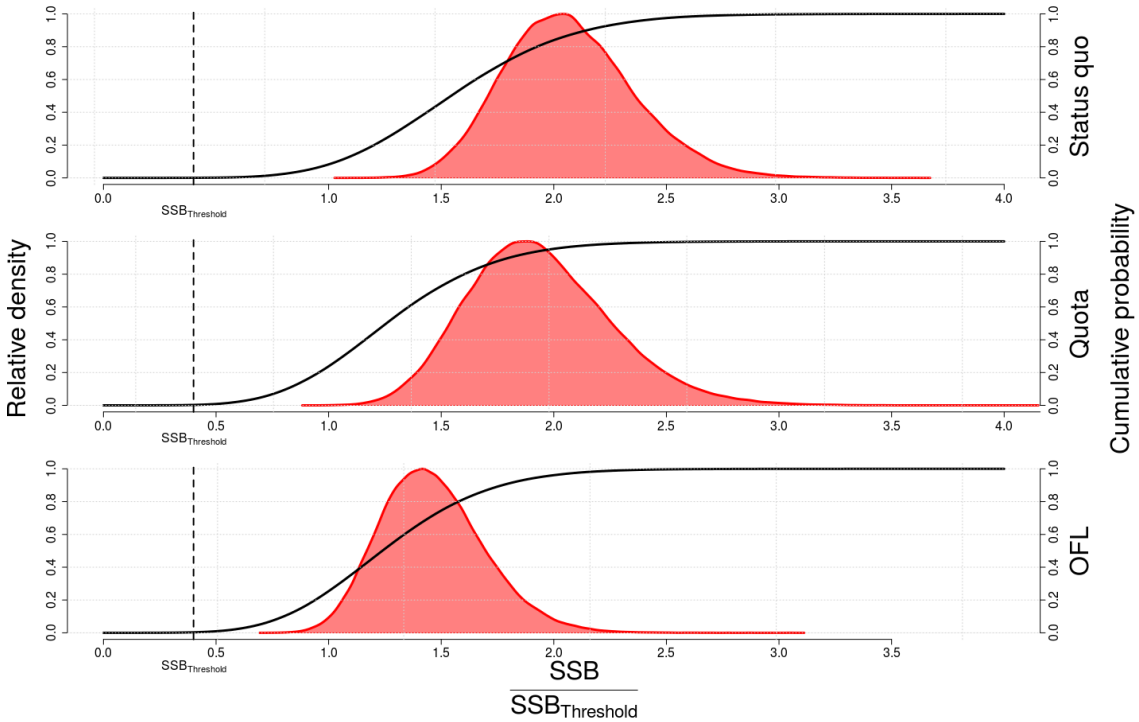

Figure 125: Probability of overfished status for ocean quahog during the projection year with the lowest biomass from 2017-2066. The different catch scenarios are in rows.

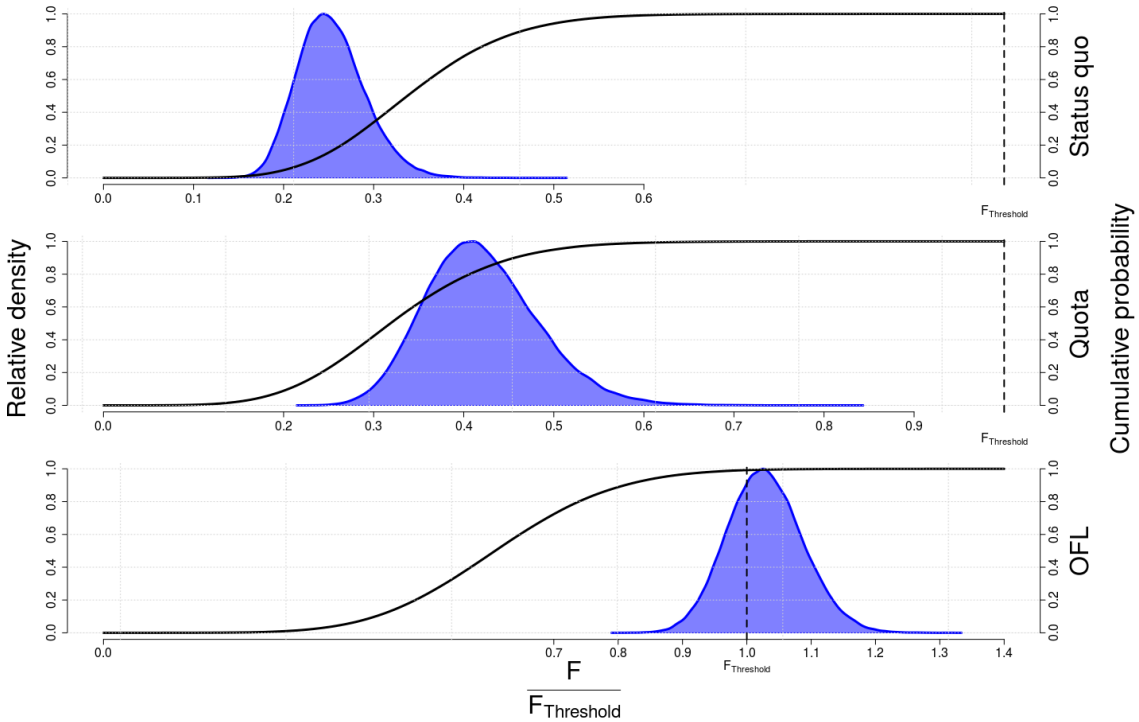

Figure 126: Probability of overfishing status for ocean quahog during the projection year with the highest F from 2017-2066. The different catch scenarios are in rows.

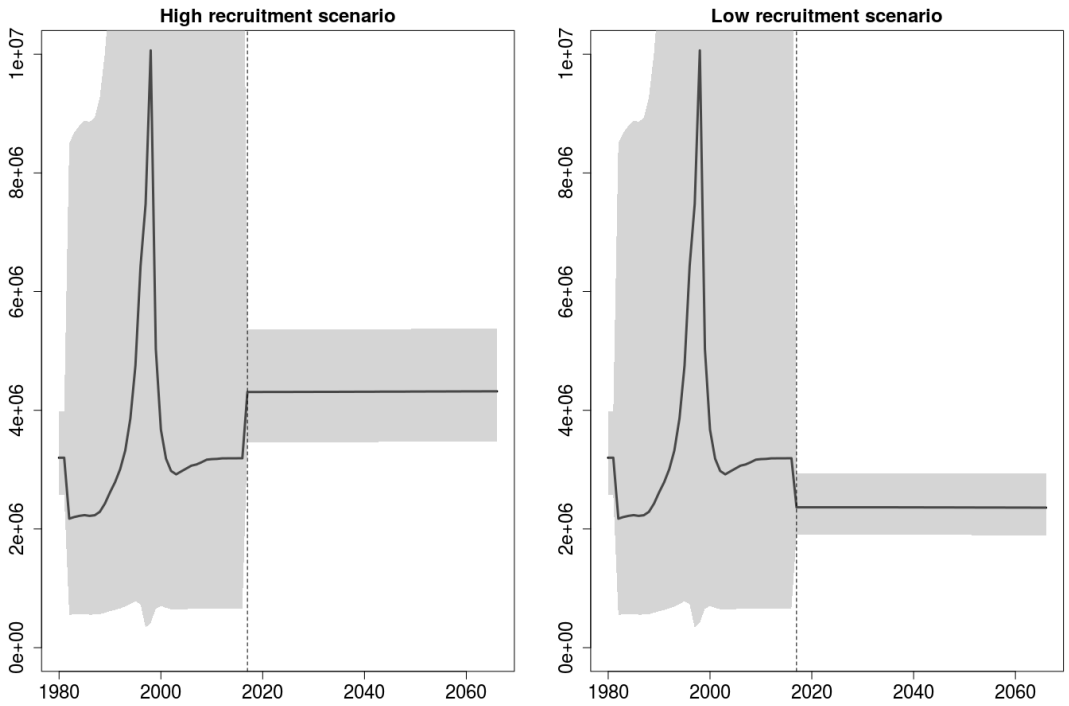

Figure 127: Forecast recruitments for the high and low recruitment scenarios in sensitivity projection runs for ocean quahog.

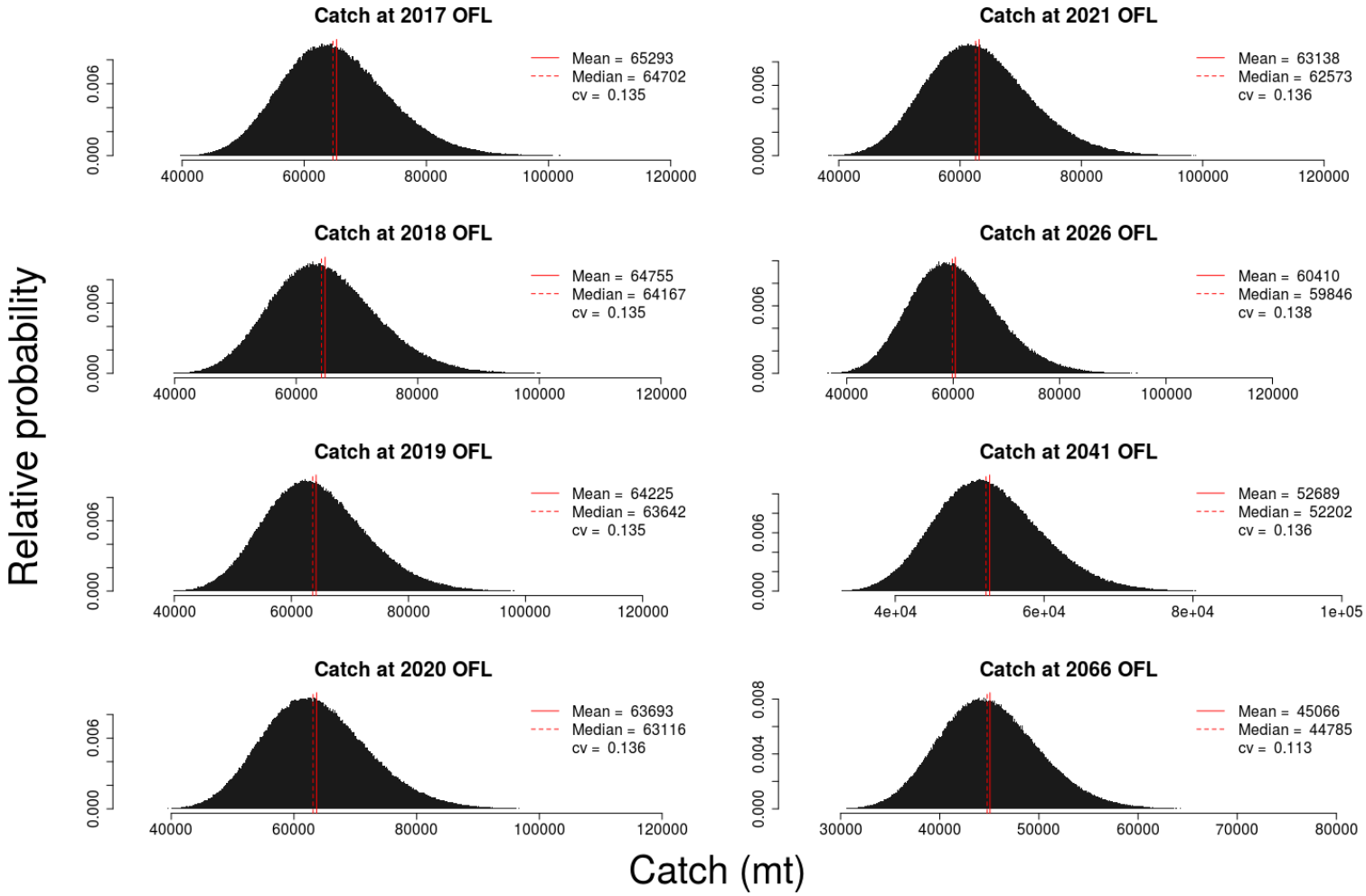

Figure 128: Distribution of catch (landings + incidental mortality) at the Overfishing Limit (OFL) from 2017-2066 for ocean quahog in four example years.